In the name of ALLAH, the most mercyful, the most beficient

Rheology of the Rate Type Fluid Models with Heat Transfer:

Analytical and Numerical Treatment

By

Aqsa

Department of Mathematics
Quaid-i-Azam University
Islamabad, Pakistan
2019

Rheology of the Rate Type Fluid Models with Heat Transfer:

Analytical and Numerical Treatment

by

Aqsa

Supervised by

Prof. Dr. Muhammad Yousaf Malik

Department of Mathematics
Quaid-i-Azam University
Islamabad, Pakistan
2019

Rheology of the Rate Type Fluid Models with Heat Transfer: Analytical and Numerical Treatment

by

Aqsa

A THESIS SUBMITTED IN THE PARTIAL FULFILLMENT OF THE REQUIREMNETS FOR THE DEGREE OF

DOCTOR OF PHILOSOPHY

IN

MATHEMATICS

Supervised by

Prof. Dr. Muhammad Yousaf Malik

Department of Mathematics
Quaid-i-Azam University
Islamabad, Pakistan
2019

Dedicated to my beloved family

Acknowledgements

All the praises and appreciations are for the omnipotent **ALLAH**, the most merciful and generous that knows better the hidden truths of the universe and HIS **Holy Prophet Muhammad (Pease Be Upon Him)** who declared it an obligatory duty of every Muslim to seek and acquire knowledge.

First and foremost I offer my sincerest gratitude to my supervisor **Prof. Dr. M. Y. Malik**, who has supported me throughout my research work with his patience and knowledge whilst allowing me the room to learn. I am really thankful to him for giving me valuable suggestions and extraordinary experiences throughout the work. I am indebted to him more than he knows..

I am much indebted to all my friends for their valuable and sincere advices and discussions. They gave me precious time along with useful comments on my research work. I have also benefited by useful suggestions from all members of FMG (Fluid Mechanics Group). For that I am very much thankful.

Where would I be without my family?

I owe my heartiest thanks to my loving and affectionate **grandparents** whose prayers have accompanied me through thick and thin. My **parents** deserve special mention for their inseparable support and prayers. I would like to pay my gratitude and thanks to my loving and dear **Khala**, my husband **Sohail**, my son **Huziafa**, my nieces **Sumaiya, Anaya, Abeeha** and nephews **Hishaam** and **Hashir** as they always revitalized and recharged me with their love and innocence, my brother **Asim Sohail** and **Muhammad Awais**, My sisters **Sania** and **Nazia** for their prayers, support and encouragement,

May Allah bless all those who pray for me (Aameen)

AQSA

Date: 24/4/2019

Author's declaration

I, AQSA hereby state that my PhD thesis entitled as **"Rheology of the Rate Type Fluid Models with Heat Transfer: Analytical and Numerical Treatment"** is my research work and has not been submitted previously for taking any degree from any university.

At any time if my statement is found to be incorrect, the university has the right to withdraw my PhD degree.

Name: Aqsa

Supervisor: Prof. Dr. M. Y. Malik

Plagiarism Undertaking

I solemnly declare that the research material presented in this thesis entitles as **"Rheology of the Rate Type Fluid Models with Heat Transfer: Analytical and Numerical Treatment"** is my research work. Small contributions are acknowledged.

I understand the zero tolerance policy of HEC and Quaidi-Azam University towards plagiarism. I as an author of the above titled thesis declare that no portion of my thesis has been plagiarized and any material used as reference is cited properly.

I undertake that if I found guilty in case of plagiarism in above titles thesis, then the university has the right to withdraw my PhD degree and that HEC nay publish my name on HEC/ University website on which the names of student are placed who submitted plagiarized thesis.

Name: Aqsa

Supervisor: Prof. Dr. M. Y. Malik

Rheology of the Rate Type Fluid Models with Heat Transfer: Analytical and Numerical treatment
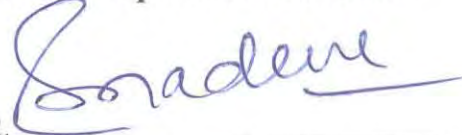
By

Aqsa

CERTIFICATE

A THESIS SUBMITTED IN THE PARTIAL FULFILLMENT OF THE REQUIREMENTS FOR THE DEGREE OF THE DOCTOR OF PHILOSOPHY

We accept this thesis as conforming to the required standard

1. _____
Prof. Dr. Muhammad Yousaf Malik
(Supervisor)

2. _____
Prof. Dr. Sohail Nadeem
(Chairman)

3. _____
Dr. Rahmat Ellahi
Associate Professor
Department of Mathematics &
Statistics Islamic University
H-10, Islamabad
(External Examiner)

4. _____
Dr. Muhammad Mushtaq
Associate Professor
Department of Mathematics,
COMSATS, Park Road
Chak Shahzad, Islamabad
(External Examiner)

Department of Mathematics
Quaid-I-Azam University
Islamabad, Pakistan
2019

Certificate of Approval

This is to certify that the research work presented in this thesis entitled **Rheology of rate Type Fluid Models with Heat Transfer: Analytical and Numerical treatment** was conducted by Ms. **Aqsa** under the supervision of **Prof. Dr. M. Yousaf Malik**. No part of this thesis has been submitted anywhere else for any other degree. This thesis is submitted to the Department of Mathematics, Quaid-I-Azam University, Islamabad in partial fulfillment of the requirements for the degree of Doctor of Philosophy in Field of Mathematics from Department of Mathematics, Quaid-I-Azam University Islamabad, Pakistan.

Student Name: **Aqsa** Signature: _____

External committee:

a) **External Examiner 1**: Signature: _____
    Name: **Dr. RahmatEllahi**
    Designation: Associate Professor
    Office Address: Department of Mathematics , IIU Islamabad

b) **External Examiner 2**: Signature: _____
    Name: **Dr. Muhammad Mushtaq**
    Designation: Associate Professor
    Office Address: Department of Mathematics , COMSATS, Islamabad

c) **Internal Examiner** : Signature: _____
    Name: **Dr. M. Yousaf Malik**
    Designation: Professor
    Office Address: Department of Mathematics, QAU Islamabad
    Supervisor Name: Signature: _____
    Prof. Dr. M. Yousaf Malik

    Name of Dean/ HOD Signature: _____

    Prof. Dr. Sohail Nadeem

Preface

The significant features of an engineering and technological field can be realized by its worth in relation to other engineering sciences. Transport phenomena in fluid mechanics have prominent aspects in chemical, thermal and mechanical engineering sciences. This field of research has enormous applications in biotechnology, microelectronics, nanotechnology, crystal growth, paper production, wire drawing, food processing etc. By getting inspiration from such broad applications, scientists and engineers have done extensive studies in this field. The strength of this subject is mainly depending on the fundamental laws of conservation. The transport phenomena like momentum, heat and mass transfer are important since they govern the velocity, temperature and concentration profiles. It has been apprehended that main attention in the preceding years has been given to the rheological problems relating to the differential type non-Newtonian fluid models. In this dissertation, the rate type non-Newtonian fluid models have been examined and the effects of heat transfer on various flow situations have been presented. Moreover, heat transfer problems have been coupled with mass transfer to investigate double diffusion. Also influence of magnetic field, suction/injection and radiations have been studied.

Chapter 1 addresses the literature review of the two and three dimensional non-Newtonian fluid models. Conservation laws and the adopted computational methodologies have been briefly describes. Advantages of different techniques which have been implemented for the analytical and numerical computations have been also discussed.

In chapter 2, investigation has been made to study the dual numerical solutions for the flow of an upper convected Maxwell (UCM) fluid in a porous medium. The influence of internal heat generation/absorption effects, chemical reaction phenomenon and magnetic field have taken into account. Stream function and similarity transformations have been employed on the governing mathematical model which results into the system of nonlinear ordinary differential equations. Shooting technique has been implemented efficiently to obtain numerical results. It has been analyzed that the dual numerical results exist in case of shrinking surface while a unique solution occurs for the stretching sheet. Results have been given to study the skin friction, local Nusselt and Sherwood numbers. The contents of this chapter have been published in **Journal of Molecular Liquids, 232 (2017) 361-366.**

In chapter 3, we have examined double-diffusivity for the Sakiadis flow of UCM nanofluid in the presence of magnetic field and heat source/ sink effects. The effects of thermal radiations have been incorporated in addition. Set of nonlinear ordinary differential equations have been achieved by applying the suitable transformations on the governing partial differential equations. Analytic and numerical solutions have been computed via homotopy analysis method and finite difference approach respectively. Comparison between the results have been presented in tabular form and seems to be in a nice agreement. Results have also been portrayed to visualize temperature and concentration profiles for the involved parameters. The contents of this chapters have been published in **Journal of Molecular Liquids, 241 (2017) 570-576.**

Chapter 4 presents the three dimensional rheology of an upper-convected Maxwell (UCM) fluid over a bidirectionally stretched surface with temperature dependent thermal conductivity effects. Flow over an exponentially stretched wall has been considered and the cases of prescribed surface temperature (PST) and prescribed surface heat flux (PSHT) have been analyzed in detail. Series solutions have been evaluated via homotopy analysis method. Results have been presented in a graphical and tabular form to visualize the effect of different physical parameters. The contents of this chapter have been submitted for publication.

Chapter 5 explores the Sakiadis rheology of Oldroyd-B fluid in the presence of magnetic field. Convective heating process has been analyzed under the effects of thermal radiations. Appropriate transformations have been invoked for conservation of partial differential equations into coupled nonlinear ordinary differential equations. Numerical as well as analytic solutions have been computed for the velocity and temperature distributions. Graphical results have been prepared observe the behavior of physical parameters. Error analysis is also presented in order to validate the obtained solutions. Bar charts have been designed to show the heat flux analysis. Comparison between the results obtained by homotopy analysis method (HAM) and finite difference method (FDM) has been given in a tabular form. The contents of this chapter are published in **Thermal Sciences (2018) Doi.org/10.2298/TSCI180426284A.**

In chapter 6, the features of Cattaneo-Christov heat flux for the flow of Burgers' fluid have been analyzed. Mathematical modelling is performed using laws of momentum and energy under the order analysis to transform the problem into the set of equations. It is shown that the term for the

hydro-magnetic rheology of the viscous model is "$\sigma B_0^2\, u/\rho$" while the generalized magnetic field term (as revealed in Eq. 6.2) is for the Burgers' model which is used in the present study. For the solution computation, homotopy analysis method is applied to compute results. Results are depicted in graphs to visualize the effect of physical parameters. Values of skin friction with heat transfer rate have been displayed in the tables. The contents of this chapter are published in **Scientia Iranica 26 (2019) 323-330.**

Chapter 7 explores the study for Jeffery nanofluid with thermophoresis and Brownian motion properties. The combined effects of viscous dissipation and heat generation/absorption have been considered. Entropy generation and inclined magnetic field for the Jeffery fluid have been analyzed. Mathematical formulations have been performed and solutions have been computed by using a homotopy approach in the spatial domain. Results have been illustrated in graphical and tabular form to study the effect of flow parameters. It is analyzed that magnetic field is a flow reducing parameter whereas Biot number behaves like a boosting factor to increase the fluid temperature. The contents of this chapter are submitted for publication.

In chapter 8, three-dimensional flow properties of an Oldroyd-B fluid model have been discussed while incorporating the effects due to the existence of nanoparticles. The present physical problem is studied under influence of nonlinear radiations. During mathematical formulation, the heat and concentration equations have been studied under thermophoresis effect and Brownian motion. Bidirectional stretching phenomenon have been taken to study the three-dimensional fluid deformation. Some suitable transformations have been utilized for conversion of derived partial differential system into coupled nonlinear ordinary differential system. Solutions are computed via homotopy approach. Several graphical and numerical illustrations have been prepared to present the behavior of involved physical quantities. The contents of this chapter are published in **Results in Physics, 8 (2018) 1038-1045.**

Table of Contents

Chapter 1

Introduction

The survey of literature relevant to the flows in steady and time dependent cases of Newtonian and non-Newtonian fluid models are described. Conservation laws along with the brief idea of solution methodologies are also presented.

1.1 Literature survey

Rheological features of the non-Newtonian fluid models show difference as associated to the Newtonian fluids. We know that the rheological properties of all the nonlinear fluids can't be anticipated by only constitutive relation between shear rate and strain rate. Non-linear fluids have nonlinear relation among the stress and strain. It is noted that the nonlinear fluids have been further characterized into three type's viz. the differential, the integral and the rate type. The constitutive equations in the last mentioned class "rate type fluids" are comparatively more complex and complicated due to the elasticity effects in addition to the viscosity. In last few years, scientists pay great attention to the rate type fluid models under different physical conditions. Harris [1] presented some literature survey in his book "the rheology and non-Newtonian flow". He primarily investigated the mathematical formulation for the laws of conservation of momentum for the Maxwell model. Later on different analysts and applied mathematicians incorporated his idea to study the rate type models under diverse flow configurations. For-instance, Zierep and Fetecau [2] have investigated the Rayleigh-Stokes equation for the Maxwell model. Tan and Masuoka [3] explored the stability of Maxwell fluid model. The authors have taken a porous medium to examine the stability values for the nonlinear rheology. Hayat and Awais [4] examined 3D flow of UCM fluid over stretched surface. Series solution has been obtained by using the homotopy approach. Abbasbandy et al. [5] investigated the numerical and analytic solutions by considering the Falkner-Skan flow. They have taken

MHD Maxwell fluid for the analysis. Later, Awais et al. [6] also considered the Maxwell fluid and studied the heat generation and absorption effects. Afify and Elgazery [7] have done the Lie group analysis to examine the chemical reaction effects. Scientists investigated the MHD flow for combined diffusion towards permeable stretching wall. Majeed et al. [8] examine the chemical reaction with heat transfer for the UCM Ferro-fluid flow with magnetic dipole. Analysis was carried out for the Soret and suction effects. Malik, Farzana and Rehman [9] also considered the Maxwell fluid model for the analysis. Scientists evaluated the MHD 3D flow in horizontal stretching surface with the convective wall. Later, Malik et al. [10] computed the numerical analysis of Williamson fluid flowing over stretched cylinder. Study has been presented by considering variable thermal and heat immersion effects. Numerical results have been calculated by using shooting method together with RK-Fehlberg approach. Awais et al. [11] observed the characteristics of micropolar fluid. Malik et al. [12] have investigated Carreau fluid and variable viscosity in spongy medium. Analysts studied under the two situations namely Poiseuille and Couette flow. Researchers have employed shooting method together with Runge-Kute-Fehlberg method to evaluate numerical results. Moreover, results displayed graphically to visualize influences of physical factors. Sakiadis [13] have scrutinized the BL behavior over solid wall. Later, Sakiadis [14] examined the behavior of boundary layer in continuous solid surface. Experts have employed numerical as well as integral method for the computation of results. Nadeem et al. [15] have evaluated the HAM solutions for flow in the regime of stagnation point. Hayat et al. [16] observed the 3D fluid motion by considering upper convected Maxwell model. Authors have discussed mixed convection with magnetic field and thermal-diffusion. Time dependent flow of the second order viscoelastic fluid model has been analyzed by Saleem et al. [17]. They have analyzed the reaction and heat immersion effects and thus calculated the analytical results. Freidoonimehr et al. [18] calculated simultaneous heat-mass transfer properties for steady, laminar, incompressible and MHD stagnation point flow. Experts have applied differential transform method together with Pade approximation to evaluate analytical results. Computed results seem to be in good agreement with the results obtained by fourth order Runge-Kutte method and already published results. Rashidi et al. [19] described the analytical and numerical results by considering the combined heat and mass transfer phenomenon. Study has been presented in the nanofluid regime from a nonlinear stretching

porous sheet. Authors have compared current HAM results with numeric consequences attained by shooting method. Furthermore, Rashidi et al. [20] analyzed the generalized the magnetic field effects for the Burger nanofluid model. Homotopy approach is employed to calculate the series solution. Results were calculated under the influence of sundr5y parameters and compared with those of already published results. Ariel [21] described the 3D flow for the steady, laminar, incompressible viscous fluid model. Analytical results were obtained via homotopy perturbation method and seem to be in good correlation with exact solutions which are already present in literature. Singh [22] investigated the 3D unsteady, incompressible flow of Newtonian model. Analysts calculated the results by using perturbation technique to visualize momentum profile, isotherms and isolines. Further, researchers discussed two cases, viz. heating case (Gr < 0) and cooling case (Gr > 0). Xu et al. [23] investigated the series solutions of the 3D unsteady natural convective flow in the stagnation point region. Mookum et al. [24] described the numerical calculations for the 3D flow. Asako and Faghri [25] evaluated three dimensional heat transfer problem in the entrance regime of rhombic duct. Zhao et al. [26] evaluated the BL nanofluid rheology. HAM has been utilized to calculate solutions and also discuss the influence of involved physical parameters. Ramzan et al. [27] investigated 3D motion of the Oldroyd-B fluid by considering Newtonian heating. Awais et al. [28] have taken the 3D Maxwell fluid model flowing on the stretching surface for the investigation. Authors have used 3-stage Lobatto IIIA formula for the analysis. Jamil et al. [29] studied the unsteady helical flows of Olroyd-B fluid through finite Hankel transforms. Hayat and Alsaedi [30] examined radiation, thermophoresis and Joul heating properties for the Oldroyd-B fluid model. Experts have also considered the influence of magneto hydrodynamics and evaluated the analytical results via homotopy analysis method. Ibrahim [31] examined the influence of magnetic effect and convective wall conditions on MHD flow. Analyst has taken the Maxwell fluid model in the existence of nanoparticles. Finally, shooting procedure has been employed to evaluate numerical calculations. Hayat and Awais [32] discussed the effects of heat along with mass transfer for the 2D second grade fluid. Scientists have considered Soret and Dufour properties and have solved the physical problem by HAM. Later, Hayat et al. [33] examined Sorat and Dufaur's effects for the 3D flow along the stretched surface. Rashidi et al. [34] evaluated approximate solutions for viscoelastic fluid on a moving stretching surface. Scientists have well taken the influence of MHD and computed the

results through homotopy analysis method. Nadeem et al. [35] explored three dimensional water-based nanofluid flowing on the stretching surface. Experts have computed the numerical results via fourth order RK technique. Alsaedi [36] examined three dimensional viscoelastic fluid flowing on an exponentially stretched surface. Mahmoud and Megahed [37] discussed the influence of viscous dissipation and heat generation/absorption of a non-Newtonian fluid. Fluid is assumed to flow on the porous flat plate and the analytic results have been calculated. Hammad and Ferdows [38] evaluated the similarity solutions for the stagnation-point flow along heated permeable sheet. Lie group analysis has been performed to demonstrate velocity profile, isotherms and isolines. Also, influence of heat immersion on flow has been examined by Alsaedi et al. [39]. Awais et al. [40] accomplished heat transfer investigation by considering third grade nanofluid. Hayat et al. [41] described convection flow for the Burger's fluid model. Effects of stratification and heat immersion are shown and finally convergent results have been evaluated for nonlinear coupled equations. Choi [42] has presented an extensive study on flow with nanoparticles. Makinde and Aziz [43] examined numerically BL flow along a stretched wall. Computed results have been displayed in graphical and tabular form to visualize the influence of considered variables on temperature and nanoparticle concentration. Also, Nadeem and Lee [44] investigated boundary layer flows along exponentially stretching sheet. Moreover, experts plotted *h*-curves to obtain convergence of the analytical results. Sheikholeslami et al. [45] investigated forced convected heat transfer problem with variable magnetic field. Further, Sheikholeslami and Ellahi [46] presented three dimensional analysis of natural convective flow of nanofluid. Dalir [47] numerically investigated heat transfer problem of a Jeffrey fluid. Cattaneo [48] initially investigated Cattaneo Christov fluid. Christov [49] studied generalization of Fourier law which is Maxwell Cattaneo model according to frame indifferent formulations. Tibullo and Zampoli [50] extend studies of Christov mentioned in ref. [49] for incompressible fluids and presented a unique solution. Haddad [51] examined thermal instability in a flow in porous media. In this study, scientist has considered Cattaneo-Christov theory in the governing equations for the flow field. Han et al. [52] have taken viscoelastic fluid while incorporating generalized heat flux. Hayat et al. [53] studied the 2D flow of Oldroyd –B fluid and included CC heat flux effects. Researchers have considered the influence of magneto-hydrodynamics with homogeneous-heterogeneous reactions and derived the series solution. Ali et al. [54] extend

7

studies for the Cattaneo-Christov heat flux by adding thermal radiation effects. Extensive studies related to Cattaneo-Christov theory have been done by the scientists and engineers mentioned in Ref. [55-60]. Ganji et al. [61] considered the 3D flow of Walter's B fluid in a vertical channel. Analysts considered the influences of viscoelasticity and inertia and examined the accuracy of VIM, ADM and HPM in solving coupled equations. Outcomes attained are in settlement with the exact results and thus displayed in tabular form. Also, Ganji et al. [62] considered MHD squeezing flow between two parallel disks. Scientists employed HAM and HPM to obtain analytic results and investigated the influence of Reynold number, magnetic number and blowing parameter. Awais et al. [63] studied unsteady 3D incompressible flow of Maxwell fluid. Series solution has been calculated via homotopy analysis method. Extensive studies for the Oldroyd B fluid has been done by the scientists in recent years for heat transfer problems in two as well as three dimensions described in Ref. [64-73].

1.2 Description of conservation laws

Conservation laws are given by

1.2.1 Continuity equation

Mathematical expression for the conservation of mass is stated as:

$$\frac{\partial \rho}{\partial t} + \nabla \cdot (\rho V) = 0. \tag{1.1}$$

For incompressible fluids

$$\nabla \cdot V = 0. \tag{1.2}$$

1.2.2 Equation of fluid motion

The mathematical form is given by

$$\rho \frac{dV}{dt} = \nabla \cdot \tau + \rho b, \tag{1.3}$$

where

$$\tau = \begin{vmatrix} \sigma_{xx} & \tau_{xy} & \tau_{xz} \\ \tau_{yx} & \sigma_{yy} & \tau_{yz} \\ \tau_{zx} & \tau_{zy} & \sigma_{zz} \end{vmatrix}. \tag{1.4}$$

Note that τ is

$$\tau = -pI + S. \tag{1.5}$$

Equation of motion become

$$\rho \frac{dV}{dt} = \nabla \cdot \tau. \tag{1.6}$$

Component forms of the above equation are

$$\rho \frac{du}{dt} = \frac{\partial(\sigma_{xx})}{\partial x} + \frac{\partial(\tau_{xy})}{\partial y} + \frac{\partial(\tau_{xz})}{\partial z},$$

$$\rho \frac{dv}{dt} = \frac{\partial(\tau_{yx})}{\partial x} + \frac{\partial(\sigma_{yy})}{\partial y} + \frac{\partial(\tau_{yz})}{\partial z}, \tag{1.7}$$

$$\rho \frac{dw}{dt} = \frac{\partial(\tau_{zx})}{\partial x} + \frac{\partial(\tau_{zy})}{\partial y} + \frac{\partial(\sigma_{zz})}{\partial z}.$$

1.2.3 Law of energy conservation

This law states that

$$\frac{\partial T}{\partial t} + V \cdot \nabla T = \alpha \nabla^2 T - \frac{1}{\rho c_p} \nabla q_r, \tag{1.8}$$

where q_r is radiative flux which is stated mathematically as

$$q_r - \frac{4\sigma}{3\alpha_R} \nabla(n^2 T^4). \tag{1.9}$$

1.2.4 Mass transfer equation

This equation is given by:

$$\frac{\partial C}{\partial t} + V \cdot \nabla C = D \nabla^2 C, \tag{1.10}$$

where C symbolizes species concentration and D represents the diffusion constant

1.3 Constitutive relations of stress tensors

The constitutive relations of stress tensors for different fluid models are given by

1.3.1 Newtonian model

The generalized tensor is

$$\tau' = -p\mathbf{I} + \mathbf{S}', \tag{1.11}$$

where extra stress tensor $\mathbf{S}'$ for Newtonian model is given by

$$\mathbf{S}' = \mu\mathbf{A}_1, \ \mu \geq 0,$$

in which the first RE tensor $\mathbf{A}_1$

$$\mathbf{A}_1 = \nabla\mathbf{V} + (\nabla\mathbf{V})^{transpose}.$$

1.3.2 Maxwell model

The tensor $\mathbf{S}'$ for an upper-convected Maxwell (UCM) model satisfies:

$$\left(1 + \lambda_1 \frac{D}{Dt}\right)\mathbf{S}' = \mu\mathbf{A}_1, \tag{1.12}$$

where λ_1 is relaxation effect and the expression for D/Dt is given by [1]

$$\frac{Da_i}{Dt} = \frac{\partial a_i}{\partial t} + u_r a_{i,r} - u_{i,r} a_r. \tag{1.13}$$

1.3.3 Oldroyd-B fluid model

For Oldroyd-B fluid model, the extra stress tensor satisfies

$$\left(1 + \lambda_1 \frac{D}{Dt}\right)\mathbf{S} = \mu\left(1 + \lambda_2 \frac{D}{Dt}\right)\mathbf{A}_1. \tag{1.14}$$

1.3.4 Jeffery fluid model

Expression of tensor in Jeffery model is

$$\mathbf{S} = \frac{\mu}{1+\lambda^*}\left(\mathbf{A}_1 + \frac{d\mathbf{A}_1}{dt}\right).$$

(1.15)

1.4 Additional forces and source terms

1.4.1 Magnetic field

The additional term in the equation of motion corresponds to the hydro magnetic flow situation is given by

$$\mathbf{F}_m = \mathbf{J} \times \mathbf{B},$$

(1.16)

$$\mathbf{J} = \sigma\left(\mathbf{E} + \mathbf{V} \times \mathbf{B}\right),$$

(1.17)

where

$$\mathbf{B} = B_0 + b.$$

After simplifications we get

$$\mathbf{F}_m = -\sigma B_0^2 \mathbf{V}.$$

(1.18)

1.4.2 Internal heat generation/absorption

The extra terms corresponds to the internal heat immersion is $\dfrac{Q_0}{\rho c_p}\left(T - T_\infty\right).$

1.4.3 Nanofluids

The extra terms representing the effects of nanofluid are given by

$$A_1 = \tau\left(D_B\frac{\partial C}{\partial y}\frac{\partial T}{\partial y} + \frac{D_T}{T_\infty}\left(\frac{\partial T}{\partial y}\right)^2\right),$$

$$A_2 = \frac{D_T}{T_\infty}\frac{\partial^2 T}{\partial y^2},$$

in which D_B represents the Brownian motion and D_T represents the thermophoresis phenomenon.

1.5 Methodology

It is analyzed through literature survey that differential systems for the Rate type non-Newtonian fluids are non-linear and complex. Such nonlinearity is more complicated when the generalized rate type fluid model are considered. For the computation of nonlinear coupled set of equations, we employed numerical techniques, namely shooting technique together with Newton Raphson method and finite difference method. To compute results analytically, we apply an effectual analytical approach namely HAM.

1.5.1 Shooting method

Shooting technique is a numerical iterative scheme used for the numerical calculations of the system. This iterative approach is applicable only on the first order initial value problem. In this technique missing initial slope at the initial (starting) interval point is supposed and then we calculate the differential equation together with initial condition. The precision of anticipated initial condition is tested by relating the calculated value of the dependent variable at the final point. If they are in good agreement then it's the solution of IVP, otherwise we continue this process by taking other value for the missing condition. These steps are repeated until the accuracy is achieved.

Solution procedure

Consider a differential equation of second order

$$\frac{d^2u}{dv^2} = f\left(u, v, \frac{du}{dv}\right). \tag{1.21}$$

The suitable wall conditions are

$$u(0) = 0 \quad \text{and} \quad u(L) = A. \tag{1.22}$$

We rewrite Eq. 1.21 in the group of two equations of first order

$$\frac{du}{dv} = w, \frac{dw}{dv} = f(u, v, w). \tag{1.23}$$

The missing initial condition is

$$\frac{du(0)}{dv} = s \quad \text{or} \quad w(0) = s. \tag{1.24}$$

13

So need to calculate "s" such that the system of ODEs satisfy the boundary condition at the second point. We can compute "s" such that:

$$u(L,s) - A = \phi(s) = 0.$$ (1.25)

By using Newton Raphson method

$$s^{(n+1)} = s^n - \frac{\phi(s^n)}{d\phi(s^n)\big/ds}.$$ (1.26)

Using above equations

$$s^{(n+1)} = s^n - \frac{y(L,s^n) - A}{\partial y(L,s^n)\big/\partial s}.$$ (1.27)

Differentiated w.r.t. s to achieve derivative of (u) with s, we have

$$\frac{dU}{dv} = W \quad \text{and} \quad \frac{dU}{dv} = \frac{\partial f}{\partial u}U + \frac{\partial f}{\partial v}V,$$ (1.28)

$$U(0) = 0 \quad \text{and} \quad W(0) = 1,$$ (1.29)

where

$$U = \frac{\partial u}{\partial s}, W = \frac{\partial w}{\partial s}.$$ (1.30)

The solution is achieved by going through following steps

1. Suppose value for s, and $s^{(1)}$ denotes the approximate value of s.
2. Solve an IVP from $x = 0$ - L.
3. Results obtained from the above step will be utilized to get

$$s^{(2)} = s^1 - \frac{y(L,s^1) - A}{Y(L,s^1)}.$$

4. Repeat the process until precision is achieved.

14

1.5.2 Finite difference technique

FDM is efficient process for the computation of BL problems. In this technique, we discretize the set of partial differential equations by replacing the differentials with the difference quotients which in result yields nonlinear algebraic equations.

Solution procedure

To achieve a numerical solution for the system of differential equations, we replace continuous variables by discrete variables. We accomplish this process by reforming the given set of equations in algebraic form by substituting differentials with difference quotients. Let we have continuous function $u(x)$. Divide x-axis on the finite no of intervals with uniform grid size $\Delta(x)$. At any three consecutive points x_{n-1}, x_n and x_{n+1}, the value of function $u(x)$ are u_{n-1}, u_n and u_{n+1}. u_{n+1} and u_{n-1} can be written in terms of u_n and $\Delta(x)$ by using Taylor series.

$$u_{n+1} = u_n + \frac{du}{dx}\Delta x + \frac{d^2u}{dx^2}\frac{(\Delta x)^2}{2!} + ... , \tag{1.31}$$

$$u_{n-1} = u_n - \frac{du}{dx}\Delta x + \frac{d^2u}{dx^2}\frac{(\Delta x)^2}{2!} - .... \tag{1.32}$$

Difference quotients for the 1st order differential terms are

Forward difference

Mathematical representation for the Forward difference of the ist-order derivatives can be obtained by using Eq. 1.31.

$$\frac{du}{dx} = \frac{u_{n+1} - u_n}{\Delta x}. \tag{1.33}$$

Backward difference

Using Eq. 1.32, we get

$$\frac{du}{dx} = \frac{u_n - u_{n-1}}{\Delta x}. \tag{1.34}$$

Central difference

15

To get central difference analogue for 1st order differentials, we subtract Eq.1.31 from Eq. 1.32.

$$\frac{du}{dx} = \frac{u_{n+1} - u_{n-1}}{2\Delta x}.$$

(1.35)

Finite difference analogue for the second order derivative terms are obtained by adding Eq. 1.31 and Eq. 1.32.

$$\frac{d^2 u}{dx^2} = \frac{u_{n+1} - 2u_n + u_{n-1}}{(\Delta x)^2}.$$

(1.36)

Similarly difference quotient for the third order derivatives is

$$\frac{d^3 u}{dx^3} = \frac{u_{n+2} - 2u_{n+1} + 2u_{n-1} - u_{n-2}}{2(\Delta x)^3}.$$

(1.37)

Using above equations in differential equations, we get nonlinear equations. Thomas algorithm is best applicable to the set of algebraic equations if they are tri-diagonal because they occupy less space.

1.5.3 Homotopy approach

This is efficient technique and researchers are employing this technique for the series solution of differential systems. We can say regarding this technique that

- HAM does not need small or large parameters. The auxiliary operator is presented to make the deformation equation of zeroth order.

- It should be noted that auxiliary operator "h", auxiliary function "$H(t)$", initial operator "L" and initial guess "$V_0(t)$"can be independently chosen.

- Convergence regime can efficiently be controlled and approximation rate for calculating the series solution is adjustable.

- Different set of base functions can be selected while implementing this approach.

Chapter 2

Analysis of UCM fluid with diffusion effects: Dual numerical results

In this chapter, we have analyzed the properties of heat immersion and reaction phenomenon in a fluid flow under magnetic effects. Characteristics of the UCM fluid model have been taken in the spongy medium to examine the absorbent effects. Diffusion equations are used to measure out the heat as well as mass transfer effects. Set of ODEs are numerically computed by using shooting technique. It is being practically examined that dual solutions occur for the flow above shrinking wall and a single solution in case of stretching surface. Properties of Deborah number, heat and mass transfer and heat immerion have been visualized graphically. Results have also been depicted in the tables to describe the dual results for skin friction, Nusselt and Sherwood number.

2.1 Construction of the equations

Consider the UCM fluid flow over a permeable wall in order to study the suction-blowing properties. The flows in the porous medium $y > 0$ is considered as revealed in the Fig. 2.1.
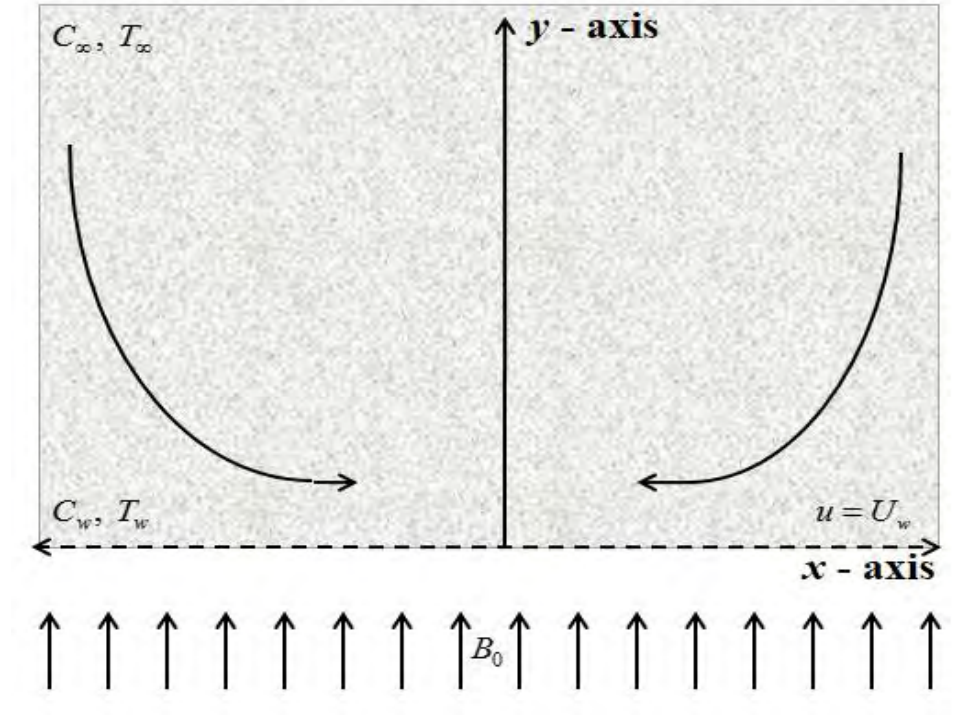
Fig. 2.1: Plan.

Mathematical model for the rheological system is

$$\frac{\partial u}{\partial x} + \frac{\partial u}{\partial y} = 0, \tag{2.1}$$

$$u\frac{\partial u}{\partial x} + v\frac{\partial u}{\partial y} + \lambda\left(u^2\frac{\partial^2 u}{\partial x^2} + v^2\frac{\partial^2 u}{\partial y^2} + 2uv\frac{\partial^2 u}{\partial x\partial y}\right) = v\frac{\partial^2 u}{\partial y^2} - \frac{\sigma B_0^2}{\rho}\left(u + \lambda v\frac{\partial u}{\partial y}\right)$$
$$-\frac{v}{k}\left(u + \lambda v\frac{\partial u}{\partial y}\right), \tag{2.2}$$

$$u\frac{\partial T}{\partial x} + v\frac{\partial T}{\partial y} = \alpha_m\frac{\partial^2 T}{\partial y^2} + \frac{Q}{\rho c_p}(T - T_\infty), \tag{2.3}$$

$$u\frac{\partial C}{\partial x} + v\frac{\partial C}{\partial y} = D\frac{\partial^2 C}{\partial y^2} - K_1 C. \tag{2.4}$$

Wall properties are of the form:

$$u = U_w, \; v = V_w, \; T = T_w, \; C = C_w \qquad \text{at} \quad y = 0,$$
$$u \to 0, \; T = T_\infty, \; C = C_\infty \qquad \text{as} \quad y \to \infty. \tag{2.5}$$

18

In the given set of equations $U_w = -cx$ signifies the shrinking velocity and V_w is suction-blowing parameter. Notice that the suction effect arises when $V_w < 0$ and $V_w > 0$ relates to blowing condition. The stream function ψ with transformations are presented

$$\psi = \sqrt{cv}\,xf(\eta), \ \eta = \sqrt{\frac{c}{v}}y, \ \theta(\eta) = \frac{T - T_\infty}{T_w - T_\infty}, \ \phi(\eta) = \frac{C - C_\infty}{C_w - C_\infty}. \tag{2.6}$$

Applying the above set of variables we get

$$f''' - (f')^2 + ff'' + \beta\left(2ff'f'' - f^2 f'''\right) + M^2\beta ff'' - M^2 f' - Kf' + K\beta ff'' = 0, \tag{2.7}$$

$$\theta'' + \Pr f\theta' + \Pr \lambda_1 \theta = 0, \tag{2.8}$$

$$\phi'' + \mathrm{Sc}\, f\phi' - \mathrm{Sc}\gamma\phi = 0. \tag{2.9}$$

The boundary conditions thus arises to be

$$f(0) = S, \ f'(0) = -1, \ \theta(0) = 1, \ \phi(0) = 1,$$
$$f'(\infty) = 0, \ \theta(\infty) = 0, \ \phi(\infty) = 0. \tag{2.10}$$

Mathematically

$$\beta = \lambda c, M^2 = \frac{\sigma B_0^2}{c\rho}, K = \frac{v}{kc}, \Pr = \frac{v}{\alpha_m}, \lambda_1 = \frac{Q}{c\rho c_p}, \mathrm{Sc} = \frac{v}{D}, \gamma = \frac{K_1}{c}, S = \frac{-V_w}{\sqrt{vc}}. \tag{2.11}$$

Physical quantities being discussed are Nu_x and Sh. These quantities are represented mathematically as

$$Nu_x / \mathrm{Re}_x^{1/2} = -\theta'(0), \mathrm{Sh}/ \mathrm{Re}_x^{1/2} = -\phi'(0). \tag{2.12}$$

19

2.2 Computational technique and results

Nonlinear coupled partial differential equations mentioned in Eqs. (2.7-2.9) are computed numerically by using boundary condition revealed in Eq. 2.10. To apply shooting technique, we apply RK method together with NR method. To calculate results numerically following variables are defined as:

$$p' = q, \quad q' = \frac{p^2 - fq - 2\beta fpq - \beta M^2 fq - \beta K_1 fq + M^2 p + K_1 p}{1 - \beta f^2},$$

$$\theta' = z, \quad \theta_1' = -\Pr \lambda_1 \theta - \Pr fz, \tag{2.15}$$

$$\phi' = u, \quad \phi_1' = \mathrm{Sc}\,\gamma\phi - \mathrm{Sc}\,fu,$$

with

$$f(0) = S, \ p(0) = -1, \ \theta(0) = 1, \ \phi(0) = 1, \tag{2.16}$$

However the solutions of $q(0)$, $u(0)$ and $z(0)$ necessarily be calculated to approximate the IVPS represented in Eqs. 2.15 and 2.16. Shooting technique is applied by selecting the suitable initial guess. Grid size is taken to be $h = 0.001$ and numerical calculations are done constantly until the tolerance of 0.00001 is accomplished. Above Eqs. 2.15 and 2.16 have physical parameters magnetic effects, Deborah number, permeability, Prandtl number, generation-absorption as well as suction-blowing. Therefore we have depicted results graphically to visualize and also we figure out the numerical results in tables. Plots for the Newtonian and UCM fluid are displayed.
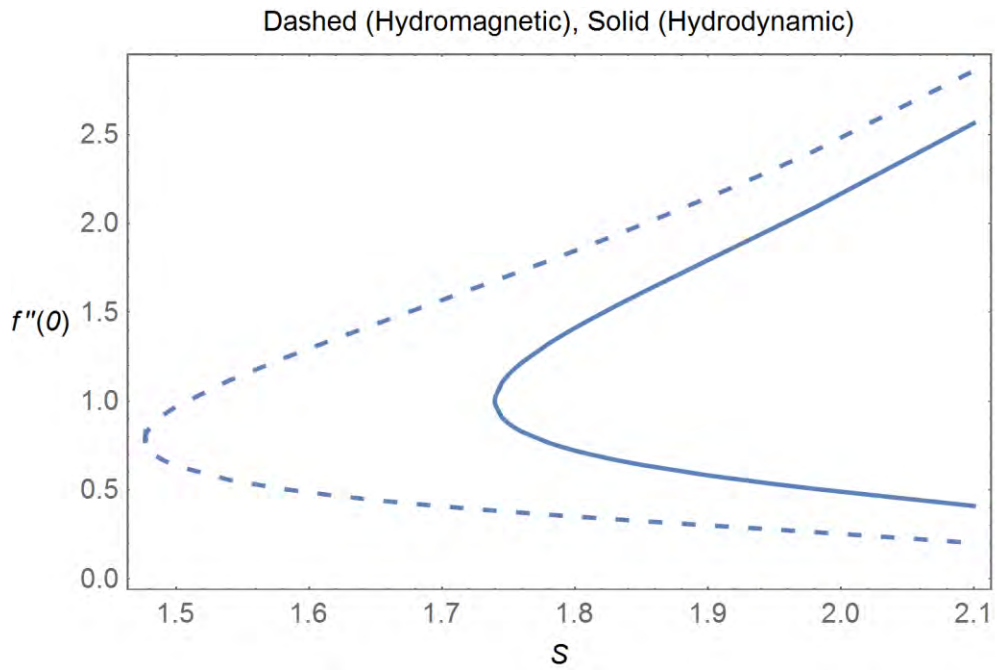
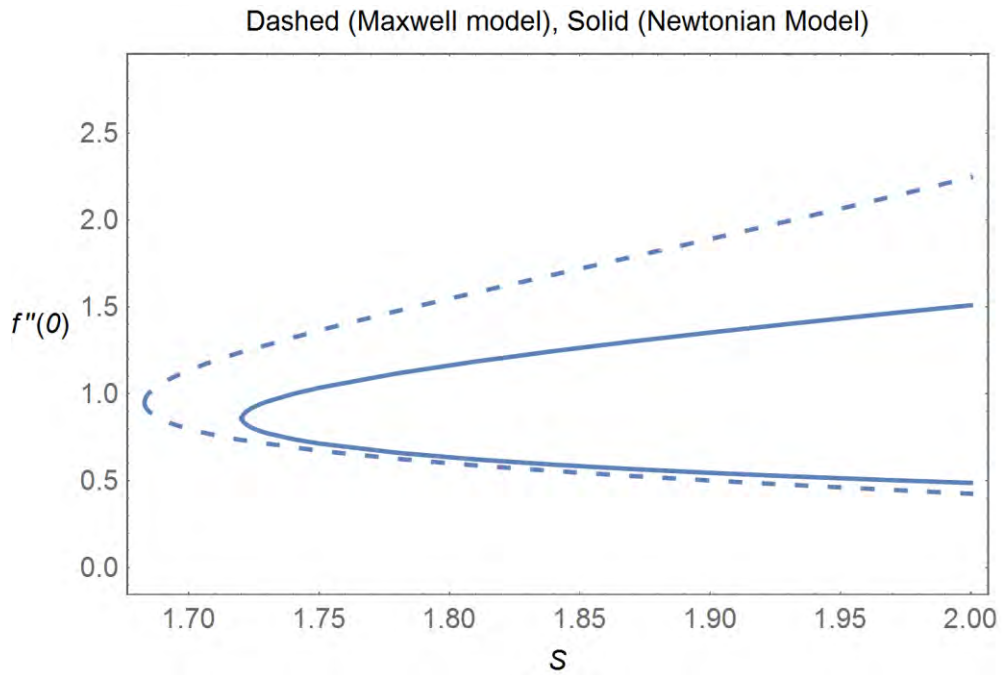Fig. 2.2: Hydromagnetic vs hydro-dynamic cases.

Fig. 2.3: UCM vs Newtonian model.

21

Skin frictions $f''(0)$ for $(M \neq 0)$ and for $(M = 0)$ flow cases are compared and displayed in the Fig. 2.2. It is visualized that the dual solution occurs in case of hydro-dynamic flow for $S > 1.7397$. However, for hydro-magnetic flow the domain rises to $S > 1.4765$. Maxwell and the Newtonian fluid are compared and displayed in Fig. 2.3. The graphs clarify that the dual solution exists in both cases though the domain in case of Maxwell fluid is comparatively greater than that of Newtonian (viscous) model over a shrinking surface.
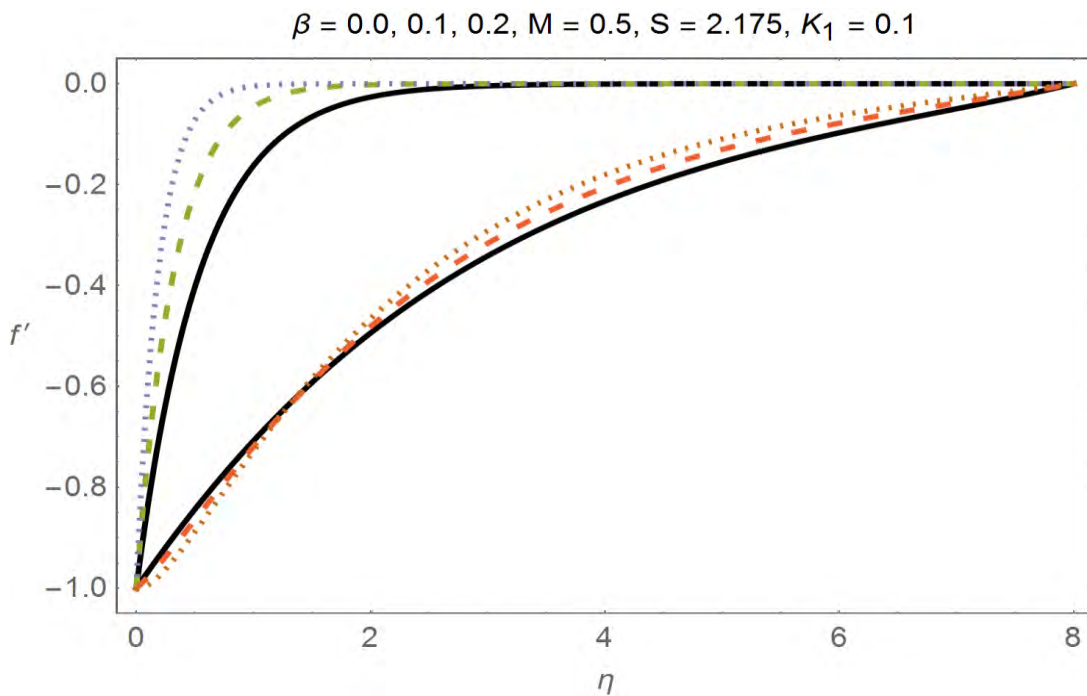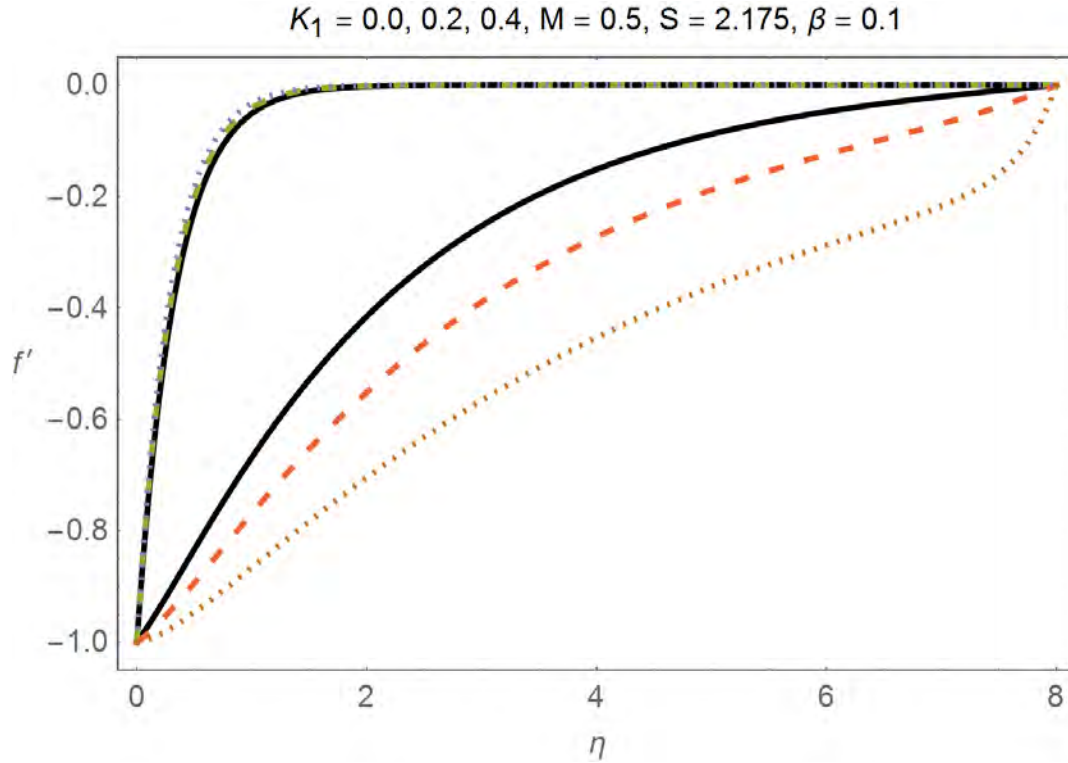

Fig. 2.4: Impact of β on f'.

Fig. 2.5: Impact of K_1 on velocity.

In Fig. 2.4, influence of β on the momentum boundary layer is displayed. It is observed that different solutions occur by changing β. Also, it is noted that flow velocity reduces with Deborah number "β" due to the elastic properties in Maxwell fluid which hinders the motion of fluid particles. Impact of porosity parameter K_1 on the fluid is presented in Fig. 2.5 and it is studied that the dual solution exists for different values of K_1. It is analyzed that the second result is significant when related with the first one. It is noted that changings in the first solution are slightly small for positive values of K_1 while the variations in second solution are acknowledgeable. Dual solutions for the thermal BL are depicted in Fig. 2.6 for various values of Pr and it is thus observed that both solutions are similar. As it is known from literature that Pr is inversely linked with diffusivity and also it is seen from the graphs that isotherms retard by growing the value of Pr. In Fig. 2.7 impact of internal heat generation/absorption is being discussed. It is clarified that temperature rises by raising hs. Effects of S on temperature are

discussed in the Fig. 2.8. It is analyzed that the boundary layer decays for greater S whereas increase in the value of S increases velocity of fluid particles. Thus, it results in higher molecular movement so the temperature reduces. The impact of the suction-blowing phenomenon on the isolines is explained in the Fig. 2.9. From this geometry it is verified that enhancement in the suction-blowing decreases the concentration. It is also noted that increasing S cause a decrease in diffusion.
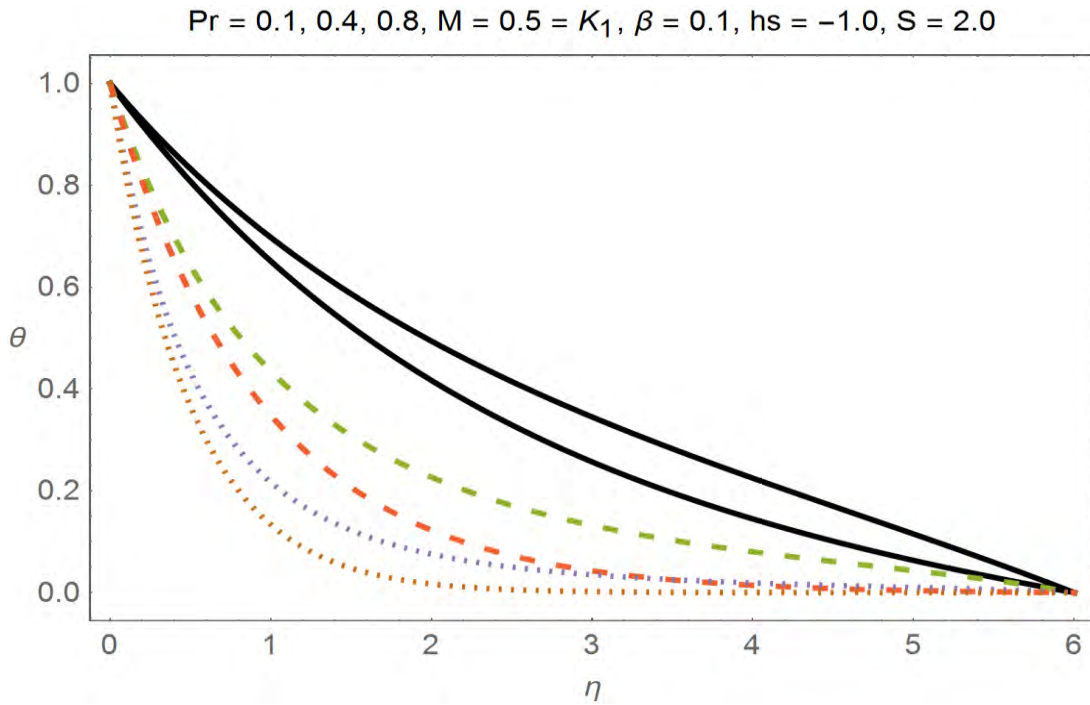

Fig. 2.6: Pr variation against θ.
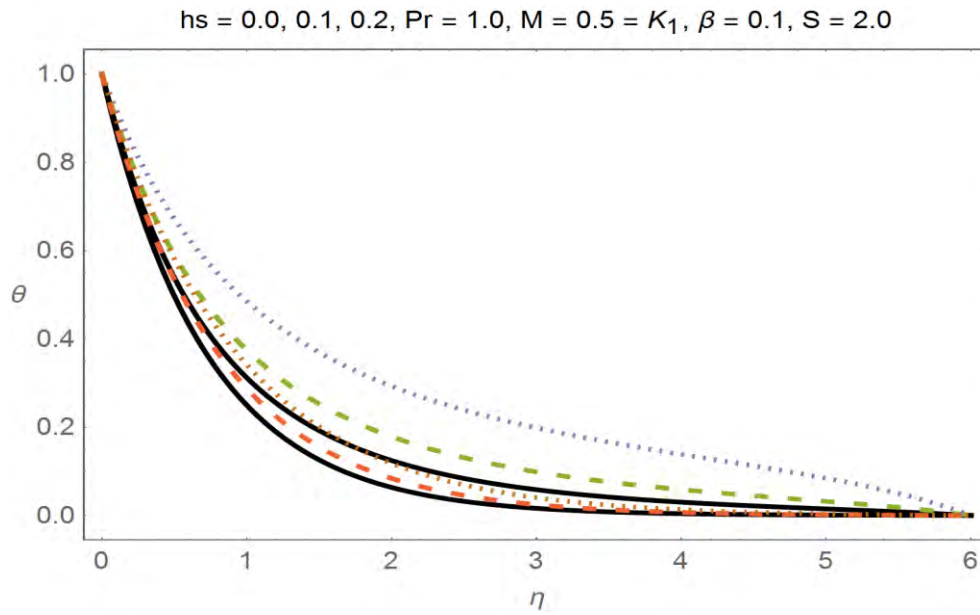
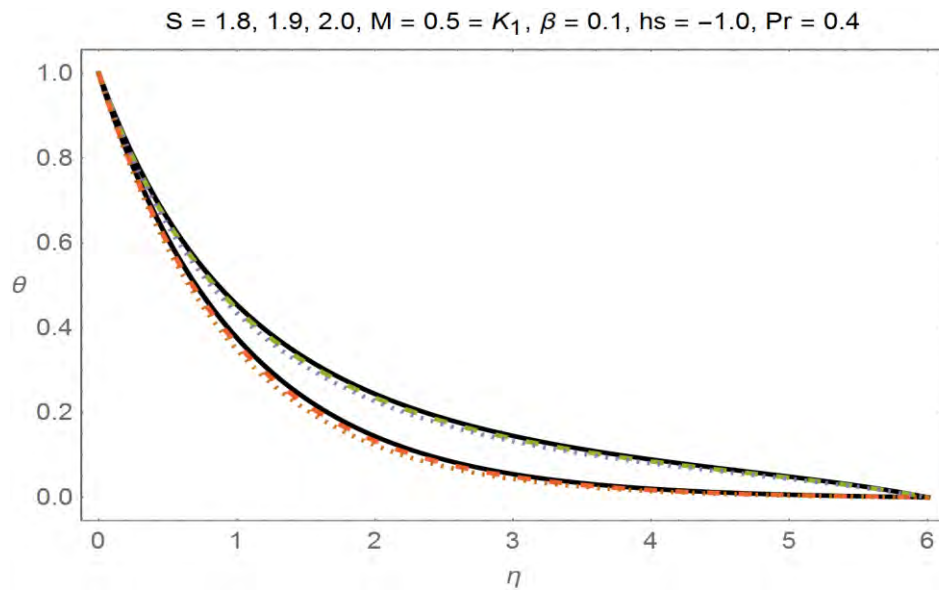Fig. 2.7: hs variations against θ.

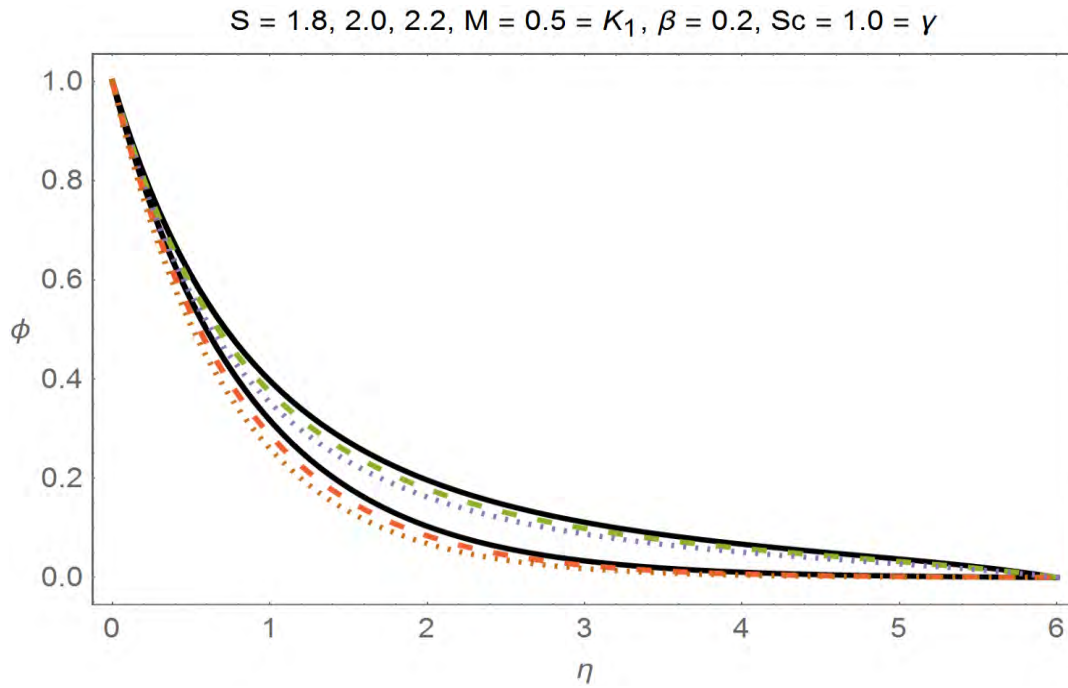Fig. 2.8: Temperature change vs S.

25

Fig. 2.9: *S* variations on concentration.

3D flow configuration is depicted in Fig. 2.10. Here the variation of velocity against the independent variables is shown. It is thus concluded that variation is maximum near the shrinking wall however the ambient values are small.
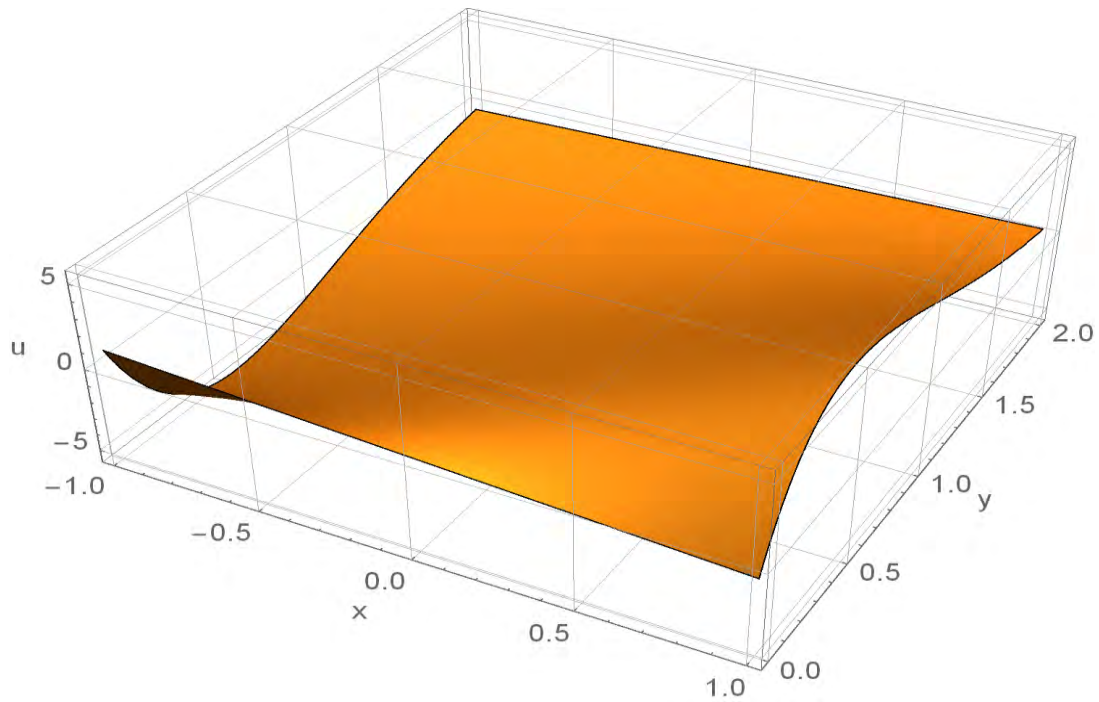
Fig. 2.10: 3D flow configuration.

The numerically computed solution of temperature-diffusion change and wall friction against β, *Pr*, *S*, *M* and *hs* have shown in the Tables (2.1-2.3). The dual results for C_f, *Nu* and *Sh* for different physical parameters are calculated and revealed which explain the characteristics of rheological behavior in computed results.

Table 2.1: Skin friction values: Dual results.

S	β	M	Skin friction $f''(0)$	
1.72	0.0	0.5	0.9555807	0.773768
1.78	0.0	0.5	1.118270	0.661129
1.87	0.0	0.5	1.301370	0.567579
1.93	0.0	0.5	1.402291	0.526234
2.00	0.0	0.5	1.509902	0.487955
1.69	0.2	0.5	1.064382	0.735073
1.87	0.2	0.5	1.788153	0.501723
1.93	0.2	0.5	1.994654	0.447306
2.00	0.2	0.5	2.245862	0.425645
1.74	0.2	0.0	1.022591	0.980014
1.80	0.2	0.0	1.411943	0.721864
1.90	0.2	0.0	1.793495	0.582473
2.10	0.2	0.0	2.563495	0.410476
1.50	0.2	0.5	0.969338	0.636261
1.62	0.2	0.5	1.351365	0.467542
1.74	0.2	0.5	1.678094	0.383745
1.82	0.2	0.5	1.903514	0.361377
1.94	0.2	0.5	2.272523	0.282457
2.10	0.2	0.5	2.85835	0.202462

Table 2.2: Nusselt number values: Dual results.

β	hs	Pr	S	Nusselt number $-\theta'(0)$	
0.0	-1.0	1.0	2.2	1.21553	1.34589
0.1	-1.0	1.0	2.2	1.21191	1.37503
0.2	-1.0	1.0	2.2	1.20607	1.40153
0.1	-1.0	1.0	2.2	1.21191	1.37503
0.1	-0.5	1.0	2.2	0.95584	1.21144
0.1	0.0	1.0	2.2	0.30947	0.99754
0.1	-1.0	0.1	2.2	0.38427	0.44265
0.1	-1.0	0.4	2.2	1.00521	1.15256
0.1	-1.0	0.8	2.2	1.84177	2.04672
0.1	-1.0	0.5	1.8	1.07013	1.19322
0.1	-1.0	0.5	2.0	1.14021	1.28300
0.1	-1.0	0.5	2.2	1.21191	1.37503

Table 2.3: Sherwood number values: Dual solutions.

S	β	M	Sherwood number $-\phi'(0)$	
1.8	0.1	0.5	1.07013	1.19322
2.0	0.1	0.5	1.14021	1.28300
2.2	0.1	0.5	1.21191	1.37503
2.0	0.0	0.5	1.14184	1.26086
2.0	0.1	0.5	1.14021	1.28300
2.0	0.2	0.5	1.13821	1.30013
2.0	0.1	0.0	1.16006	1.27801
2.0	0.1	0.25	1.15464	1.27938
2.0	0.1	0.5	1.14021	1.28300

2.3 Conclusive remarks

This analysis aims to compute numerical results for UCM fluid model. Heat-mass transfer problem is studied with magnetic properties, reaction phenomenon and heat immersion. Numerically calculated results are illustrated in graphs and also shown in tabular form. Conclusive remarks about the present study are

- Dual results occur for the double diffusive flow over shrinking surface.
- Unique (single) solution happens only for stretching surface.
- Momentum boundary layer turn to be thinner as the magnetic field retards the motion of fluid particles.
- Second result is significant as compare to first for the porosity (permeability) effect.
- Suction phenomenon reduces the temperature as well as concentration profiles.

Chapter 3

Magnetic properties in Sakiadis flow of non-Newtonian nanofluid

This chapter reveals the study of Sakiadis flow for nano material with magnetic properties and heat immersion effects. Double diffusivity is briefly examined with thermal radiations. During mathematical modelling, the physical problem is transfigured to the set of PDEs which are further altered to nonlinear ODEs via appropriate transformations. Calculated results are shown in graphs to visualize the effect of involved parameters.

3.1 Mathematical modelling

Combined heat-mass transfer effects with magnetic field in sakiadis flow of UCM nanomaterial is investigated. Flow dynamics in a absorbent medium with convective wall properties have been considered. Conservation laws are

$$\frac{\partial u}{\partial x} + \frac{\partial v}{\partial y} = 0 , \tag{3.1}$$

$$u\frac{\partial u}{\partial x} + v\frac{\partial u}{\partial y} + \lambda\left(u^2\frac{\partial^2 u}{\partial x^2} + v^2\frac{\partial^2 u}{\partial y^2} + 2uv\frac{\partial u}{\partial x\partial y}\right) = v\frac{\partial^2 u}{\partial y^2} - \left(\frac{\sigma B^2_0}{\rho} + \frac{v}{K}\right)\left(u + \lambda v\frac{\partial u}{\partial y}\right), \tag{3.2}$$

$$u\frac{\partial T}{\partial x} + v\frac{\partial T}{\partial y} = -\frac{1}{\rho c_p}\left(\frac{\partial q_r}{\partial y}\right) + \alpha_m\frac{\partial^2 T}{\partial y^2} + \frac{Q_0}{\rho c_p}(T - T_\infty) + \tau\left(D_B\frac{\partial C}{\partial y}\frac{\partial T}{\partial y} + \frac{D_T}{T_\infty}\left(\frac{\partial T}{\partial y}\right)^2\right), \tag{3.3}$$

31

$$u \frac{\partial C}{\partial x} + v \frac{\partial C}{\partial y} = D_B \frac{\partial^2 C}{\partial y^2} + \frac{D_T}{T_\infty} \frac{\partial^2 T}{\partial y^2}, \tag{3.4}$$

The wall conditions are

$$u = U, \ v = 0, \ -k \frac{\partial T}{\partial y} = h_f \left(T_f - T \right), -D \frac{\partial C}{\partial y} = h_c \left(C_f - C \right) \quad \text{at} \quad y = 0,$$

$$u \to 0, \ T \to T_\infty, \ C \to C_\infty \qquad \qquad \text{as} \quad y \to \infty. \tag{3.5}$$

Where q_r is

$$q_r = -(4\sigma^3 / 3k^*) \partial T^4 / \partial y. \tag{3.6}$$

Utilizing

$$\eta = \sqrt{\frac{U}{\nu x}} y, u = Uf', \ v = -\frac{1}{2} \sqrt{\frac{\nu U}{x}} \left(f - \eta f' \right), \ \theta(\eta) = \frac{T - T_\infty}{T_f - T_\infty}, \ \phi(\eta) = \frac{C - C_\infty}{C_f - C_\infty}. \tag{3.7}$$

We get

$$f''' + \frac{1}{2} f f'' - \frac{D_e}{2} \left(2 f f f'' + \eta f'^2 f'' + f^2 f''' \right)$$

$$- M^2 \left(f' - D_e \left(f - \eta f' \right) f'' \right) - K_1 f' + K_1 D_e \left(f f'' - \eta f f'' \right) = 0, \tag{3.8}$$

$$\theta'' + \Pr \left(\frac{1}{2} f \theta' + N_b \theta' \phi' + N_t \theta'^2 + h s \theta \right) + \frac{4}{3} R d \theta'' = 0, \tag{3.9}$$

$$\phi'' + Sc \left(\frac{1}{2} f \phi' \right) + \frac{N_t}{N_b} \theta'' = 0, \tag{3.10}$$

32

along with wall properties

$$f(0) = 0,$$
$$f'(0) = 1,$$
$$\theta'(0) = -\gamma_1\left(1 - \theta(0)\right), \quad \phi'(0) = -\gamma_2\left(1 - \phi(0)\right),$$
$$f'(\infty) \to 0, \quad \theta(\infty) \to 0, \quad \phi(\infty) \to 0.$$

(3.11)

Mathematically

$$M^2 = \frac{\sigma B_0^2}{\rho U},$$

$$Rd = \frac{4\sigma^* T_\infty^3}{kk^*},$$

$$K_1 = \frac{\nu}{KU},$$

$$D_e = \frac{\lambda U}{2x},$$

$$Sc = \frac{\nu}{D_B},$$

$$N_t = \frac{\tau D_T\left(T_f - T_\infty\right)}{\nu T_\infty},$$

$$N_b = \frac{\tau D_B\left(C_f - C_\infty\right)}{\nu},$$

$$\Pr = \frac{\nu}{\alpha_m},$$

$$hs = \frac{Q}{U\rho c_p}.$$

The numerical treatment is computed using finite-difference approach (FDM) as shown in Table 1.

3.2 Solution computations

In this part of chapter, we aim to investigate the impact of physical parameters including Deborah number *De*, heat generation-absorption parameter *hs,* thermophoresis parameter N_t. Further, effect of magnetic field *M*, Biot numbers (γ_1, γ_2) and Brownian motion N_b is also been studied on the velocity, temperature and species concentration. During solution computation errors are evaluated and depicted in Fig. (3.1-3.3). It is observed that errors in the results are quite negligible. It is revealed in Fig 3.4 that Deborah number *De* retards the motion of fluid particles near the boundary. Fig 3.5 reveals the effect of magnetic strength *M*. This geometry clarifies that boundary layer decreases with *M*. From literature, it is studied that apparent viscosity of the fluid increases as the magnetic field is applied on it. Likewise, in Fig 3.6 effect of magnetic field on θ is presented. It is shown that θ increases close to the convective wall. Impact of *hs* on θ is discovered in Fig 3.7. Also for (*hs < 0.0*), the temperature reduces while for (*hs > 0.0*), the temperature rises. Also, thermal slip is observed in both cases because of the convective properties of surface. Influence of γ_1 on the temperature is discussed in the Fig. 3.8. It is witnessed from this picture that temperature increases close to the wall and decreases far from the convective surface. Effects of (N_t, N_b) on θ are exposed in Fig. 3.9. Consequently, it is studied that nanoparticles enhance the temperature. Effect of *M* on the graph of concentration is observed in Fig. 3.10. It is verified that species concentration is in direct relation with magnetic field. Enhancement in the value of *M* gives rise to concentration profile. Impact of Biot number γ_2 on the isolines is displayed in the Fig. 3.11. It is witnessed that the concentration profile in increased near to the convective wall. Influences of (N_t, N_b) on the species mass distribution are portrayed in the Fig. 3.12. It is discovered that ϕ rises by enhancing the thermophoresis and Brownian motion (N_t, N_b).
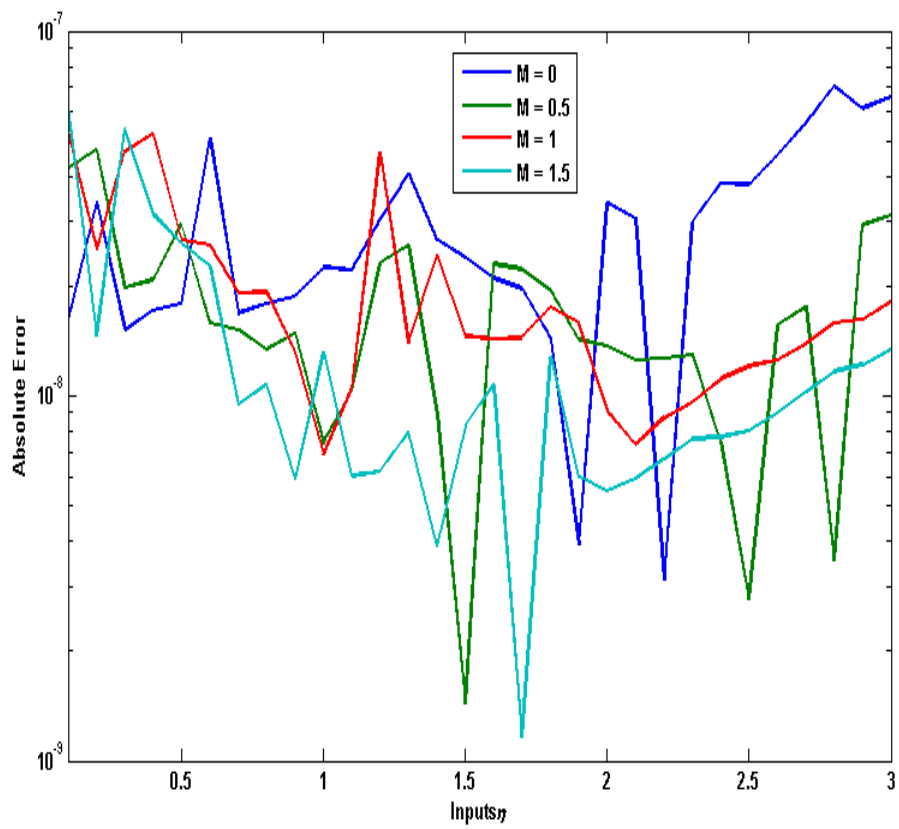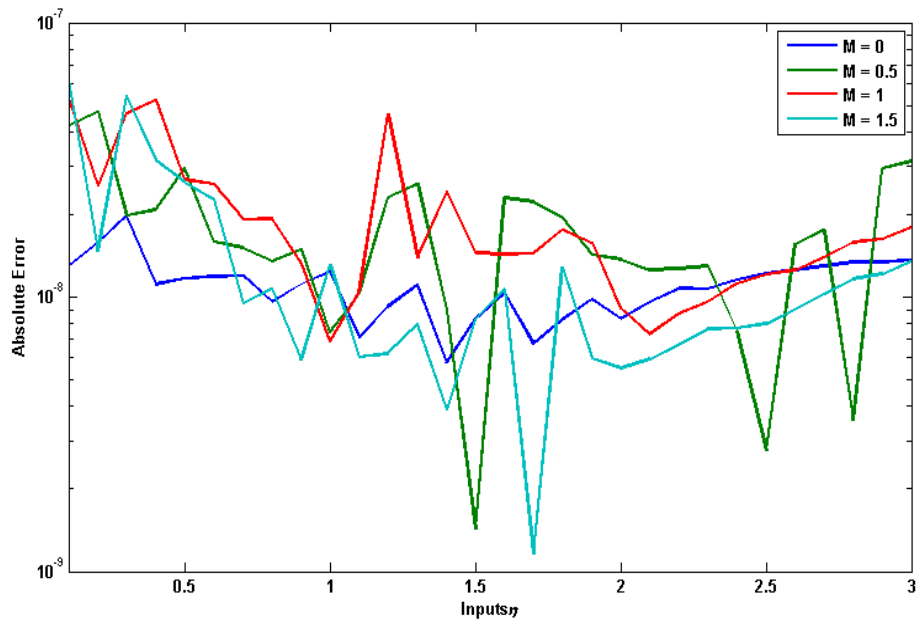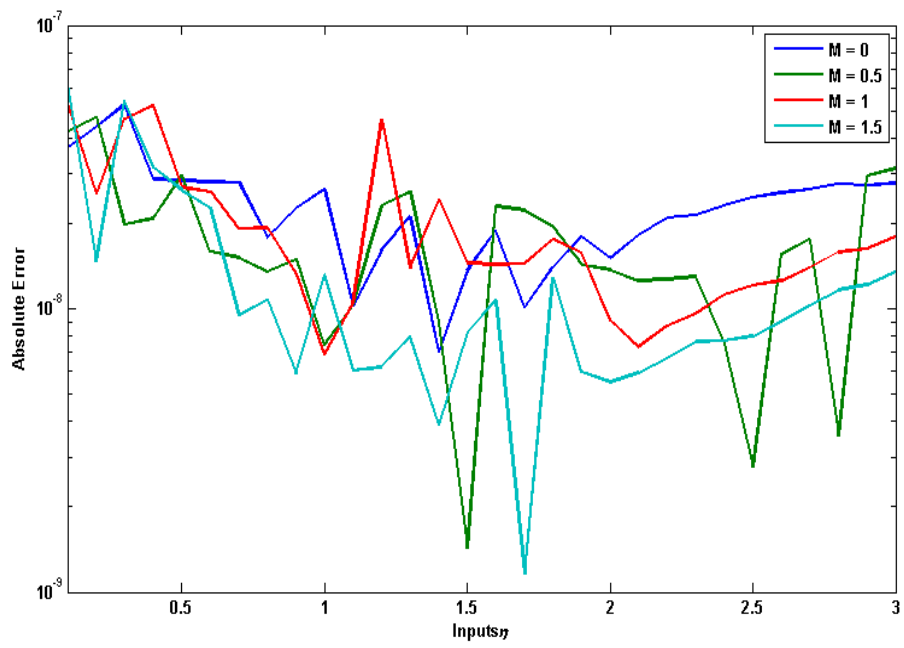
Fig. 3.1: Error in *f*.

Fig. 3.2: Error in θ.
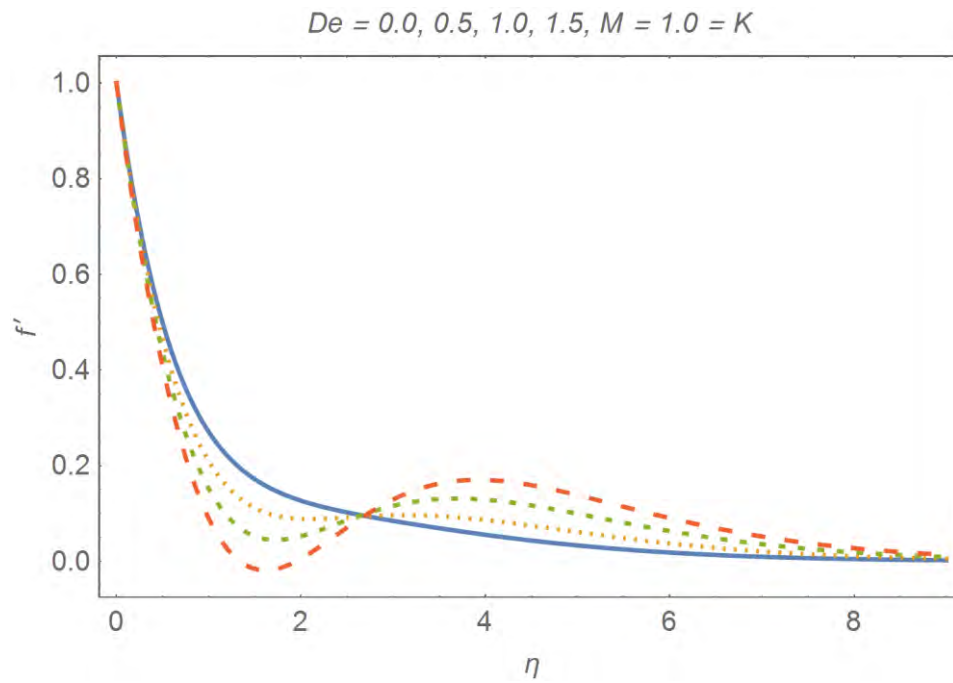

Fig. 3.3: Error in ϕ.

Fig. 3.4: *De* variation on f'.
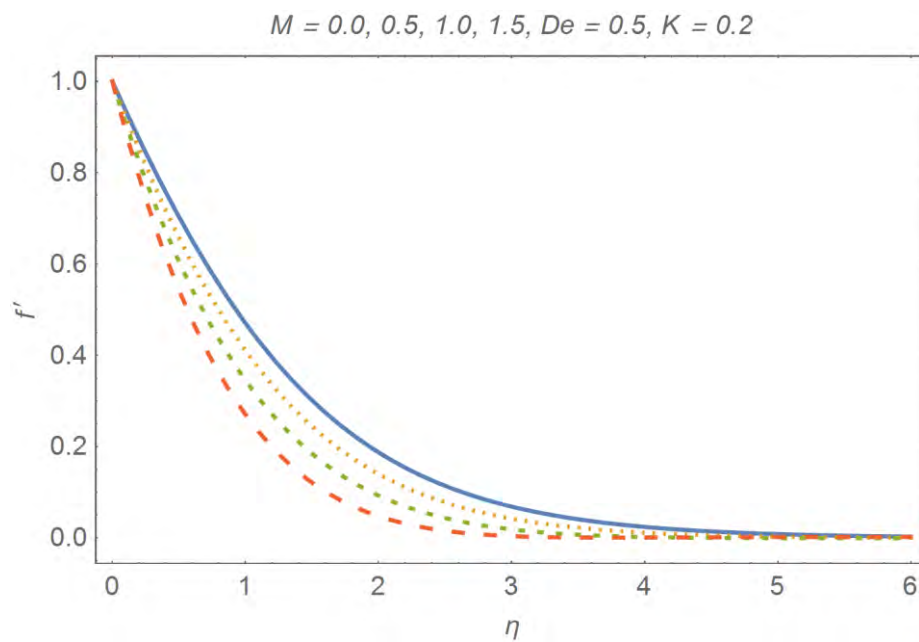
Fig. 3.5: *M* variation on f'.
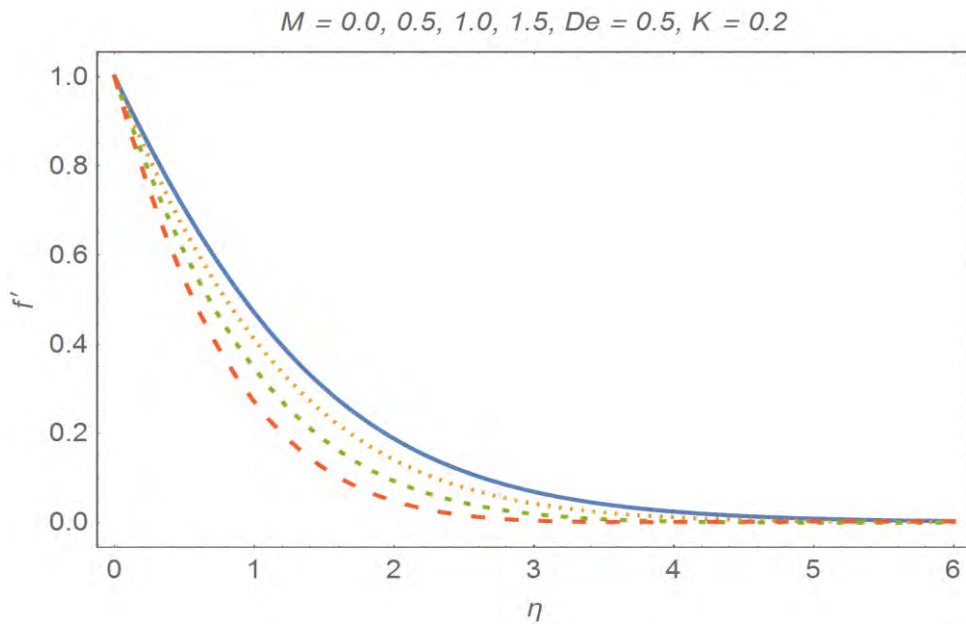
Fig. 3.6: *M* variation on θ.
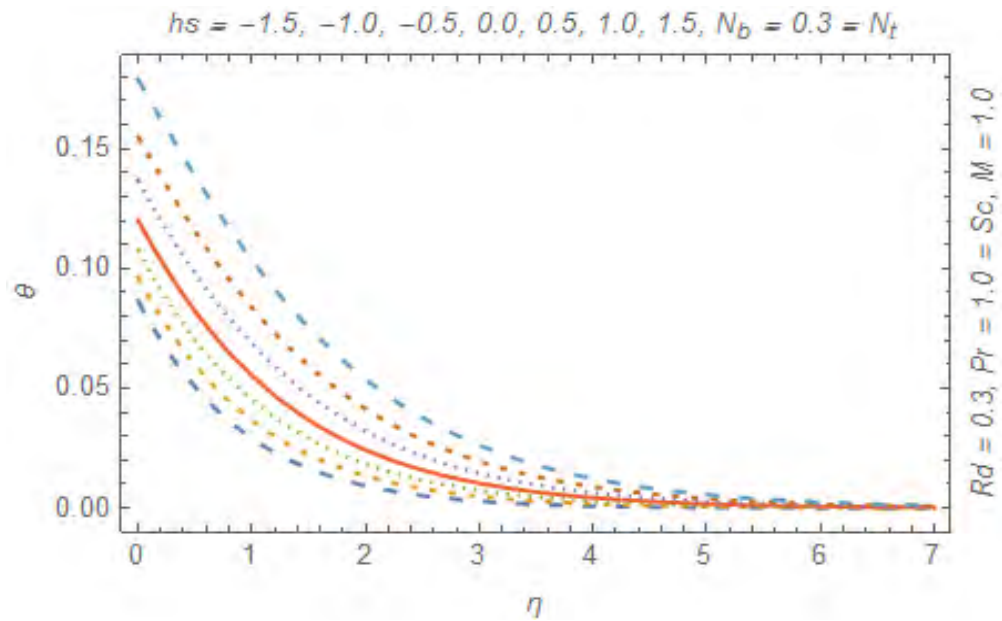
Fig.3.7: *hs* variation on θ.
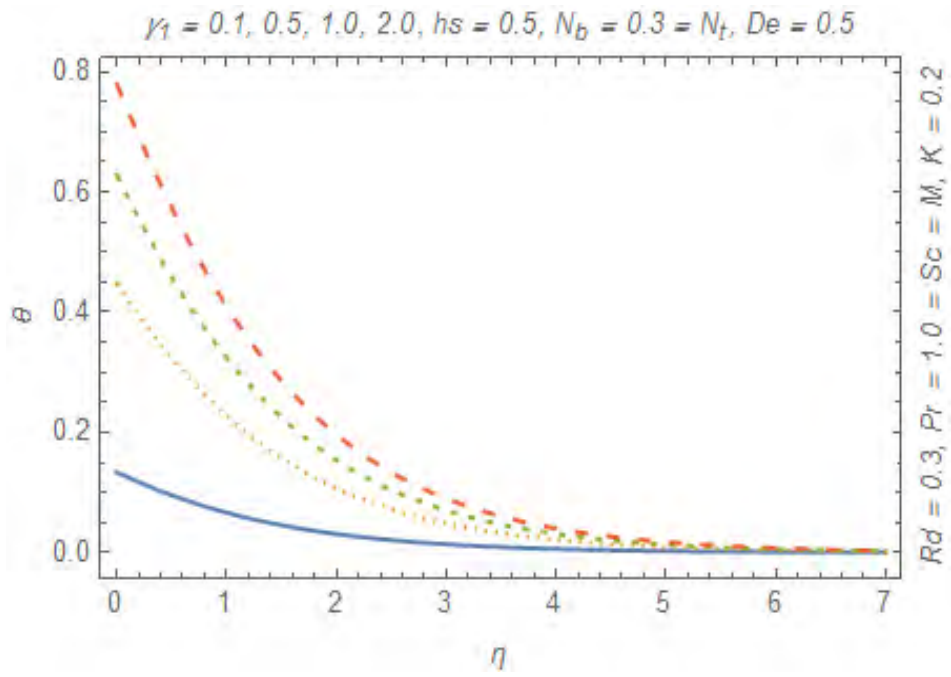
Fig. 3.8: γ_1 variation on θ.

Fig. 3.9: (N_b, N_t) variation on θ.

M = 0.0, 0.6, 1.3, 2.0, De = 0.5, K = 0.2, Pr = 1.0 = Sc

Rd = 0.3, hs = 0.5 = N_t = N_b

Fig. 3.10: *M* variatons on ϕ.

γ_2 = 0.1, 0.3, 0.6, 1.0, N_b = N_t = 0.5, M = 1.0, De = 0.5

Rd = 0.3, hs = 0.5, Pr = 1.0 = Sc
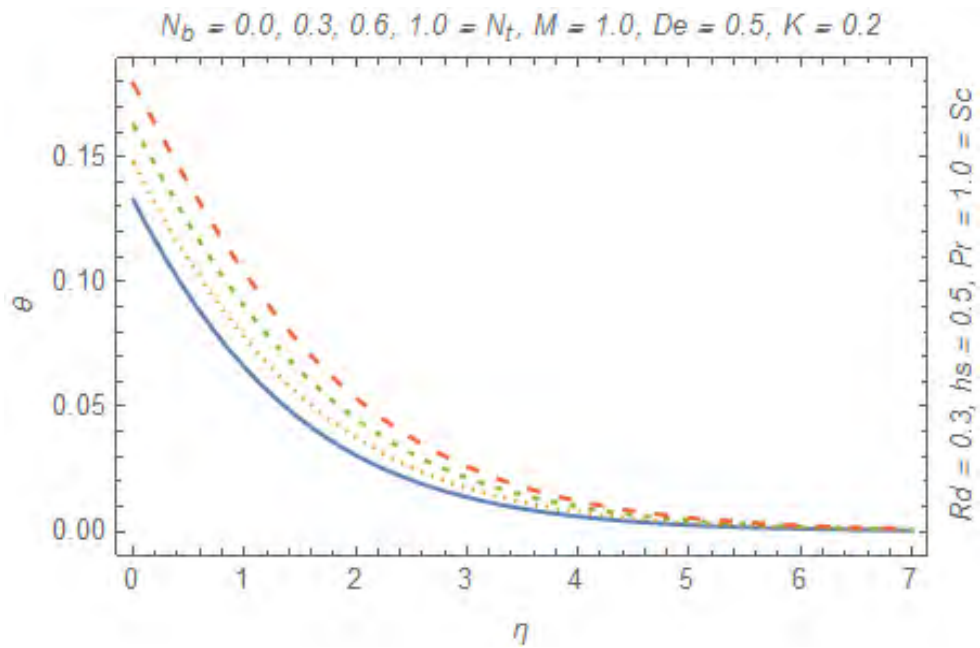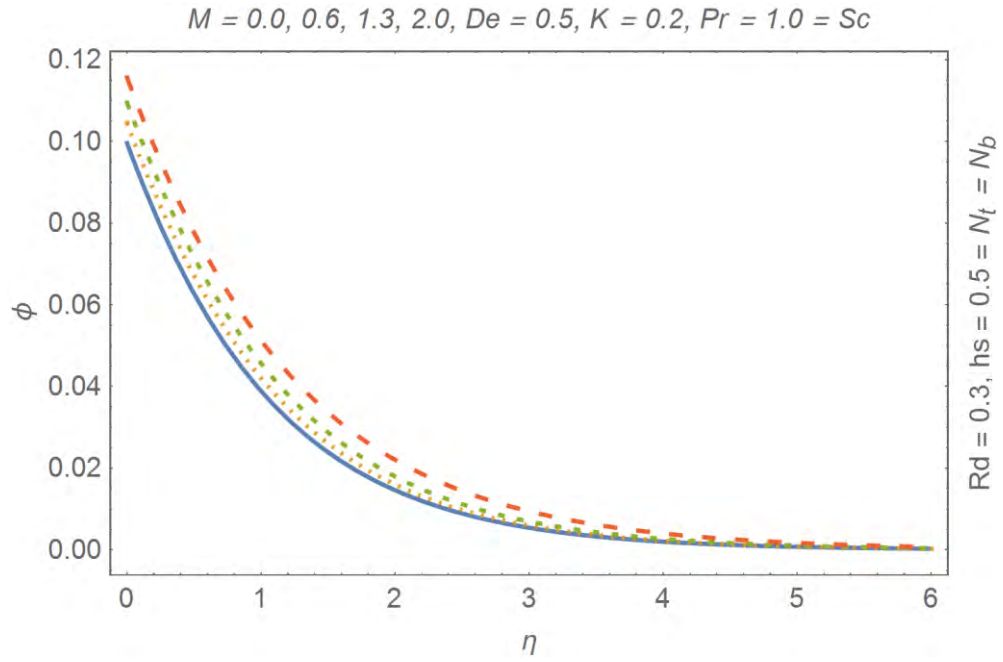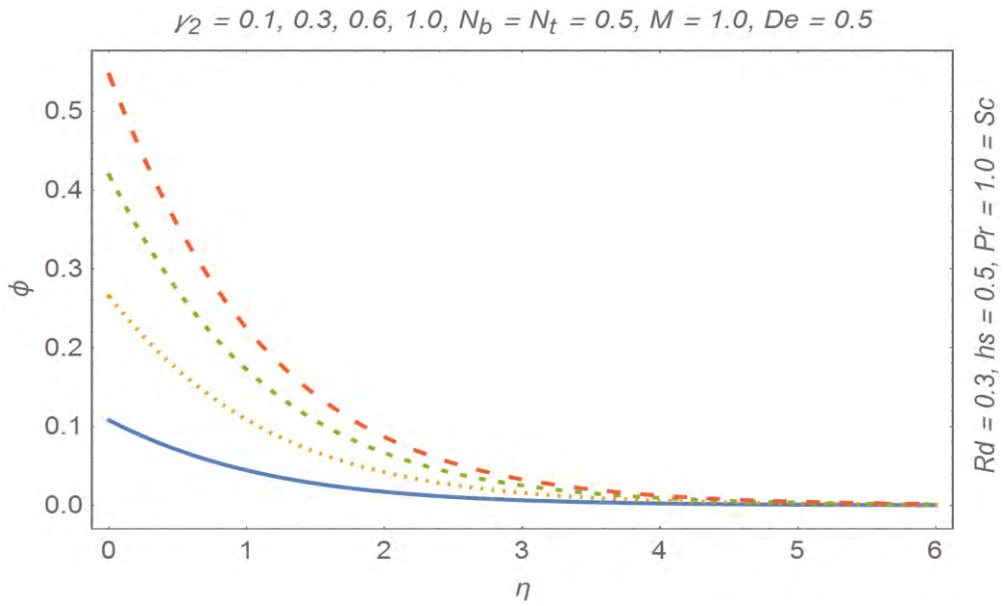
Fig. 3.11: γ_2 variations on ϕ.
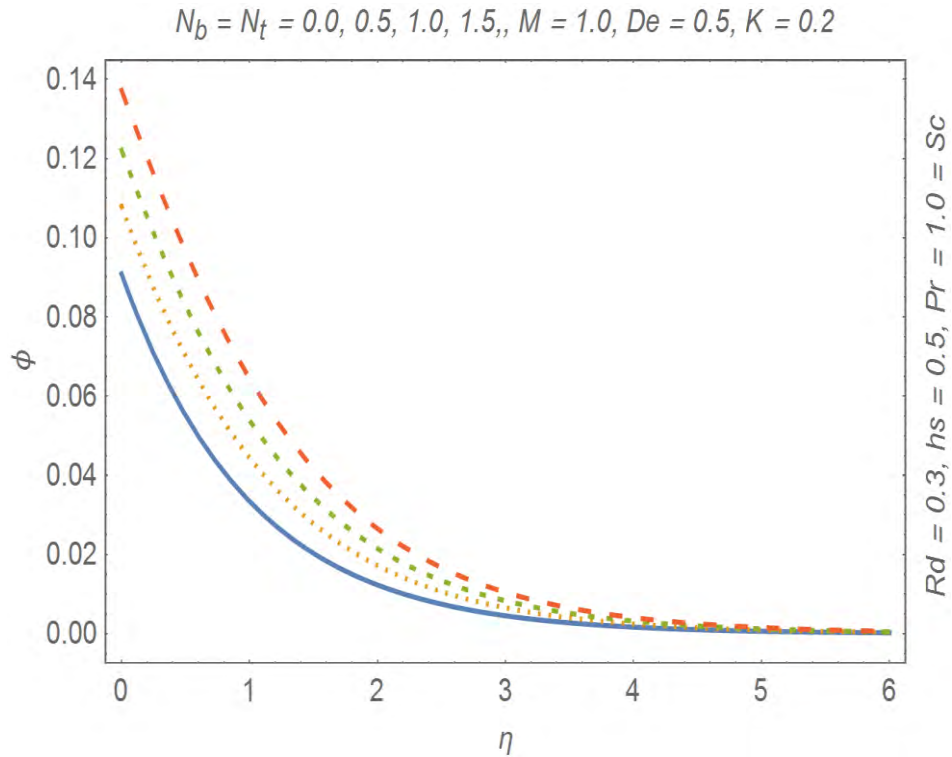
Fig. 3.12: (N_b, N_t) variations on ϕ.

Table 3.1: Comparison table.

Parameters							FD Solution		HAM Solution	
De	hs	M	N_b	N_t	γ_1	γ_2	$-\left(1+\dfrac{4}{3}Rd\right)\theta'(0)$	$-\phi'(0)$	$-\left(1+\dfrac{4}{3}Rd\right)\theta'(0)$	$-\phi'(0)$
0.0	0.5	1.0	0.3	0.3	0.5	0.3	0.247136	0.248907	0.247260	0.248890
0.5	0.5	1.0	0.3	0.3	0.5	0.3	0.246492	0.249193	0.246578	0.249295
1.0	0.5	1.0	0.3	0.3	0.5	0.3	0.245687	0.249552	0.248952	0.249513
1.5	0.5	1.0	0.3	0.3	0.5	0.3	0.2447057	0.249958	0.2447057	0.249955
0.5	-1.5	1.0	0.3	0.3	0.5	0.3	0.4769977	0.139383	0.4769977	0.139374
0.5	-1	1.0	0.3	0.3	0.5	0.3	0.4519256	0.151260	0.4519232	-0.151241

0.5	-0.5	1.0	0.3	0.3	0.5	0.3	0.4157199	0.168457	0.4157214	0.168467
0.5	0	1.0	0.3	0.3	0.5	0.3	0.3576959	0.196092	0.3576458	0.196089
0.5	0.5	1.0	0.3	0.3	0.5	0.3	0.2464949	0.249193	0.2464875	0.249188
0.5	1.0	1.0	0.3	0.3	0.5	0.3	-0.0672411	0.399351	-0.0672547	0.399340
0.5	1.5	1.0	0.3	0.3	0.5	0.3	-6.5635507	3.514316	-6.5635259	3.514320
0.5	0.5	0.0	0.3	0.3	0.5	0.3	0.2562556	0.245268	0.2562456	0.245270
0.5	0.5	0.5	0.3	0.3	0.5	0.3	0.2532122	0.246472	0.2532312	0.246472
0.5	0.5	1.0	0.3	0.3	0.5	0.3	0.2464949	0.249193	0.2464859	0.249193
0.5	0.5	1.5	0.3	0.3	0.5	0.3	0.2394121	0.252142	0.2394251	0.252142
0.5	0.5	1.0	0.1	0.3	0.5	0.3	0.2539361	0.336783	0.2539245	0.336783
0.5	0.5	1.0	0.3	0.3	0.5	0.3	0.2464949	0.249193	0.2464925	0.249193
0.5	0.5	1.0	0.6	0.3	0.5	0.3	0.2351707	0.227337	0.2351817	0.227337
0.5	0.5	1.0	1.0	1	0.5	0.3	0.2197855	0.218640	0.2197875	0.218641
0.5	0.5	1.0	0.3	0.1	0.5	0.3	0.2565104	0.214782	0.2565104	0.214781
0.5	0.5	1.0	0.3	0.3	0.5	0.3	0.2464949	0.249193	0.2464957	0.249192
0.5	0.5	1.0	0.3	0.6	0.5	0.3	0.2313545	0.313103	0.2313542	0.313102
0.5	0.5	1.0	0.3	1.0	0.5	0.3	0.2110014	0.421578	0.2110014	0.421577
0.5	0.5	1.0	0.3	0.3	0.1	0.3	0.1038475	0.218254	0.1038457	0.218254
0.5	0.5	1.0	0.3	0.3	0.5	0.3	0.2462949	0.249193	0.2462857	0.249193
0.5	0.5	1.0	0.3	0.3	1.0	0.3	0.2945056	0.261406	0.2945514	0.261406
0.5	0.5	1.0	0.3	0.3	2.0	0.3	0.3253130	0.269785	0.3253128	0.269784
0.5	0.5	1.0	0.3	0.3	0.5	0.1	0.2543187	0.105175	0.2543187	0.105175
0.5	0.5	1.0	0.3	0.3	0.5	0.3	0.2464949	0.249193	0.2464947	0.249195
0.5	0.5	1.0	0.3	0.3	0.5	0.6	0.2393645	0.378966	0.2393545	0.378964
0.5	0.5	1.0	0.3	0.3	0.5	1.0	0.2338329	0.478731	0.2338358	0.478735

3.3 Conclusive remarks

Convective heat-mass transport effects have studied for the Sakiadis rheology of UCM nanomaterial. Brownian and thermophoretic effects are discussed in the present study. Final results are listed in some steps as:

- Boundary layers decrease by increasing the value of Deborah effects.
- Magnetic effect opposes the fluid motion and delays the velocity.
- The temperature is directly related with magnetic field. Enhancement in temperature increases with magnetic field.
- Heat immersion parameter has contrary behavior on the temperature.
- Thermophoreses and Brownien motion both improve the temperature and concentration.

Chapter 4

3D dynamics of UCM model over exponentially stretched wall: Variable properties

This part portrays the 3D flow of UCM over exponential stretched wall. The energy equation with temperature dependent conductivity has been studied in detail. Analytical solutions are computed via HAM. Comparison with the already published data is presented for the limiting case. Various graphs and tables are illustrated to show the real insight of the problem.

4.1 Problem development

Consider the dynamics of UCM fluid over a bidirectional stretching wall. Analysis is performed in *(x,y,z)* coordinates. Constitutive mathematical relations are

$$\frac{\partial \widetilde{u}}{\partial \widetilde{x}} + \frac{\partial \widetilde{v}}{\partial \widetilde{y}} + \frac{\partial \widetilde{w}}{\partial \widetilde{z}} = 0, \tag{4.1}$$

$$\widetilde{u}\frac{\partial \widetilde{u}}{\partial \widetilde{x}} + \widetilde{v}\frac{\partial \widetilde{u}}{\partial \widetilde{y}} + \widetilde{w}\frac{\partial \widetilde{u}}{\partial \widetilde{z}} = \upsilon\frac{\partial^2 \widetilde{u}}{\partial \widetilde{z}^2} - \lambda\left(\widetilde{u}^2\frac{\partial^2 \widetilde{u}}{\partial \widetilde{x}^2} + \widetilde{v}^2\frac{\partial^2 \widetilde{u}}{\partial \widetilde{y}^2} + \widetilde{w}^2\frac{\partial^2 \widetilde{u}}{\partial \widetilde{z}^2}\right)$$
$$+ 2\lambda\left(\widetilde{u}\widetilde{v}\frac{\partial \widetilde{u}^2}{\partial \widetilde{x}\partial \widetilde{y}} + \widetilde{v}\widetilde{w}\frac{\partial \widetilde{u}^2}{\partial \widetilde{y}\partial \widetilde{z}} + \widetilde{u}\widetilde{w}\frac{\partial \widetilde{u}^2}{\partial \widetilde{x}\partial \widetilde{z}}\right), \tag{4.2}$$

$$\tilde{u}\frac{\partial \tilde{v}}{\partial \tilde{x}}+\tilde{v}\frac{\partial \tilde{v}}{\partial \tilde{y}}+\tilde{w}\frac{\partial \tilde{v}}{\partial \tilde{z}}=\upsilon\frac{\partial^2 \tilde{u}}{\partial \tilde{z}^2}-\lambda\left(\tilde{u}^2\frac{\partial^2 \tilde{v}}{\partial \tilde{x}^2}+\tilde{v}^2\frac{\partial^2 \tilde{v}}{\partial \tilde{y}^2}+\tilde{w}^2\frac{\partial^2 \tilde{v}}{\partial \tilde{z}^2}\right)$$
$$+2\lambda\left(\tilde{u}\tilde{v}\frac{\partial^2 \tilde{v}}{\partial \tilde{x}\partial \tilde{y}}+\tilde{v}\tilde{w}\frac{\partial^2 \tilde{v}}{\partial \tilde{y}\partial \tilde{z}}+\tilde{u}\tilde{w}\frac{\partial^2 \tilde{v}}{\partial \tilde{x}\partial \tilde{z}}\right).$$

(4.3)

Wall effects are

$$\tilde{u}=U_w=U_0 e^{\frac{x+y}{L}},\quad \tilde{v}=V_w=U_0 e^{\frac{x+y}{L}},\quad \tilde{w}=0,\quad at\quad \tilde{z}=0,$$

and $\tilde{u}\to 0,\quad \tilde{v}\to 0,\quad as\quad \tilde{z}\to\infty.$

(4.4)

Introducing the transformations:

$$\eta=\sqrt{\frac{U_0}{2L\upsilon}}e^{\frac{x+y}{2L}}\tilde{z},\quad \tilde{u}=U_0 e^{\frac{x+y}{L}}f'(\eta),\quad \tilde{v}=U_0 e^{\frac{x+y}{L}}g'(\eta),$$

$$w=-\sqrt{\frac{\upsilon U_0}{2L}}e^{\frac{x+y}{2L}}\left(f(\eta)+g(\eta)+\eta(f'(\eta)+g'(\eta))\right).$$

(4.5)

Eqs. (4.2) and (4.3) become

$$f'''-2(f'+g')f'+(f+g)f''-\beta\left(2(f'+g')^2 f'-\frac{\eta}{2}(f'+g')^2 f''\right)$$
$$-\beta\left(\frac{1}{2}(f+g)^2 f'''-3f(f'+g')f''-3g(f'+g')f''\right)=0,$$

(4.6)

$$g'''-2(f'+g')g'+(f+g)g''-\beta\left(2(f'+g')^2 g'-\frac{\eta}{2}(f'+g')^2 g''\right)$$
$$-\beta\left(\frac{1}{2}(f+g)^2 g'''-3f(f'+g')g''-3g(f'+g')g''\right)=0,$$

(4.7)

whereas the boundary conditions altered after subjected to transformations are written below:

$$f = 0, \quad g = 0, \quad f' = 1, \quad g' = \alpha, \quad at \quad \eta = 0 \quad and \qquad f' \to 0, \quad g' \to 0, \quad as \quad \eta \to \infty, \qquad (4.8)$$

where $\beta = \dfrac{\lambda U_0 e^{\frac{x+y}{L}}}{L}$ denotes the Deborah number and $\alpha = \left(\dfrac{V_0}{U_0}\right)$ symbolizes stretching ratio

parameter. Observe that $\alpha = 0$ shows that, the three dimensional flow is changed to two-dimensional flow which is stated as:

$$f''' - 2af'^2 + ff'' - \beta\left(2af'^3 - \frac{\eta}{2}f''f'^2 + \frac{1}{2}\eta f^2 f''' - 3ff'f''\right) = 0, \qquad (4.9)$$

$$f = 0, \quad f' = 1, \quad as \quad \eta = 0 \quad and \quad f' \to 0 \quad as \quad \eta \to \infty. \qquad (4.10)$$

Note that for $\alpha = 1$, we have $f = g$ that describes axisymmetric flow and with the similar boundary conditions (4.10).

4.1.1 Energy diffusion analysis

By taking the effects of radiation, we get

$$\tilde{u}\frac{\partial \tilde{T}}{\partial \tilde{x}} + \tilde{v}\frac{\partial \tilde{T}}{\partial \tilde{y}} + \tilde{w}\frac{\partial \tilde{T}}{\partial \tilde{z}} = \frac{1}{\rho c_p}\frac{\partial}{\partial \tilde{z}}\left(\left(k + \frac{16T_\infty^3 \sigma^*}{3k^*}\right)\frac{\partial \tilde{T}}{\partial \tilde{z}}\right), \qquad (4.11)$$

whereas the wall conditions for the PST and PHF cases are:

$$\tilde{T} = \tilde{T}_w = T_\infty + T_0 e^{\frac{A(x+y)}{2L}} \quad at \quad \tilde{z} = 0 \text{ and } \tilde{T} \to T_\infty \quad as \quad \tilde{z} \to \infty,$$

$$-k_\infty\left(\frac{\partial \tilde{T}}{\partial \tilde{z}}\right)_w = T_1 e^{\frac{(B+1)(x+y)}{2L}} \quad at \quad \tilde{z} = 0 \text{ and } \quad \tilde{T} \to T_\infty \quad as \quad \tilde{z} \to \infty. \qquad (4.12)$$

Thermal conductivity (*k*) is expressed mathematically as:

PST case: $\quad k = k_\infty\left(1 + \gamma.\theta(\eta)\right),$

PHF case: $\quad k = k_\infty\left(1 + \gamma.\phi(\eta)\right). \qquad (4.13)$

A similarity transformation is presented as

$$\tilde{T} = T_\infty + T_0 e^{\frac{A(x+y)}{2L}} \theta(\eta) \quad \text{and} \quad \tilde{T} = T_\infty + \frac{T_1}{k_\infty}\sqrt{\frac{2\upsilon L}{U_0}} e^{\frac{B(x+y)}{2L}} \phi(\eta). \tag{4.14}$$

Eq. (4.11) is reduced to the following form by applying Eq. (4.14):

$$(1 + Rn + \gamma\theta)\theta'' + \Pr(f + g)\theta' - A.\Pr(f' + g')\theta + \gamma\theta'^2 = 0, \tag{4.15}$$

$$(1 + Rn + \gamma\varphi)\varphi'' + \Pr(f + g)\varphi' - B.\Pr(f' + g')\varphi + \gamma\varphi'^2 = 0. \tag{4.16}$$

 And wall effects are

$$\theta = 1, \quad \phi' = -\frac{1}{1+\lambda}, \quad at \quad \eta = 0, \text{ and } \theta \to 0, \quad \phi' \to 0, \quad at \quad \eta \to \infty, \tag{4.17}$$

where $\Pr = {\mu c_p}\big/{k_\infty}$ and $Rn = {16\sigma * T_\infty^3}\big/{3kk*}$ respectivly.

4.2 Series solutions

The analytic solutions of Eqs. (4.6), (4.7), (4.15) and (4.16) subject to the conditions (4.8) and (4.17) are computed by utilizing homotopy approach. The suitable initial guesses and linear operator are:

$$f_0(\eta) = 1 - e^{-\eta}, \quad g_0(\eta) = \alpha(1 - e^{-\eta}), \quad \theta_0(\eta) = e^{-\eta}, \quad \phi_0(\eta) = \frac{e^{-\eta}}{1+\gamma}, \tag{4.18}$$

$$L_f(f) = f''' - f', \quad L_g(g) = g''' - g', \quad L_\theta(\theta) = \theta'' - \theta, \quad L_\phi(\phi) = \phi'' - \phi. \tag{4.19}$$

A MATHEMATICA code is constructed and we suppose $(h_f, h_g, h_\theta$ and $h_\varphi)$ for the function $(f, g, \theta$ and $\phi)$. It is observed experimentally that the convergence is achieved and it depends on these auxiliary parameters. Convergence of the solution are well presented in tabular form (Table 4.1).

47

Table 4.1: Convergence of the series solution.

Order of approximation	$-f''(0)$	$-g''(0)$	$-\theta'(0)$	$\phi''(0)$
1	1.44813	0.72406	0.87333	0.51570
4	1.75472	0.86584	0.70194	0.21325
8	1.78138	0.88897	0.64558	0.18583
12	1.78208	0.89124	0.62985	0.18581
16	1.78303	0.89148	0.62395	0.18618
20	1.78303	0.89148	0.62135	0.18634
30	1.78303	0.89148	0.62135	0.18634

4.3   Results and analysis

Here we wish to present the graphical and numerical illustration for the involved physical parameters. Therefore, Figs. (4.1-4.10) and Tables (4.2-4.3) are constructed. Influence of β on f and f' is examined in Fig. 4.1 and Fig. 4.2. Thus, we notice that β is in inverse relation with fluid velocity. Fluid motion slows down by enhancing Deborah number. From literature, we study that $(\beta < 1)$ resembles with the fluids in which the relaxation time is fewer than the deformation time. Therefore, non-Newtonian fluids act like viscous fluid. Contrary to that the fluid particles act like a solid material. Figs. 4.3 and 4.4 are constructed to study the influence of stretching ratio parameter α on $g(\eta)$ and $g'(\eta)$ correspondingly. It is shown in these geometries that the velocity of fluid particles increases by enhancing the value of $\alpha = (0.0, 0.3, 0.6, 1.0)$. From above observation, we determine that when $\alpha = 0,$ the flow diminishes to two dimensional form, while for $\alpha > 0,$ the flow resembles to three-dimensional (for the reason that surface is bidirectional stretching) as apparent from Fig. 4.4. In addition, the flow turns to be axisymmetric when $\alpha = 1.0$. The impact of temperature dependent thermal conductivity γ on PST and PHF cases are portrayed in Fig. 4.5 and Fig. 4.6. It is observed from geometry that

$\gamma = (0.0, 0.5, 1.0, 1.5)$ is directly related with $\theta(\eta)$ and inversely proportional to $\phi(\eta)$. Variation of the radiation parameter Rn is presented in Figs. 4.7 and 4.8. It is perceived that by increasing the radiation there is growth in temperature for (PST and PHF). The effect of stretching ratio parameter by considering $\Pr = (0.7 \text{ and } 0.02)$ against the temperature profile is shown in Figs. 4.9 and 4.10 respectively. PST and PHF cases exhibit eloquent overshoot for small value of Prandtl number $(\text{liquid metals} = 0.02)$ though for greater Prandtl number $(\text{air} = 0.7)$ the temperature variations are not very much momentous. Physically, we can say that the reaction of stretching ratio parameter is effective for the liquid metals $(\Pr = 0.02)$ because they are less viscous. However, for greater Prandtl number, fluid turns to be more viscous so there is less overshoot. Computed results are compared in table 4.2 and 4.3 and it is clear that numerical solution and HAM results are in an agreement.
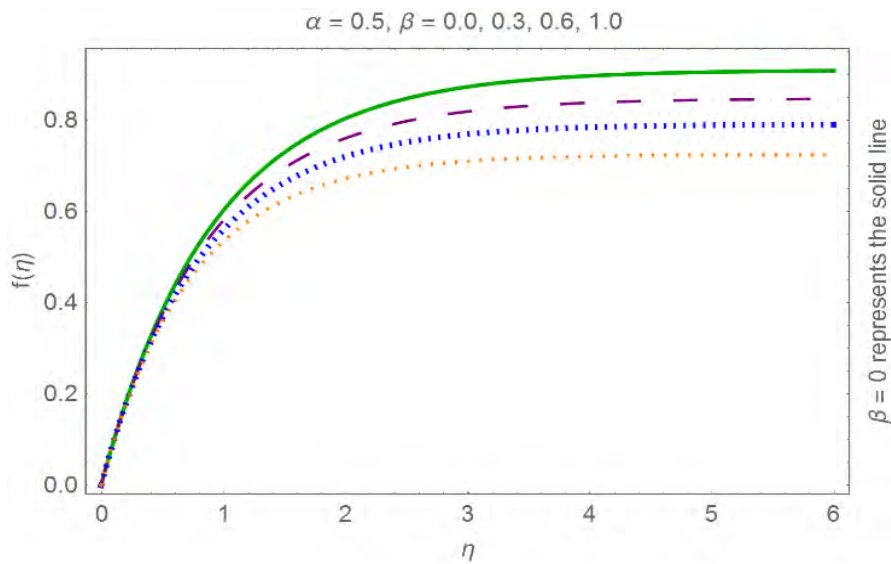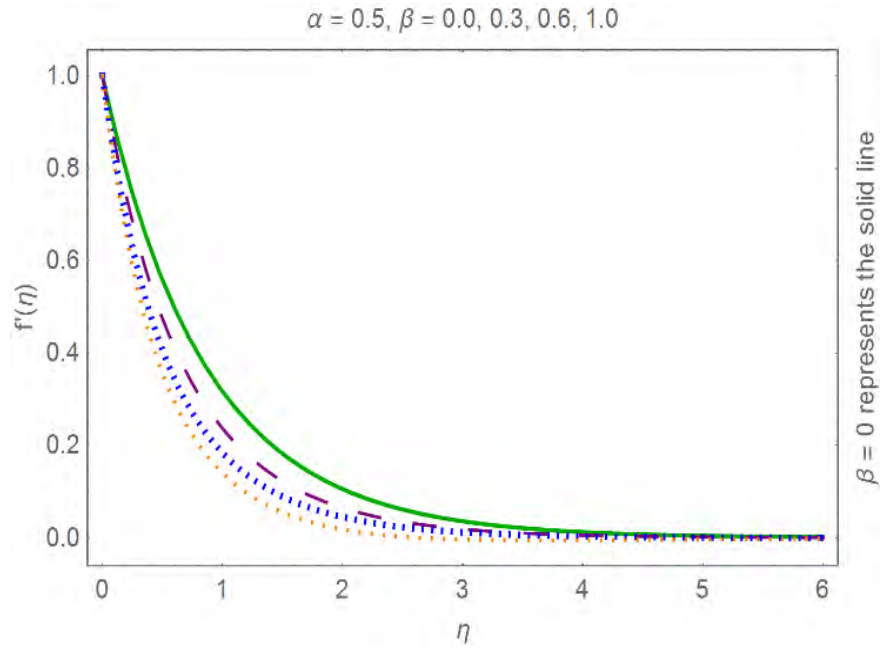
Fig. 4.1: Deborah number variations on f.

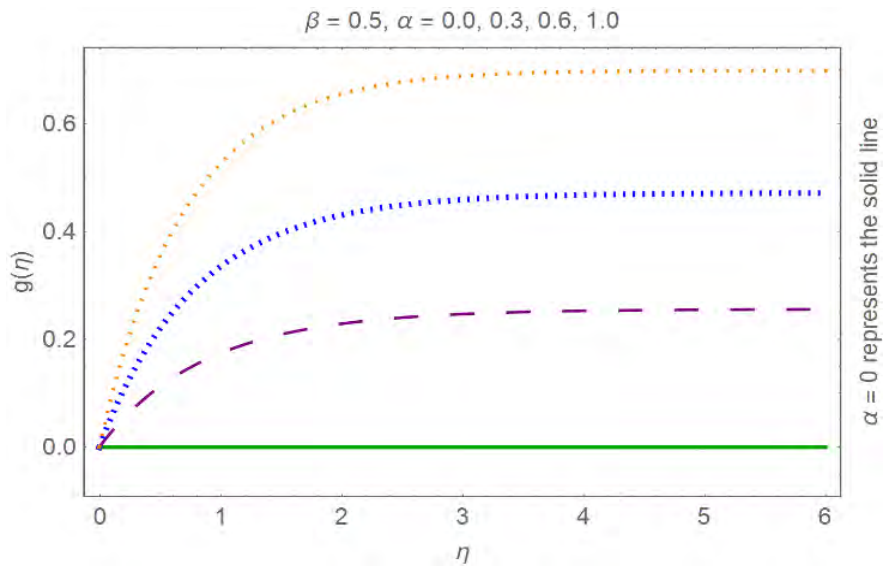49

Fig. 4.2: Deborah number variations on f'.

Fig. 4.3: α variations on g.

Fig. 4.4: α variatiosn on g'.

Fig. 4.5: γ variations on θ for PST

51
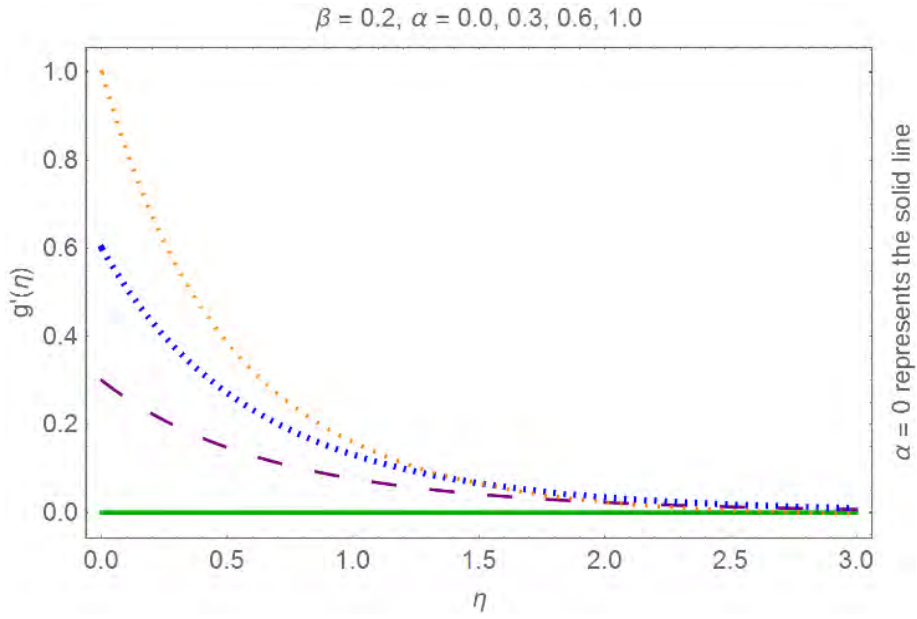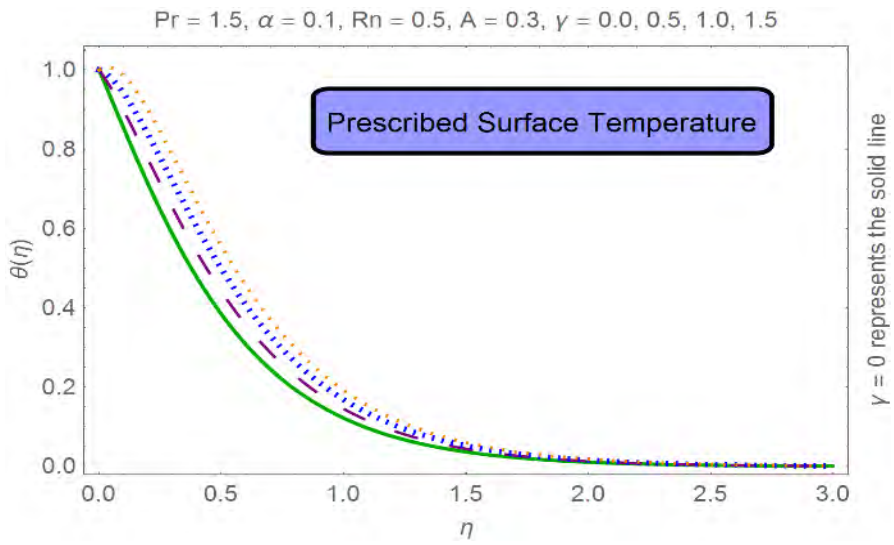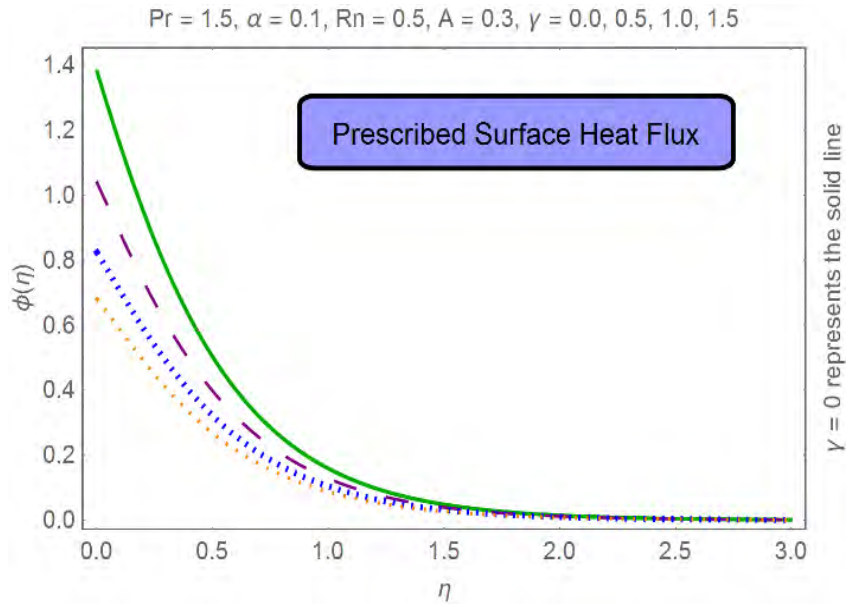
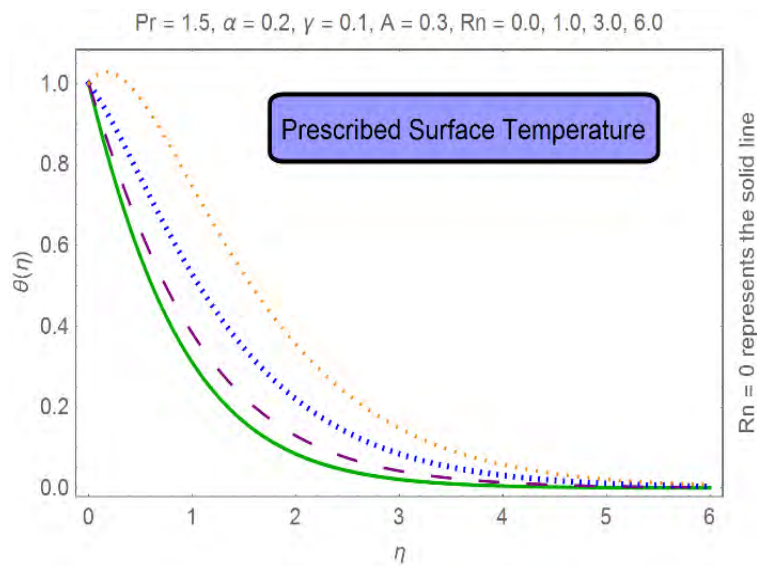Fig. 4.6: γ variations on ϕ for PSHF.

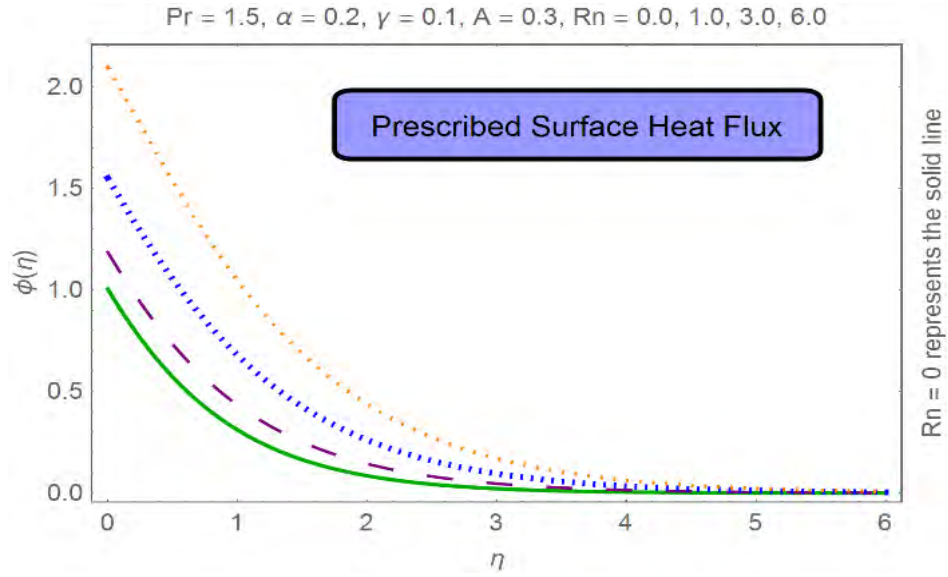Fig. 4.7: Rn variations on θ for PST.

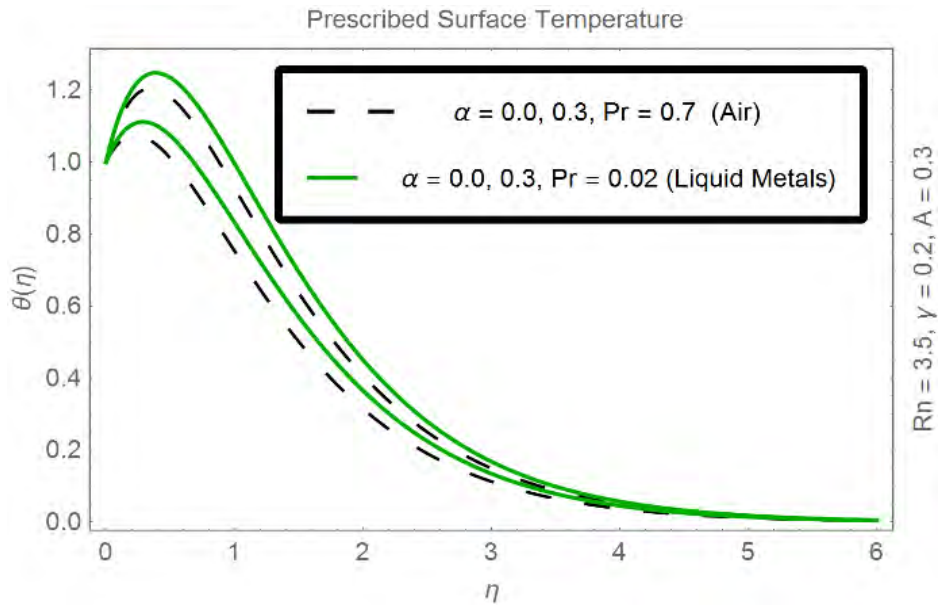Fig. 4.8: Rn changes on ϕ for PHF.
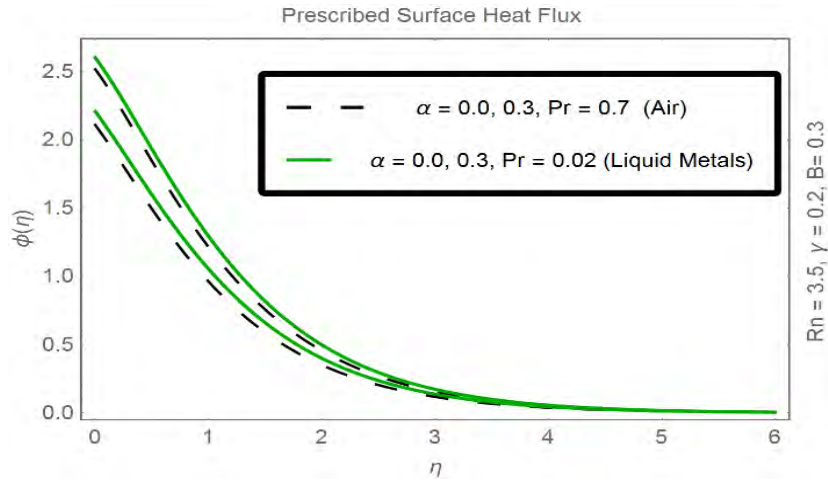
Fig. 4.9: Comparison of results: Air vs liquid metals on θ.

Fig. 4.10: Comparison of results: Air vs liquid metals on ϕ.

Table 4. 2: Evaluation table.

Parameters		(Awais et al. 28)		Present	
α	β	$f''(0)$	$g''(0)$	$f''(0)$	$g''(0)$
0.0	0.2	-1.56105	0.0	-1.56101	0.0
0.3		-1.86446	-0.55934	1.86443	-0.55934
0.6		-2.15823	-1.29494	-2.15824	-1.29493
0.5	0.0	-1.57001	-0.78501	-1.57002	-0.78501
	0.2	-1.78309	-0.89156	-1.78300	-0.89155
	0.4	-1.97288	-0.98645	-1.97288	-0.98644

Table 4.3: PST vs PHF cases: Analysis

Parameters		PST $\theta(\eta)$			PHF $\phi(\eta)$		
α	Rn	$\eta = 0.0$	$\eta = 2.5$	$\eta = 5.0$	$\eta = 0.0$	$\eta = 2.5$	$\eta = 5.0$
0.0	5.0	1.00000	0.28385	0.03857	1.93112	0.34177	0.04194
2.5		1.00000	0.16762	0.01665	1.70385	0.21745	0.02048
5.0		1.00000	0.05138	-0.0052	1.47658	0.09312	-0.0009
0.2	0.0	1.00000	0.06934	0.00313	1.00385	0.07065	0.00347
	3.0	1.00000	0.19247	0.02334	1.54931	0.22736	0.02552
	6.0	1.00000	0.31559	0.04355	2.09476	0.38406	0.04757

4.4 Conclusive remarks

Conclusive remarks about the present study are:

- Deborah number stops fluid and hence the velocity of the fluid particles reduces.
- Non-Newtonian fluid acts like a viscous (Newtonian) fluid as the Deborah number "De" is greater than one.
- Three dimensional flow lessens to two dimensional flow when $(\alpha = 0)$.
- Temperature dependent thermal conductivity has conflicting impact in both PST and PHF cases.
- Radiation parameter seems to be the source of enhancement in fluid temperature.
- Stretching parameter has a better over shoot for liquid metals.

Chapter 5

Rheology of Oldroyd-B model with magnetic and heat immersion effects: Analytical and numerical treatment

Sakiadis rheology of Oldroyd-B model with magnetic and heat immersion effect has been discussed in this chapter. Convective heating process is analyzed in the presence of thermal radiations. Appropriate variables are applied to alter PDEs into coupled nonlinear ODEs. Numerical as well as analytic solutions have been computed. Results are revealed in graphs to observe the performance of all parameters. Error plots are also presented during the analysis.

5.1 Mathematical description

Consider the Oldroyd-B fluid flowing in a absorbent medium where magnetic properties are also present. Analysis on convective heat transfer process is performed. Equations for the flow field are:

$$\nabla \cdot V = \mathbf{0},$$

(5.1)

$$\rho \frac{D\mathbf{V}}{Dt} = -\nabla p + \operatorname{div} \mathbf{S},$$

(5.2)

$$\left(1 + \lambda_1 \frac{D}{Dt}\right) S = \mu \left(1 + \lambda_2 \frac{D}{Dt}\right) A_1,$$

(5.3)

$$\frac{Da_i}{Dt} = \frac{\partial a_i}{\partial t} + u_r a_{i,r} - u_{i,r} a_r, \tag{5.4}$$

$$\rho c_p \frac{d\,\mathbf{T}}{dt} = k^* \nabla^2 \mathbf{T} + \bar{q}, \tag{5.5}$$

Eqs. (5.2-5.5) are further simplified as

$$u\frac{\partial u}{\partial x} + v\frac{\partial u}{\partial y} + \lambda_1 \left(u^2 \frac{\partial^2 u}{\partial x^2} + v^2 \frac{\partial^2 u}{\partial y^2} + 2uv\frac{\partial u}{\partial x\partial y} \right) = -\left(\frac{\sigma B^2_{\,0}}{\rho} + \frac{v}{k} \right)\left(u + \lambda_1 v\frac{\partial u}{\partial y} \right) +$$

$$v\left\{ \frac{\partial^2 u}{\partial y^2} + \lambda_2 \left(u\frac{\partial^3 u}{\partial x\partial y^2} + v\frac{\partial^3 u}{\partial y^3} - \frac{\partial u}{\partial x}\frac{\partial^2 u}{\partial y^2} - \frac{\partial u}{\partial y}\frac{\partial^2 v}{\partial y^2} \right) \right\}, \tag{5.6}$$

$$u\frac{\partial T}{\partial x} + v\frac{\partial T}{\partial y} = \alpha_m \frac{\partial^2 T}{\partial z^2} - \frac{1}{\rho C_p}\frac{\partial q_r}{\partial y} + \frac{Q_0}{\rho C_p}\left(T - T_\infty \right). \tag{5.7}$$

We acquire the results for Maxwell model when λ_2 attains zero value. Also, the results for the Newtonian fluid (viscous) model can be acquired by setting $\lambda_1 = \lambda_2 = 0$.

The wall conditions are

$$u = U, v = 0, -k\frac{\partial T}{\partial y} = h_f \left(T_f - T \right), \qquad \text{at } y = 0,$$

$$u \to 0, v \to 0, T \to T \to T_\infty \qquad \text{as } y \to \infty, \tag{5.8}$$

Applying

$$\eta = \sqrt{\frac{U}{vx}}\, y, u = Uf', v = -\frac{1}{2}\sqrt{\frac{vU}{x}}\left(f - \eta f' \right), \theta(\eta) = \frac{T - T_\infty}{T_f - T_\infty}. \tag{5.9}$$

Eqs. (5.5-5.8) becomes

$$f''' + \left(\frac{1}{2}\right)ff'' - \frac{D_e}{2}\left(2ff'f'' + \eta f'^2 f'' + f^2 f'''\right) - M^2\left(f' - D_e(f - \eta f')f''\right)$$

$$- Kf' + KD_e\left(ff'' - \eta ff''\right) + D_s\left(2(\eta f'f''' + \eta ff'''' - ff''') - ff'''' - f''^2\right) = 0, \tag{5.10}$$

$$\theta'' + \Pr\left(\frac{1}{2}f\theta' + hs\theta\right) + \frac{4}{3}Rd\theta'' = 0, \tag{5.11}$$

And wall effects are

$$f(0) = 0,\ f'(0) = 1,\ \theta'(0) = -\gamma_1(1 - \theta(0)),$$
$$f'(\infty) \to 0,\ \theta(\infty) \to 0. \tag{5.12}$$

Notice that

$$D_e = \lambda_1 U / 2x,$$

$$D_s = \lambda_2 U / 2x,$$

$$K = v / kU,$$

$$M = \sqrt{\delta \beta_\circ^2 / \rho U},$$

$$R_d = 16\delta^* T_\infty^3 / 3k'k^*,$$

$$hs = Q_\circ / U\rho C_p$$

and

$$\Pr = \upsilon / \alpha_m.$$

5.2 Error analysis

The system of Eqs. (5.10 and 5.11) along with wall properties (5.12) are nonlinear and coupled. Thus, error analysis is executed to get the certified calculations. We have constructed Figs. 5.1 and 5.2 which display the error in momentum and thermal distribution. Geometries witnesses that error in the calculations are insignificant.
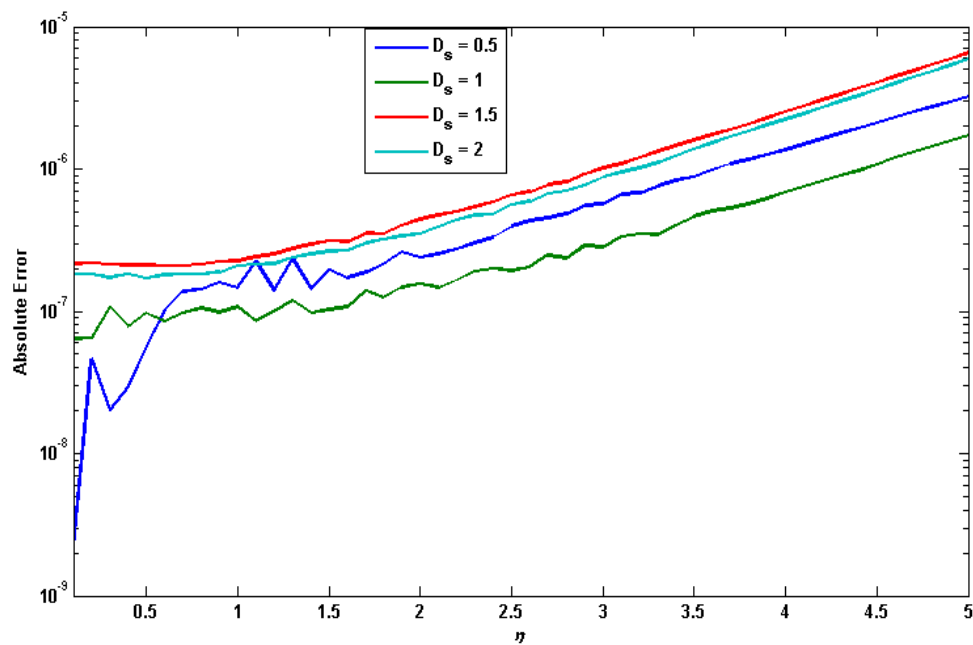

Fig. 5.1: Error in f.
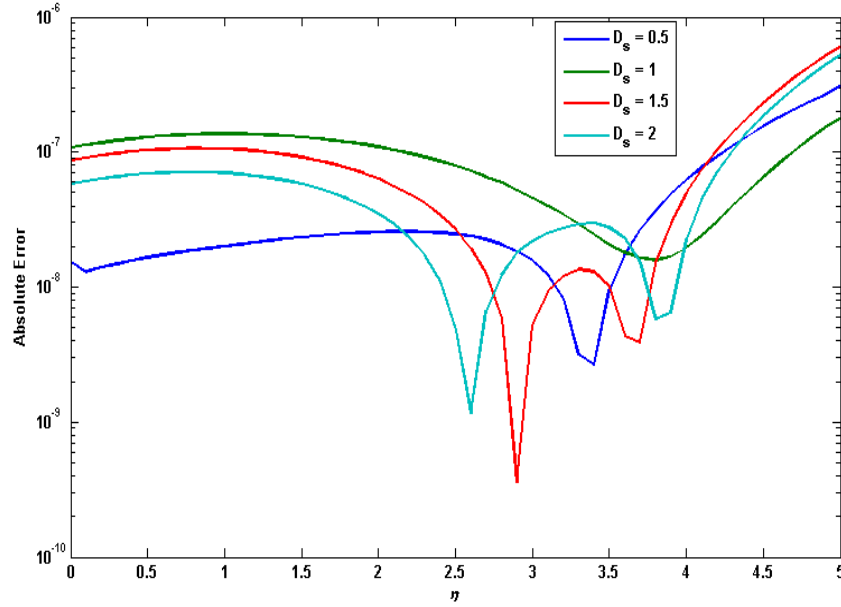
Fig. 5.2: Error in θ.

5.3 Results and analysis

We observe that the system of nonlinear equations (5.10-5.12) include different physical quantities comprising of Deborah number, wall convection parameter, magnetic field, internal heat generation/ absorption etc. Thus, we construct Figs. (5.3-5.11) and table 5.1 to examine the effect of various parameters on the momentum distribution and isotherms. Fig. 5.3 and 5.4 gives the heat transfer against magnetic field M and permeability K. Front bar demonstrates the results of Propane while back bar display the solutions of Ethylene glycol. Further, it is observed growth in magnetic and porosity parameter tends to decrease heat transfer rate. Figs. 5.5 and 5.6 explain the impact of Deborah numbers. It is witnessed that velocity reduce against Deborah number De rises however in case of Ds, velocity enhances. Deborah numbers (De, Ds <<1) indicates the flow motion but their large values (De, Ds >>1) relates to solid-like behavior. Fig. 5.7 interprets the effect of magnetic field M on the velocity profile. We notice that magnetic parameter and velocity are inversely proportional. Fig. 5.8 illustrates the variation in temperature profile for different values of magnetic field M. It is noticed that isotherms and isolines develops for higher magnetic parameter M. we know that the magnetic parameter depend on the Lorentz force. In

result of the enhancement of magnetic force, the Lorentz force gets stronger which yields growth in the temperature profile. In Fig. 5.9 effect of *hs* on the temperature profile is shown. Notice that, its negative value relates to heat absorption whereas its positive value characterizes heat generation. It is investigated that the temperature profile is decreasing function of heat absorption while temperature rises for the case of heat generation. Biot number γ_1 effect on the thermal distribution is demonstrated in Fig 5.10. It is shown from the geometry that there is growth in the temperature for the greater values of γ_1. Fig. 5.11 describes the 3D flow pattern of the present study. This graph noticeably shows that maximum change is close to the moving wall where falloffs slowly and tends to uniform free stream. Table 5.1 and 5.2 portray several results.
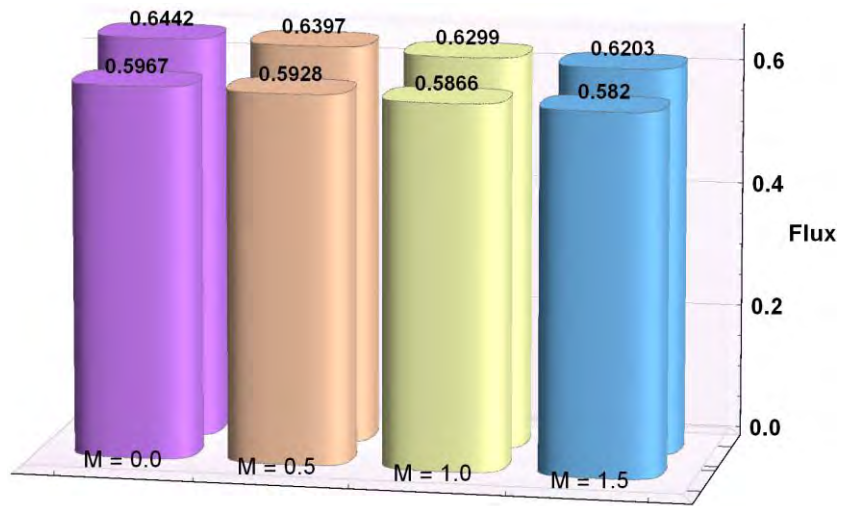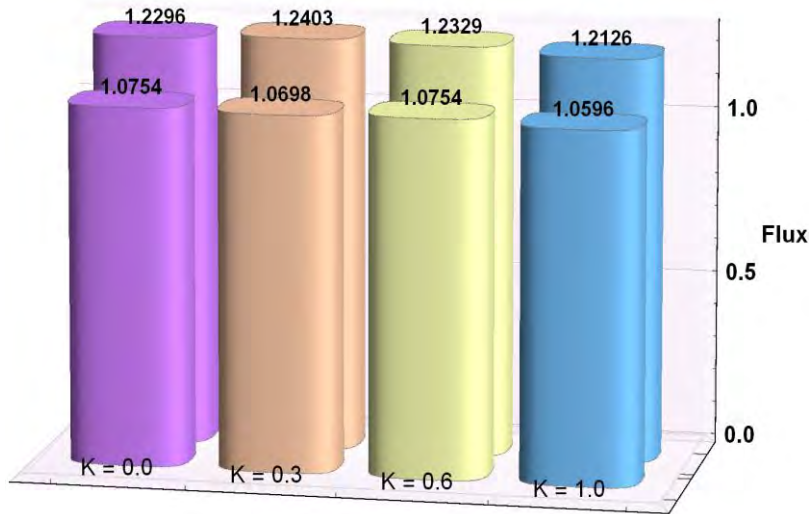
Fig. 5.3: Rate of heat transfer against *M*.
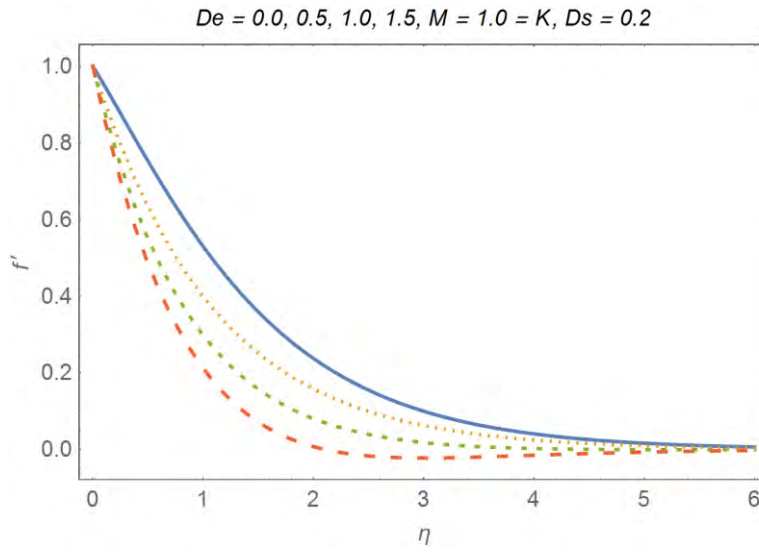

Fig. 5.4: Rate of heat transfer against *K*.
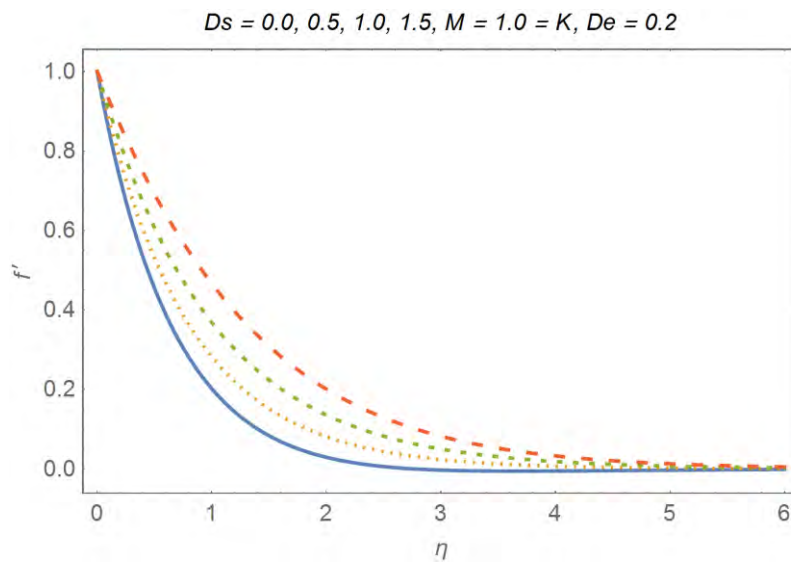
Fig. 5.5: *De* effects on f'.

Fig. 5.6: *Ds* effects on f'.
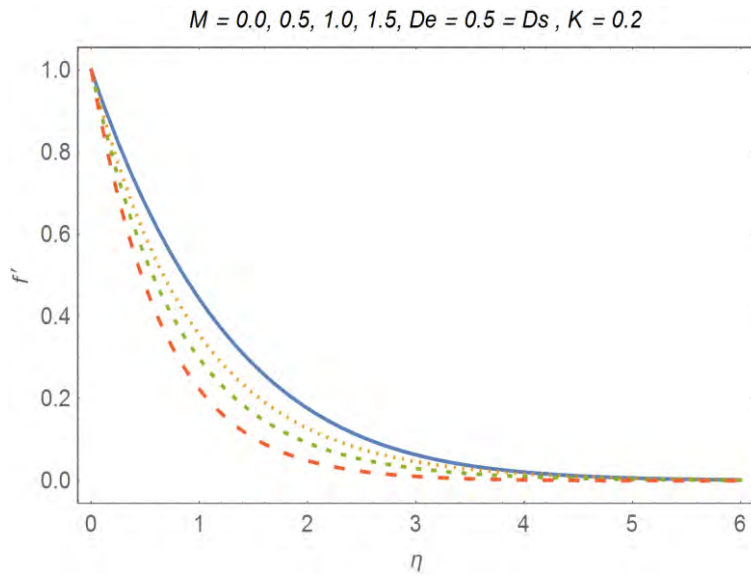
Fig. 5.7: M variations on f'.
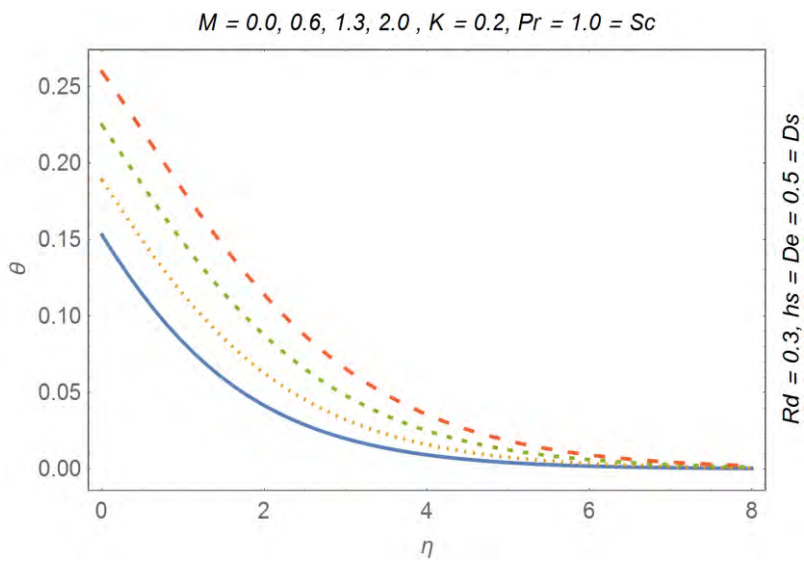
Fig. 5.8: M variations on θ.
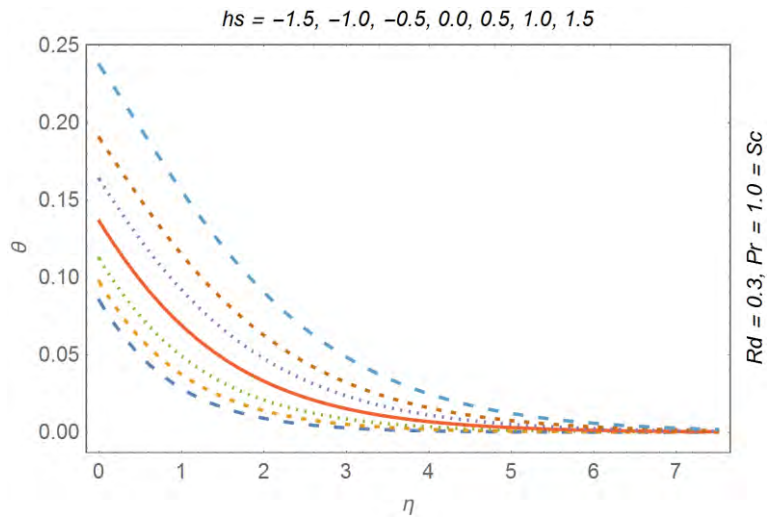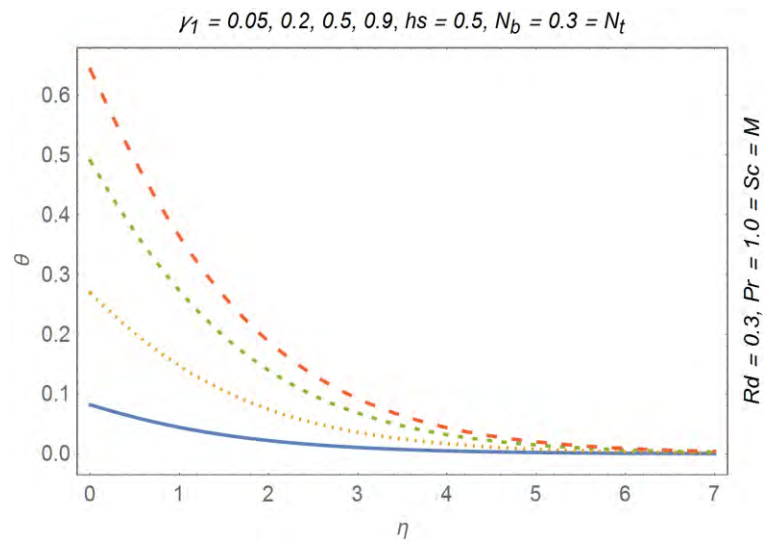
Fig. 5.9: *hs* variations on θ.

Fig. 5.10: γ_1 variations on θ.
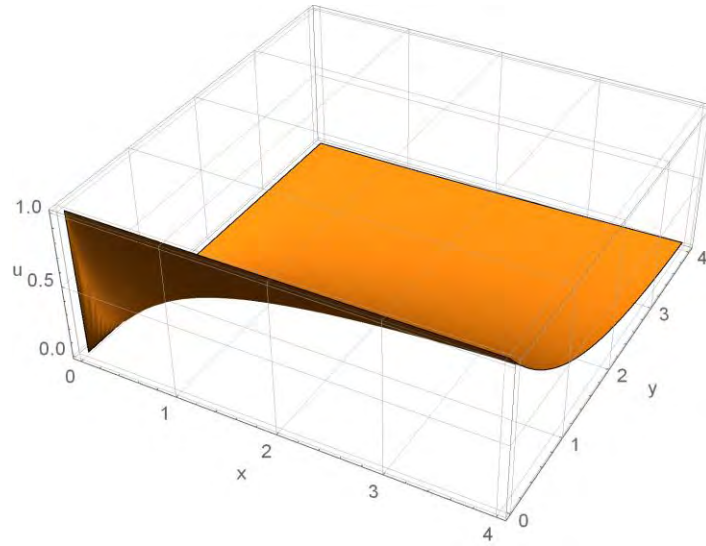
Fig. 5.11: Velocity plot in 3D configuration.

Table 5.1: Comparison values of skin friction.

Parameters							HAM solutions	Numerical solutions
De	hs	M	Ds	Pr	K	γ_1	$-f''(0)$	$-f''(0)$
0.0	0.5	1.0	0.5	1.0	0.5	0.5	1.91694324	1.91694813
0.5	0.5	1.0	0.5	1.0	0.5	0.5	1.97353017	1.97333087
1.0	0.5	1.0	0.5	1.0	0.5	0.5	2.03664843	2.03665842
1.5	0.5	1.0	0.5	1.0	0.5	0.5	2.10465408	2.10475407
0.5	-1.5	1.0	0.5	1.0	0.5	0.5	1.97343077	1.97333087
0.5	-1.0	1.0	0.5	1.0	0.5	0.5	1.97334088	1.97333087
0.5	-0.5	1.0	0.5	1.0	0.5	0.5	1.97333067	1.97333088
0.5	0.0	1.0	0.5	1.0	0.5	0.5	1.97333128	1.97333088
0.5	0.5	1.0	0.5	1.0	0.5	0.5	1.97763087	1.97333087

0.5	1.0	1.0	0.5	1.0	0.5	0.5	1.97333087	1.97333087
0.5	1.5	1.0	0.5	1.0	0.5	0.5	1.97480543	1.97480543
0.5	0.5	0.0	0.5	1.0	0.5	0.5	1.25597299	1.25587299
0.5	0.5	0.5	0.5	1.0	0.5	0.5	1.46804033	1.46704033
0.5	0.5	1.0	0.5	1.0	0.5	0.5	1.97223087	1.97333087
0.5	0.5	1.3	0.5	1.0	0.5	0.5	2.34456601	2.34576601
0.5	0.5	1.0	0	1.0	0.5	0.5	1.30360674	1.30360942
0.5	0.5	1.0	0.5	1.0	0.5	0.5	1.97333091	1.97333087
0.5	0.5	1.0	1.0	1.0	0.5	0.5	4.16623092	4.16623093
0.5	0.5	1.0	1.5	1.0	0.5	0.5	11.86444761	11.86444756
0.5	0.5	1.0	0.5	0.1	0.5	0.5	1.97333098	1.97333088
0.5	0.5	1.0	0.5	0.5	0.5	0.5	1.97333188	1.97333088
0.5	0.5	1.0	0.5	1.0	0.5	0.5	1.97333077	1.97333087
0.5	0.5	1.0	0.5	1.5	0.5	0.5	1.97333077	1.97333087
0.5	0.5	1.0	0.5	1.0	0.0	0.5	1.65264429	1.65264492
0.5	0.5	1.0	0.5	1.0	0.5	0.5	1.97333077	1.97333087
0.5	0.5	1.0	0.5	1.0	1.0	0.5	2.24931857	2.24931874
0.5	0.5	1.0	0.5	1.0	1.5	0.5	2.49518554	2.49518541
0.5	0.5	1.0	0.5	1.0	0.5	0.1	1.97333087	1.97333088
0.5	0.5	1.0	0.5	1.0	0.5	0.5	1.97333054	1.97333087
0.5	0.5	1.0	0.5	1.0	0.5	1.0	1.97333076	1.97333087
0.5	0.5	1.0	0.5	1.0	0.5	1.5	1.97333088	1.97333085

Table 5.2: Comparison values of temperature gradient.

Parameters							Numerical solutions	HAM solutions
De	Hs	M	Ds	Pr	K	γ_1	$-(1+4R_d/3)\theta'(0)$	$-(1+4R_d/3)\theta'(0)$
0.0	0.5	1.0	0.5	1.0	0.5	0.5	0.88626087	0.88626167
0.5	0.5	1.0	0.5	1.0	0.5	0.5	0.87047844	0.87047845
1.0	0.5	1.0	0.5	1.0	0.5	0.5	0.85857029	0.85857129
1.5	0.5	1.0	0.5	1.0	0.5	0.5	0.84965734	0.84965754
0.5	-1.5	1.0	0.5	1.0	0.5	0.5	0.47848456	0.47848356
0.5	-1	1.0	0.5	1.0	0.5	0.5	0.44917061	0.44917151
0.5	-0.5	1.0	0.5	1.0	0.5	0.5	0.39803006	0.39803116
0.5	0	1.0	0.5	1.0	0.5	0.5	0.25191604	0.25191594
0.5	0.5	1.0	0.5	1.0	0.5	0.5	0.87047844	0.87046844
0.5	1.0	1.0	0.5	1.0	0.5	0.5	0.35714342	0.35714842
0.5	1.5	1.0	0.5	1.0	0.5	0.5	0.72566043	0.72566043
0.5	0.5	0.0	0.5	1.0	0.5	0.5	0.96221819	0.96221819
0.5	0.5	0.5	0.5	1.0	0.5	0.5	0.92237457	0.92236757
0.5	0.5	1.0	0.5	1.0	0.5	0.5	0.87047844	0.87048844
0.5	0.5	1.3	0.5	1.0	0.5	0.5	0.85099774	0.85097874
0.5	0.5	1.0	0	1.0	0.5	0.5	−0.01897348	−0.01898304
0.5	0.5	1.0	0.5	1.0	0.5	0.5	0.87047844	0.87047834
0.5	0.5	1.0	1.0	1.0	0.5	0.5	0.84028696	0.84028896
0.5	0.5	1.0	1.5	1.0	0.5	0.5	0.82674776	0.82674786
0.5	0.5	1.0	0.5	0.1	0.5	0.5	0.15693718	0.15693728

0.5	0.5	1.0	0.5	0.5	0.5	0.5	−0.44869951	−0.44868951
0.5	0.5	1.0	0.5	1.0	0.5	0.5	0.87047844	0.87047944
0.5	0.5	1.0	0.5	1.5	0.5	0.5	0.52974335	0.52974345
0.5	0.5	1.0	0.5	1.0	0.0	0.5	0.21824554	0.21824564
0.5	0.5	1.0	0.5	1.0	0.5	0.5	0.87047844	0.87047854
0.5	0.5	1.0	0.5	1.0	1.0	0.5	0.85515317	0.85515337
0.5	0.5	1.0	0.5	1.0	1.5	0.5	0.84547170	0.84547180
0.5	0.5	1.0	0.5	1.0	0.5	0.1	0.14570719	0.14570719
0.5	0.5	1.0	0.5	1.0	0.5	0.5	0.87047844	0.87047854
0.5	0.5	1.0	0.5	1.0	0.5	1.0	2.30145457	2.30145467
0.5	0.5	1.0	0.5	1.0	0.5	1.5	5.09132362	5.09132372

5.5 Conclusive remarks

Sakiadis fluid motion for the Oldroyd-B model over a porous wall is investigated in the present study. Conclusive remarks deduced from graphical and tabular solution are as follows:

- Enhancement in the value of *De* tends to lessen momentum distribution while by improving the values of *Ds* we get growth in the value of velocity profile.
- Magnetic field *M* tends to slow down the fluid motion.
- The temperature distribution progresses by enhancing magnetic field.
- Heat generation-absorption both have opposed behavior on isolines.
- Large γ_1 intensify the temperature.

Chapter 6

Dynamics of Burgers' fluid with generalized heat flux with heat immersion and magnetic field

This chapter presents the features of CC heat flux for the flow of Burgers' fluid. To investigate the thermal relaxation properties together with heat source/sink we present the Cattaneo-Christov model rather than Fourier's law. Mathematical modelling is performed using laws of momentum and energy under the order analysis to transform the problem into the set of equations. It is shown that the term "$\sigma B_0^2 \, u / \rho$" is for the hydro-magnetic rheology of the viscous model while the generalized magnetic field term (as revealed in Eq. 6.2) is for the Burgers' model which is used in the present study. For the solution computation, homotopy analysis method is applied to compute results. Results are depicted in graphs to visualize the effect of physical parameters. Values of skin friction with heat transfer rate have been displayed in the tables.

6.1 Governing equations

Consider the dynamics of Burgers' fluid past a conducting wall in the region of stagnation point. The conducting wall is situated along x-axis and an incompressible Burgers' fluid fills the space $y > 0$ as displayed in the Fig. 6.1.
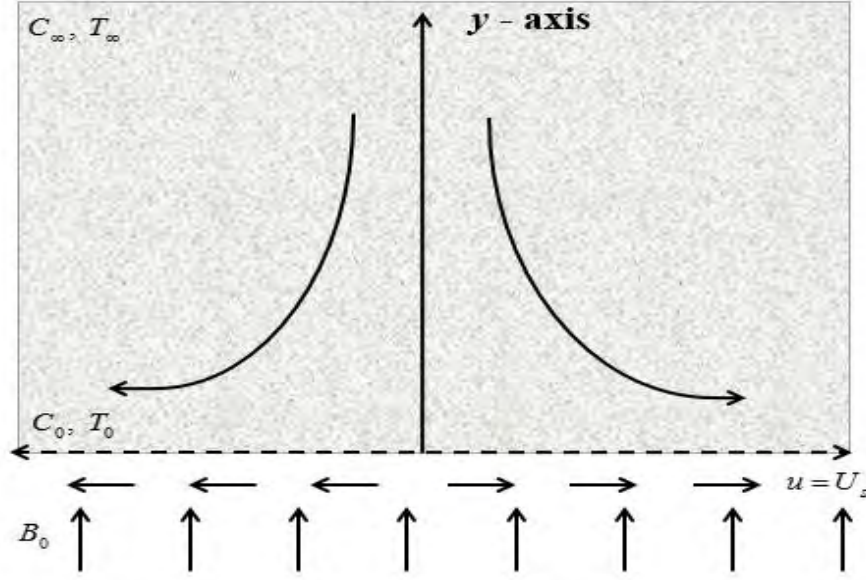
Fig. 6.1: Geometry.

A uniform magnetic field $\mathbf{B} = \{0, B_0, 0\}$ is applied along y-axis and the influence of influenced magnetic field is ignored by supposing slight magnetic Reynolds' number. A conducting wall go through a stretched phenomenon with $U_s(x)$, while $U_e(x)$ is the free stream. The equations are of the form:

$$\frac{\partial u}{\partial x} + \frac{\partial v}{\partial y} = 0,$$ (6.1)

$$u\frac{\partial u}{\partial x} + v\frac{\partial u}{\partial y} + \lambda_1 \left(\begin{array}{c} u^2 \dfrac{\partial^2 u}{\partial x^2} + v^2 \dfrac{\partial^2 u}{\partial y^2} \\[2mm] +2uv\dfrac{\partial^2 u}{\partial x \partial y} \end{array} \right) + \lambda_2 \left(\begin{array}{c} u^3 \frac{\partial^3 u}{\partial x^3} + v^3 \frac{\partial^3 u}{\partial y^3} + u^2 \left(\frac{\partial^2 u}{\partial x^2}\frac{\partial u}{\partial x} - \frac{\partial u}{\partial y}\frac{\partial^2 v}{\partial x^2} + 2\frac{\partial v}{\partial x}\frac{\partial^2 u}{\partial x \partial y} \right) \\[2mm] +3v^2 \left(\frac{\partial v}{\partial y}\frac{\partial^2 u}{\partial y^2} + \frac{\partial u}{\partial y}\frac{\partial^2 u}{\partial x \partial y} \right) + 3uv\left(u\frac{\partial^3 u}{\partial x^2 \partial y} + v\frac{\partial^3 u}{\partial x \partial y^2} \right) \\[2mm] +2uv\left(\frac{\partial u}{\partial y}\frac{\partial^2 u}{\partial x^2} + \frac{\partial v}{\partial x}\frac{\partial^2 u}{\partial y^2} + \frac{\partial v}{\partial y}\frac{\partial^2 u}{\partial x \partial y} - \frac{\partial u}{\partial y}\frac{\partial^2 v}{\partial x \partial y} \right) \end{array} \right) =$$

$$v\left\{ \frac{\partial^2 u}{\partial y^2} + \lambda_3 \left(u\frac{\partial^3 u}{\partial x \partial y^2} + v\frac{\partial^3 u}{\partial y^3} - \frac{\partial u}{\partial x}\frac{\partial^2 u}{\partial y^2} - \frac{\partial u}{\partial y}\frac{\partial^2 v}{\partial y^2} \right) \right\} - \frac{\sigma B_0^2}{\rho}\left(u - U_e + \lambda_1 v\frac{\partial u}{\partial y} \right) + U_e \frac{du}{dx}$$

$$-\frac{\sigma B_0^2 \lambda_2}{\rho}\left(u\frac{\partial v}{\partial x}\frac{\partial u}{\partial y}-v\frac{\partial u}{\partial x}\frac{\partial u}{\partial y}+uv\frac{\partial^2 u}{\partial x \partial y}+v^2\frac{\partial^2 u}{\partial y^2}\right), \tag{6.2}$$

The wall effects are:

$$u=U_s=cx,\ v=0 \quad \text{at} \quad y=0,$$
$$u=U_e=ax \quad \text{as} \quad y\to\infty, \tag{6.3}$$

Moreover, the solution for Newtonian fluid can be achieved for $\lambda_1=\lambda_2=\lambda_3=0$.

The generalized heat flux model is:

$$q+\lambda(\frac{\partial q}{\partial t}+V.\nabla q-q.\nabla V+(V.\nabla)q)=-k\nabla T, \tag{6.4}$$

Equation written above corresponds to Fourier's law when $\lambda=0$. The energy equation takes the following form when the internal heat generation/absorption effects are present.

$$\rho c_p V.\nabla T=-\nabla.q+Q(T-T_\infty). \tag{6.5}$$

Substituting Eq. 6.4 into Eq. 6.5, we get

$$u\frac{\partial T}{\partial x}+v\frac{\partial T}{\partial y}+\lambda\left(u^2\frac{\partial^2 T}{\partial x^2}+v^2\frac{\partial^2 T}{\partial y^2}+2uv\frac{\partial^2 T}{\partial x \partial y}+u\frac{\partial u}{\partial x}\frac{\partial T}{\partial x}+u\frac{\partial v}{\partial x}\frac{\partial T}{\partial y}+v\frac{\partial v}{\partial y}\frac{\partial T}{\partial y}\right)$$
$$-\frac{Q(T-T_\infty)}{\rho c_p}+\frac{Q}{\rho c_p}\lambda\left(u\frac{\partial T}{\partial x}+v\frac{\partial T}{\partial y}\right)=\frac{k}{\rho c_p}\left(\frac{\partial T^2}{\partial x^2}+\frac{\partial T^2}{\partial y^2}\right). \tag{6.6}$$

The conditions are

$T = T_w$ at $y = 0$,

$T \to T_\infty$ as $y \to \infty$, $\qquad$ (6.7)

where Q, c_p, T_w and T_∞ are the heat generation-absorption coefficient, the specific heat constant, wall temperature and the free stream temperature respectively.

The expression for stream function is

$$u = \frac{\partial \psi}{\partial y} \text{ and } v = -\frac{\partial \psi}{\partial x}, \qquad (6.8)$$

where

$$\psi = \sqrt{cv} \, x f(\eta), \quad \theta(\eta) = \frac{T - T_\infty}{T_w - T_\infty}, \quad \eta = \sqrt{\frac{c}{v}} y. \qquad (6.9)$$

Applying the above mentioned transformations, we get

$$f''' - f'^2 + ff'' + \beta_1 \left(2ff'f'' - f^2 f''' \right) + \beta_2 \left(f^3 f'''' - 2ff'^2 f'' - 3f^2 f''^2 \right)$$
$$+ \beta_3 \left(f''^2 - ff'''' \right) - M^2 \left(f' - \beta_1 ff'' + \beta_2 f^2 f''' \right) + A^2 + M^2 A = 0, \qquad (6.10)$$

$$\theta'' + \Pr(f\theta' + h_s \theta + \gamma(f^2 \theta'' + ff'\theta' - h_s f\theta')) = 0. \qquad (6.11)$$

Along with associated wall conditions

$$f'(\eta) = 1, \, f(\eta) = 0, \, \theta(\eta) = 1 \qquad \text{at} \quad \eta = 0,$$
$$f'(\eta) = A, \, \theta(\eta) = 0 \qquad \text{as} \quad \eta \to \infty, \qquad (6.12)$$

where

$$\beta_1 = c\lambda_1, \; \beta_2 = c^2 \lambda_2, \; \beta_3 = c\lambda_3, \; \Pr = \frac{v}{\alpha}, \; M^2 = \frac{\sigma B_0^2}{\rho c}, \; A = \frac{a}{c}. \qquad (6.13)$$

6.2 Results and discussion

Here we analyze the influence of different physical parameters involving Deborah numbers, thermal relaxation parameter, stagnation point, Prandtl number, heat source/sink etc on solution set. Thus, we construct Figs. 6.2-6.10 and Tables 6.1-6.3 to visualize the results graphically and in tabular form. Figs. 6.2 and 6.3 display the stream line behavior for the viscous and Burger fluid which show that streamlines for Burgers' fluid are different as compared to the streamlines for Newtonian fluid. It is because of the occurrence of several relaxation and retardation times in the stress tensor of Burger's model. Fig. 6.4 shows the variation of stagnation point A on the velocity field. By increasing A, the velocity increases and the momentum boundary-layer deceases in the region $0.0 < A < 1.0$. However, when $A > 1.0$ the momentum boundary-layer grows. Thus, we say that the bigger values of A together with greater free stream which improves the fluid's velocity and the momentum boundary layer. Also, for $A = 1.0$ both velocity and momentum boundary layer disappears. Therefore, $A = 1.0$ is a critical point at which the behavior of the momentum boundary layer varies. Fig. 6.5 show the comparison of Newtonian and Burger's fluid. It is perceived that the magnitude of velocity profile and momentum boundary layer is lesser in magnitude for the rheology of Burger's model when equated with the rheology of Newtonian model. The extra physical quantities β_1, β_2 and β_3 are positive for Burger fluid. Values of β_1, β_2 and β_3 signifies to viscous and elastic effects which slow down the flow. Fig. 6.6 displays the impact of magnetic field on the flow profile. Note that the velocity profile decreases by increasing magnetic field parameter M. The apparent viscosity rises due to the effects of magnetic strength. So, the ability of fluid particles to transmit force is increased. The influence of thermal relaxation time on the temperature distribution is shown in Fig 6.7. It is studied that the temperature profile and its relaxation time have opposite relationship. It is seen that the temperature reaches free stream rapidly for the greater values of thermal relaxation parameter. The effect of Pr on the temperature profile is given in Fig 6.8. Isolines tends to reduce as Pr increases. The thermal diffusivity is smaller for higher Prandtl number because of the decrease in thermal diffusion. Observe that the decline in thermal diffusion rate results into a decrease in temperature. The result of internal heat generation/absorption parameters hs on the temperature profile are portrayed in the Figs. 6.9 and 6.10. It is seen that the temperature profile

$\theta(\eta)$ reduces when the heat sink is present. However, the temperature profile expands for the case of heat source. The heat source and sink play important role in controlling the temperature. This is significant due to its many applications in industry as the product mainly depends on the heat transfer rate. The comparison of the present computed results and the published results are shown in table 6.1 and it is verified that both are in a nice agreement. Table 6.2 displays the behavior of $f''(0)$ against different values of Burgers parameter β_2. Note that the numerical values of skin friction $f''(0)$ improves for bigger values of Burgers parameter β_2. The calculated values of heat transfer rate at the wall $\theta'(0)$ against different quantities are shown in the table 6.3. It is analyzed that the magnitude of $\theta'(0)$ falls for Burgers parameter, thermal relaxation time and internal heat source/sink quantity.
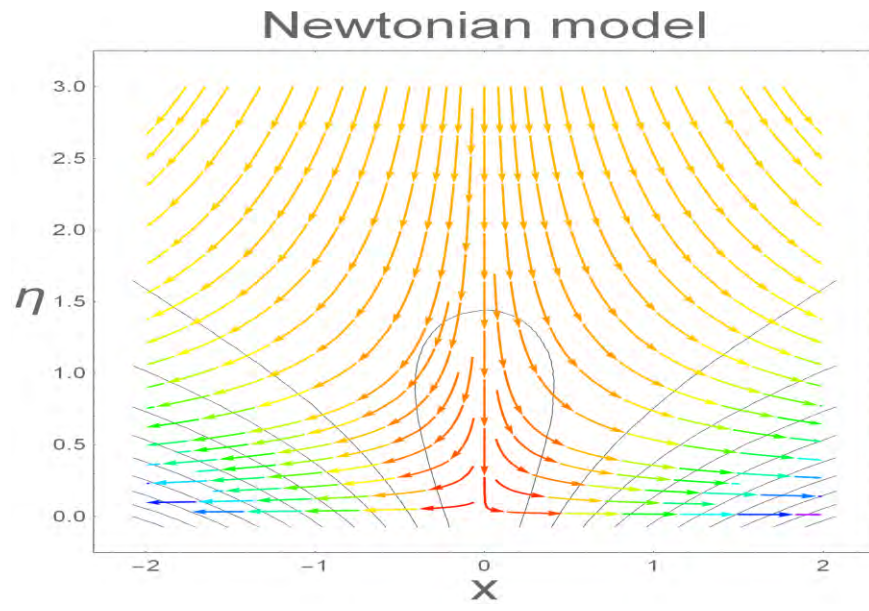
Fig. 6.2: Rheology of Newtonian model.
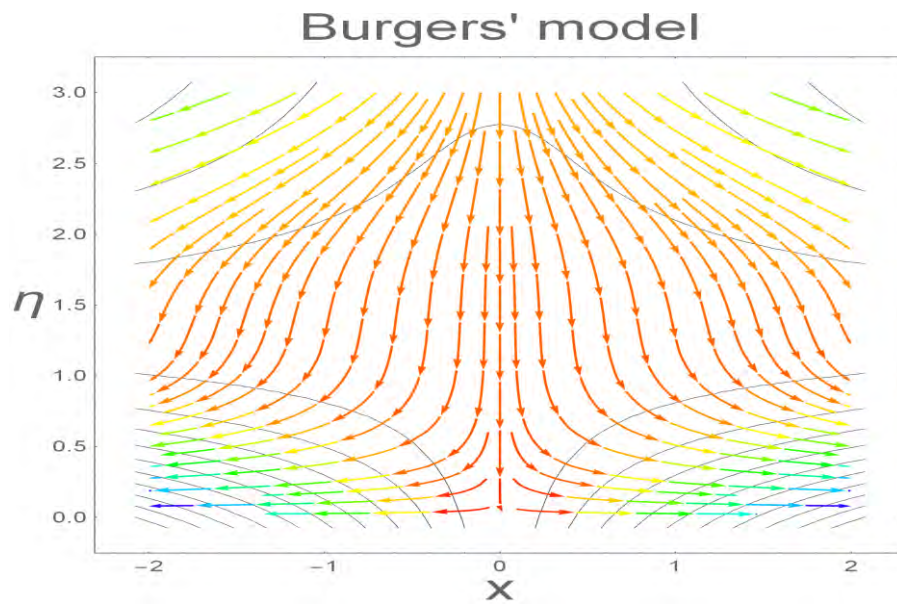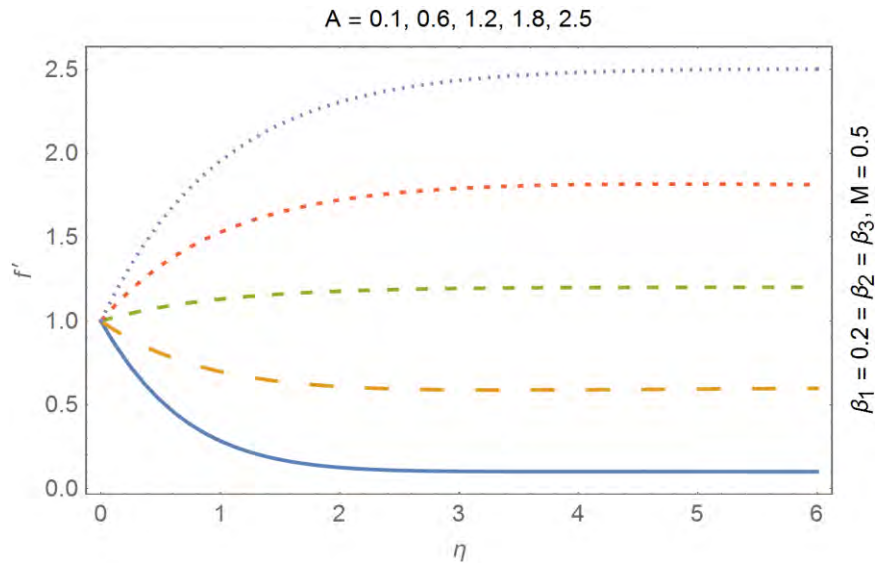

Fig. 6.3: Rheology of Burgers model.

Fig. 6.4: *A* variations on the velocity.

Fig. 6.5: Newtonian vs Burgers model.
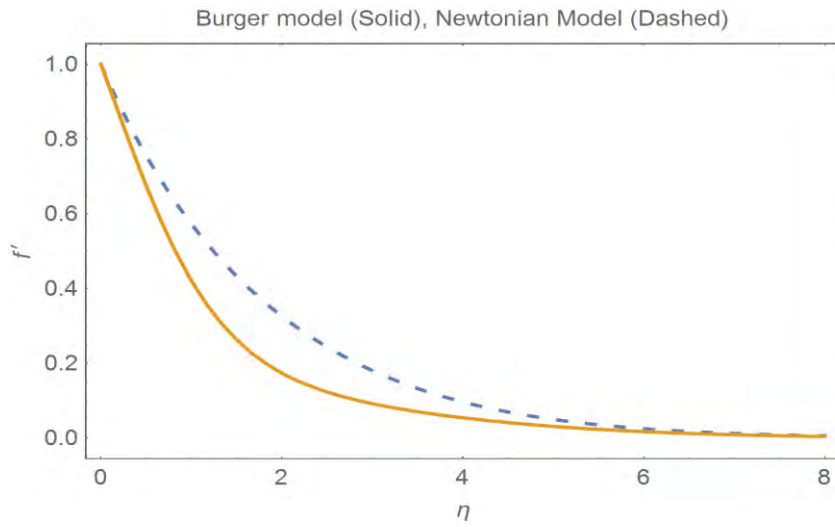
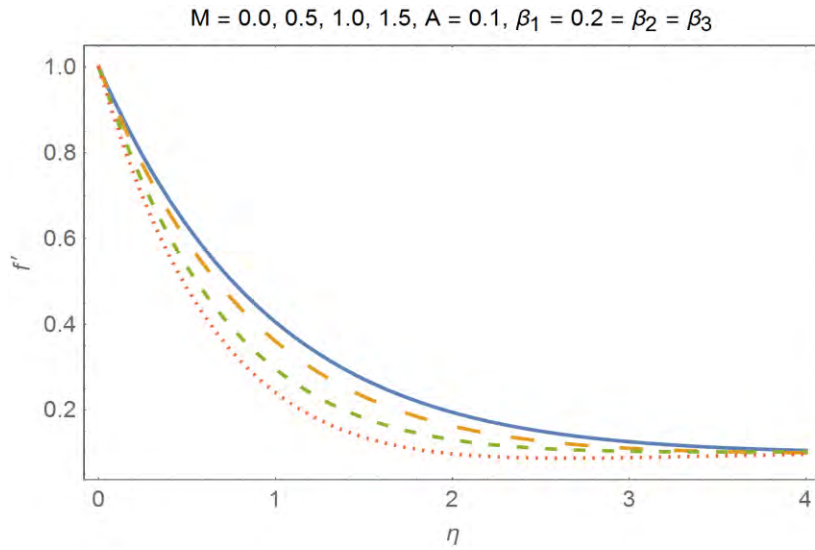M = 0.0, 0.5, 1.0, 1.5, A = 0.1, $\beta_1 = 0.2 = \beta_2 = \beta_3$

Fig. 6.6: Velocity distribution vs M.

γ = 0.0, 0.5, 1.0, 1.5, Pr = 1.0, hs = 0.5

$\beta_1 = 0.2 = \beta_2 = \beta_3$, M = 0.5, A = 0.1
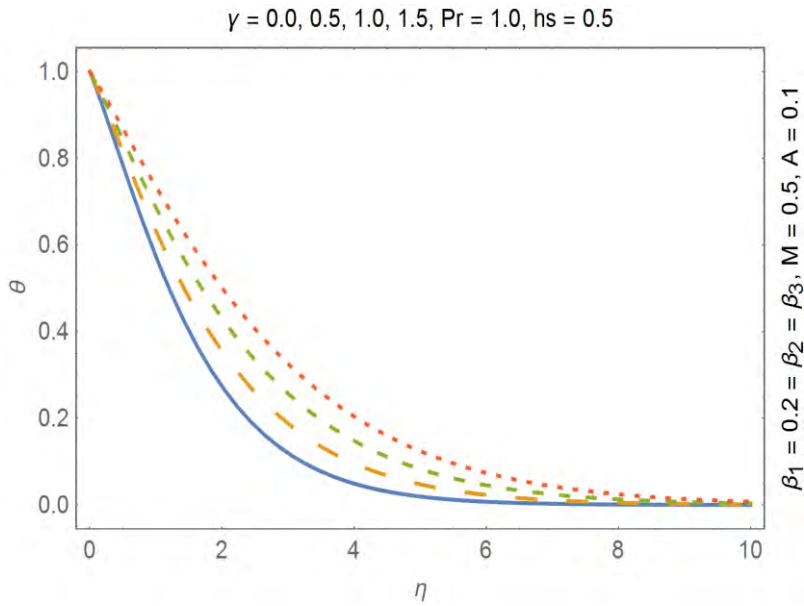
Fig. 6.7: Temperature distribution vs γ.
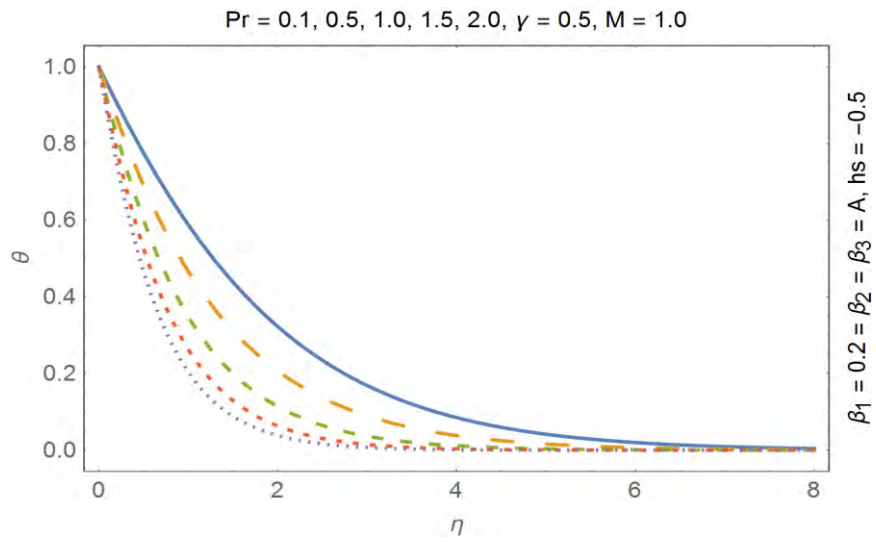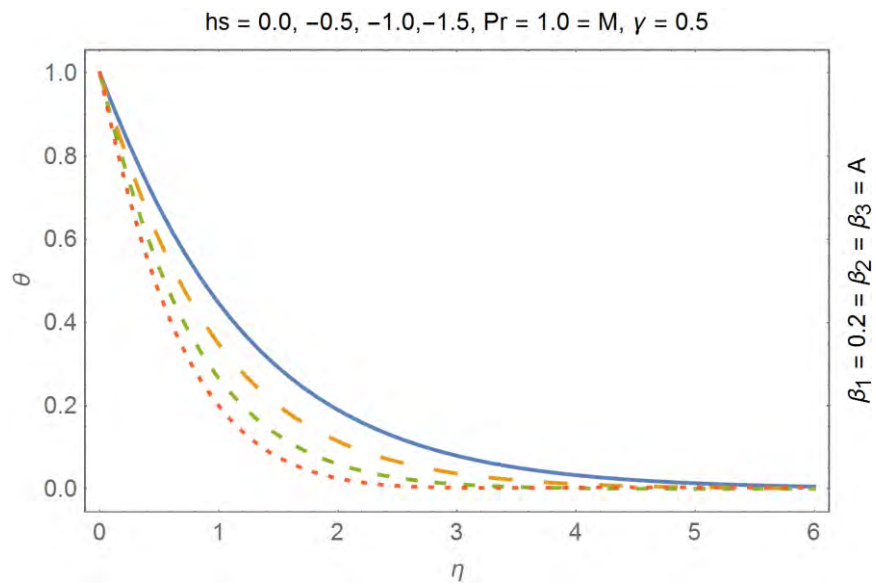
Fig. 6.8: Temprature change vs *Pr*.

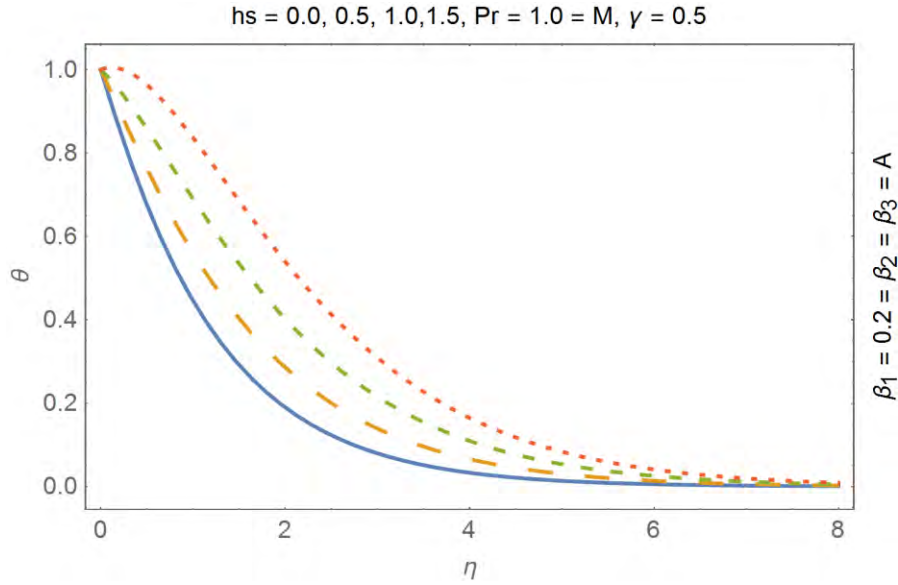Fig. 6.9: Temperature variation vs heat sink.

Fig. 6.10: Temperature change vs heat source.

Table 6.1: Evaluation of $f''(0)$ with published results when $A = 0.0 = \beta_2 = \beta_3 = M$.

β_1	Our results	Sadghey et al. [78]	Mukhopadhyay [79]
0.0	1.000000	1.00000	0.999999
0.4	1.101904	1.10084	1.101851
0.8	1.196712	1.19872	1.196693

Table 6.2: Behavior of $f''(0)$ for various values of Burgers parameter β_2.

β_2	$-f''(0)$
0.0	0.96652
0.2	0.97951
0.4	0.99328
0.6	1.00773
0.8	1.01582
1.0	1.05219

Table 6.3: Numerical values of $\theta'(0)$ for various physical parameters.

β_2	γ	h_s	$-\theta'(0)$
0.0	0.3	-0.2	0.76621
0.2			0.75992
0.4			0.74165
0.2	0.0		0.76105
	0.3		0.75992
	0.6		0.74319
	0.3	-0.2	0.75992
		0.0	0.60445
		0.2	0.41284

6.3 Conclusive remarks

We discussed the CC heat flux for the Burger's fluid model. Some observations are

- Velocity profile and the boundary layer are quite lessor because of the additional viscoelastic effects.
- Streamlines are different for Newtonian and Burger model.
- Temperature distribution is quite smaller for the CC model when compared with the basic Fourier's law.
- A reduction in temperature profile is noted for greater Prandtl number.
- Presence of heat source/sink in the system can efficiently control the temperature to the desired value.

Chapter 7

Second law analysis of Jeffery nanomaterial with magnetic field

We investigate the entropy generation and inclined magnetic field for the Jeffery fluid. Moreover, viscous dissipation and heat generation-absorption effects are considered. Boundary layer is applied to develop the leading equations. Solutions have been computed by using a homotopy approach in the spatial domain. Results are illustrated in graphical form to study the effect of flow parameters. It is analyzed that magnetic field is a flow reducing parameter whereas Biot number behaves like a boosting factor to increase the fluid temperature. The present work is also discussed for Newtonian fluid $(\lambda_1 \rightarrow 0)$

7.1 Problematic development

The dynamics of the Jeffery fluid over stretching wall ($y = 0$) is studied. The material holds onto the region $y > 0$. Magnatic field B_0 is employed at an angle Ψ to the positive direction of the $y-$axes. The considered physical problem is modelled by using a Cartesian coordinate system by taking $x-$axes sideways the stretching surface and $y-$axes in a upright direction. The systematic picture of physical situation and coordinates system is portrayed in Figure 7.1.
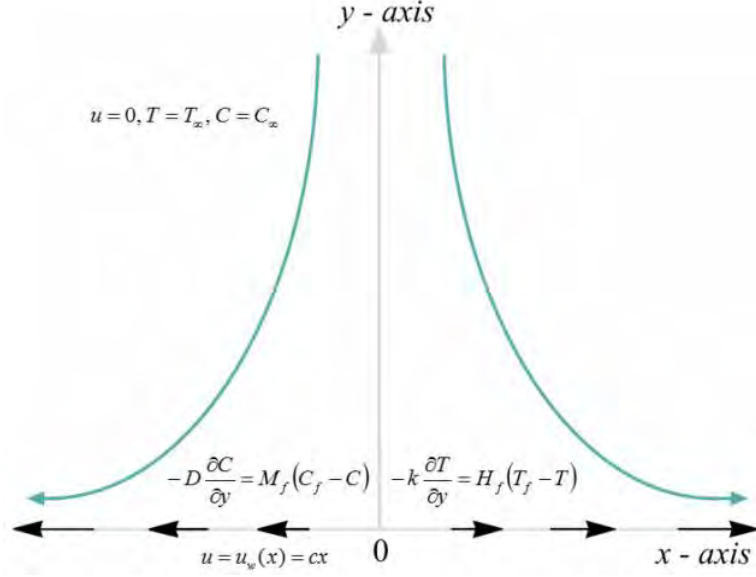
Fig. 7.1: Geometry

Governing equations for the rheology of the viscoelastic nanomaterial are

$$\frac{\partial u}{\partial x} + \frac{\partial v}{\partial y} = 0, \tag{7.1}$$

$$u\frac{\partial u}{\partial x} + v\frac{\partial u}{\partial y} = \frac{\upsilon}{1+\lambda_1}\left[\frac{\partial^2 u}{\partial y^2} + \lambda_2\left(\frac{\partial u}{\partial y}\frac{\partial u^2}{\partial x \partial y} + u\frac{\partial u^3}{\partial x \partial y^2} + \frac{\partial v}{\partial y}\frac{\partial u^2}{\partial y^2} + v\frac{\partial u^3}{\partial y^3}\right) - \frac{\sigma}{\rho}B_0^2\,Sin^2(\Psi)u\right], \tag{7.2}$$

$$u\frac{\partial T}{\partial x} + v\frac{\partial T}{\partial y} = \alpha_m\frac{\partial^2 T}{\partial y^2} + \frac{Q_0}{\rho c_p}(T - T_\infty) + \tau\left[D_B\frac{\partial C}{\partial y}\frac{\partial T}{\partial y} + \frac{D_T}{T_\infty}\left(\frac{\partial T}{\partial y}\right)^2\right] + \frac{\upsilon}{c_p}\left(\frac{\partial u}{\partial y}\right)^2, \tag{7.3}$$

$$u\frac{\partial C}{\partial x} + v\frac{\partial C}{\partial y} = D_B\frac{\partial^2 C}{\partial y^2} + \frac{D_T}{T_\infty}\left(\frac{\partial T}{\partial y}\right)^2, \tag{7.4}$$

Note that Eqs. 7.1-7.4 are deduced from the continuity equation, law of momentum, law of energy and law of concentration respectively.

The supported wall properties are:

$$u = u_w = cx, v = 0, -k\frac{\partial T}{\partial y} = H_w(T_w - T), -D\frac{\partial C}{\partial y} = M_w(C_w - C), \text{ at } y = 0,$$

$$u = 0, v = 0, \ T \to T_\infty, \ C \to C_\infty \text{ as } y \to \infty, \tag{7.5}$$

where (u, v) represent the velocities, σ the electric conductivity, υ the kinematics viscosity, ρ the density, τ the ratio of the heat capacities, α_m the thermal diffusivity constant, D_T the thermophoretic effect, D_B the Brownian diffusion. Moreover, specific heat, heat generation/absorption, mass diffusivity, coefficient of heat transfer, coefficient of mass transfer, thermal conductivity are denoted by c_p, Q_0, D, H_w, M_w, k respectively. Also, T, T_w, T_∞, C, C_w, C_∞ stand for fluid temperature, wall temperature, ambient temperature, concentration, species concentration at the surface and ambient concentration correspondingly.

In the upcoming steps, we apply the suitable transformation in order to convert the set of partial differential equations to the system of ordinary differential equations.

$$\eta = \sqrt{\frac{c}{\upsilon}}y, u = cxf'(\eta), v = -\sqrt{c\upsilon}f(\eta), \theta(\eta) = \frac{T - T_\infty}{T_w - T_\infty}, \ \varphi(\eta) = \frac{C - C_\infty}{C_w - C_\infty}. \tag{7.6}$$

Substitute Eqn. (7.6), in Eqs. $(7.1 - 7.4)$ we have:

$$f''' + (1 + \lambda_1)\left(ff'' - (f')^2 - M \ Sin^2(\Psi)f'\right) + \beta\left((f'')^2 - ff''''\right) = 0, \tag{7.7}$$

$$\theta'' + Pr\left(f\theta' + \lambda\theta + N_b\phi'\theta' + N_t(\theta')^2 + Ec \ (f'')^2\right) = 0, \tag{7.8}$$

$$\varphi'' + Le \ f\varphi' + \frac{N_t}{N_b}\theta'' = 0. \tag{7.9}$$

The dimensionless boundary conditions

$$f(0) = 0, f'(0) = 1, \theta'(0) = -\gamma_1(1 - \theta(0)), \ \phi'(0) = -\gamma_2(1 - \phi(0)),$$

$$f(\infty)=0, \quad \theta(\infty)=0, \quad \phi(\infty)=0, \tag{7.10}$$

where $\beta, Le, Ec, \gamma_1, \gamma_2, \Pr$ specifies the dimensionless Deborah, Lewis, Eckert, heat transfer and mass transfer Biot numbers and Prandtl number respectively. While M denote the magnetic field, N_b the Brownian motion and N_t the thermophoresis. Note that $\lambda > 0$ and $\lambda < 0$ shows heat source and sink respectively and are stated as:

$$\beta = \lambda_2 c, \; Ec = \frac{u_w^2}{c_p\left(T_w - T_\infty\right)}, \; Le = \frac{\upsilon}{D_B}, \; \Pr = \frac{\upsilon}{\alpha_m}, \; \gamma_1 = \frac{H_w}{k}\sqrt{\frac{\upsilon}{c}}, \; \gamma_2 = \frac{M_w}{D}\sqrt{\frac{\upsilon}{c}},$$

$$M = \frac{\sigma}{c\rho}B_0^{\;2}, \; N_t = \tau \, D_T \frac{\left(T_w - T_\infty\right)}{\upsilon T_\infty}, \; N_b = \tau \frac{D_B\left(C_w - C_\infty\right)}{\upsilon}, \; \lambda = \frac{Q_0}{c\rho c_p}. \tag{7.11}$$

The exact solution of Eq. 7.7 for $\Psi = \pi/2$ is

$$f(\eta) = \frac{1 - e^{-m\eta}}{m}, \; m = \left(\frac{1+\lambda_1}{1+\beta}\right)^{1/2}.$$

Notice that its second derivative for velocity $f''(\eta) = -me^{-m\eta}$ which further gives the velocity gradient at the wall with the exact result to be $f''(0) = -m$.

The volumetric entropy generation term $\left(S_G\right)$ and the characteristic entropy generation rate $\left(S_g\right)$ are expressed as:

$$S_G = \frac{k}{T_\infty^{\;2}}\left(\frac{\partial T}{\partial y}\right)^2 + \frac{\mu}{T_\infty}\left(\frac{\partial u}{\partial y}\right)^2 + \frac{\sigma B_0^2}{T_\infty}Sin(\Psi)u^2, \quad S_g = \frac{k}{T_\infty^{\;2}}\left(\frac{\Delta T}{l}\right)^2. \tag{7.12}$$

The entropy generation Ns in non-dimensional form is

$$Ns = \frac{S_G}{S_g} = \mathrm{Re}_l\left(\theta'\right)^2 + \frac{\mathrm{Re}_l \, Br}{\zeta}\left(f''\right)^2 + \frac{Ha^2 \, Br}{\zeta}Sin(\Psi)\left(f'\right)^2. \tag{7.13}$$

Eq. 7.12 describes the three roots for the generation of entropy:

- Ist term is achieved because of the heat transfer N_H irreversibility.

- We get the second term for the reason that the effects of viscous dissipation N_V are present.

- The third expression is accomplished since the effects of magnetic field N_M are present.

Additionally the dimensionless numbers apperaing in the system of equations are "Reynolds number (Re_l), Hartman number (Ha), finite temperature difference (ζ), Brinkmann number (Br)" and expressed as:

$$\mathrm{Re}_l = \frac{u_l}{\upsilon} l, \; Br = \frac{\mu}{k\,\Delta T} u_w^2(x), \; Ha^2 = B_0 \sqrt{\frac{\sigma}{\mu}} l, \; \zeta = \frac{\Delta T}{T_\infty}. \tag{7.14}$$

The series solution of Eqs. $(7.7-7.9)$ under conditions 7.10 are calculated via homotopy approach. The guesses and operators for f, θ and ϕ are defined below

$$f_0(\eta = 1 - \exp(-\eta), \; \theta_0(\eta) = \frac{\gamma_1}{1+\gamma_1} \exp(-\eta), \; \phi_0(\eta) = \frac{\gamma_2}{1+\gamma_2} \exp(-\eta),$$

and

$$L_f(f) = f''' - f', \; L_\theta(\theta) = \theta'' - \theta, \; L_\varphi(\varphi) = \varphi'' - \varphi. \tag{7.15}$$

A MATHEMATICA computer program has been constructed for HAM. The exact and HAM solutions are portrayed in Figure 7.2 and 7.3. Both exact solution and the series solution are in an agreement.
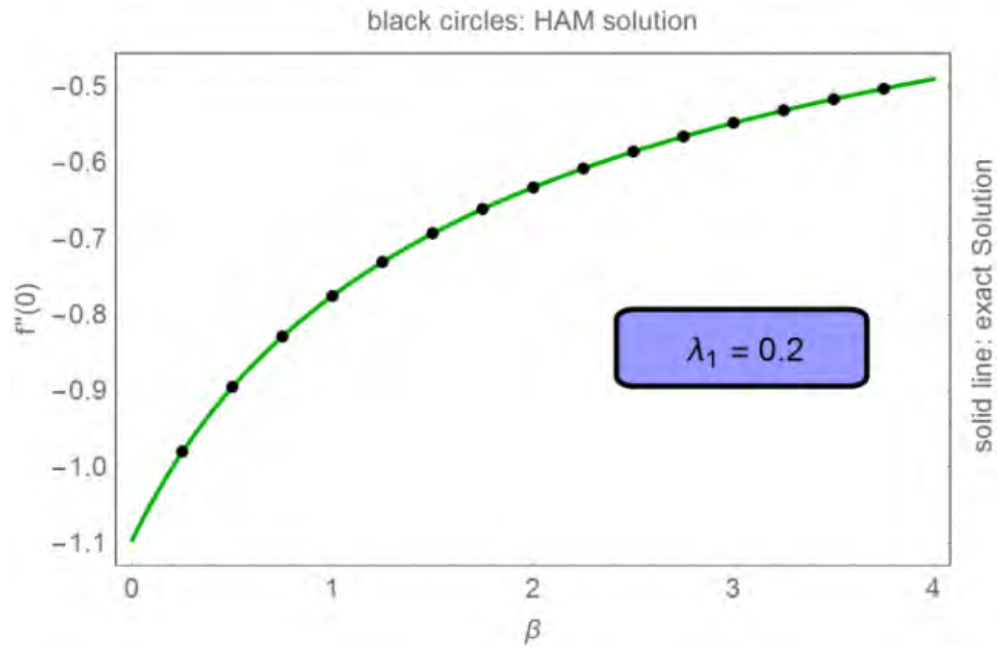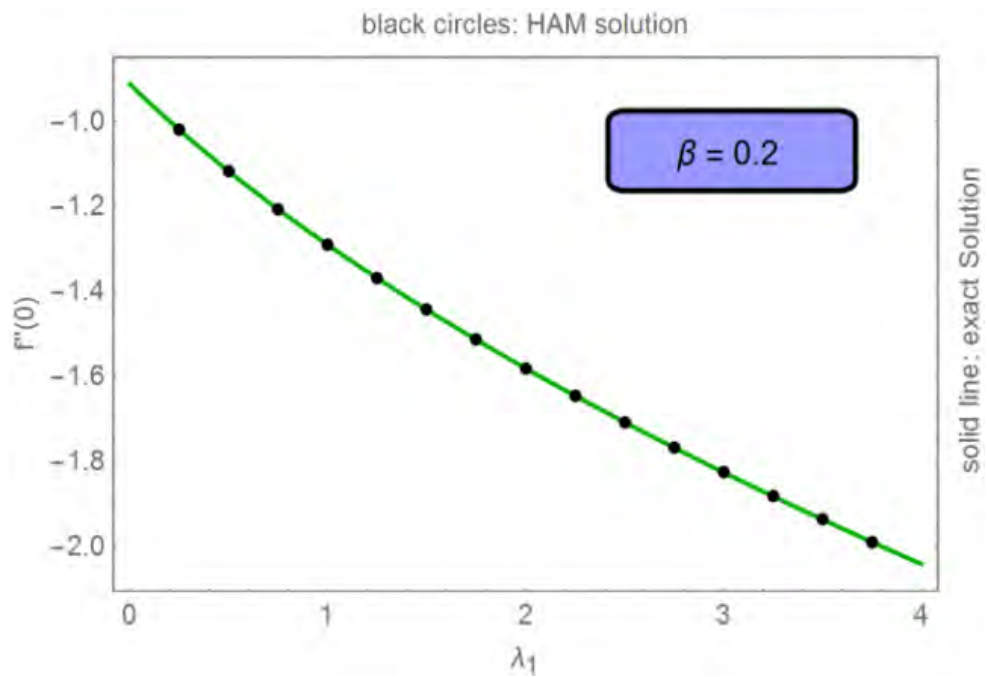
Fig. 7.2: Impact in $f''(0)$ with β.

Fig. 7.3: Impact of $f''(0)$ with λ_1.

7.2 Results and discussion

Results are sketched to demonstrate the performance of various evolving constraints for the momentum, thermal and concentration distributions. Fig. 7.4 gives the effect of β on the velocity graph. It is perceived that when a magnetic field is constant the Deborah number develop the flow configuration. Both the elasticity and viscosity are led by the Deborah number. As the Deborah number takes the low value the material acts like viscous whereas for greater values of β, the fluid acts to be non-Newtonian. Using this concept results are graphed for lesser values of Deborah number. Fig. 7.5 is portrayed to visualize the behavior of angle of inclination Ψ on the velocity. It is noted by increasing the value of Ψ, the velocity profile decreases. We have studied that by increasing the angle of inclination, the influence of magnetic field rises and thus the Lorentz force enhance. In results of that velocity profile decays. Fig. 7.6 explains the behavior of N_b and N_t on temperature field. Notice that growing value of both N_b and N_t improves temperature profile rapidly. Brownian motion appears due to the size of nanoparticles which disturbs the rate of heat transfer. Enhancement in the magnitude of the Brownian motion results into the efficient movement in the nanoparticles. So the thermal conductivity of the fluid particles is improved. Fig. 7.7 portrays the impact of Biot number γ_1 on $\theta(\eta)$. It is the relation of the heat conduction resistances at the interior and at the exterior of material. It is noticed that as Biot number increases the temperature of the fluid rises. When Biot number is less than 0.1, it specifies that heat transfer inside the material is greater than the convection away from its surface. Fig. 7.8 shows the impact of Brownian motion and thermophoresis parameter on concentration. It is apparent that by increasing the magnitude of Brownian motion and thermophoresis the nanoparticle concentration grows. Fig. 7.9 is organized to examine the effect of γ_2 on mass concentration $\phi(\eta)$. It specifies that increase of mass Biot number improves the concentration field. Results are well compared and presented in tabular form. It is detected that $f''(0)$ decreases with the improvement in β, but $f''(0)$ grow as $\lambda_1 \to \infty$.
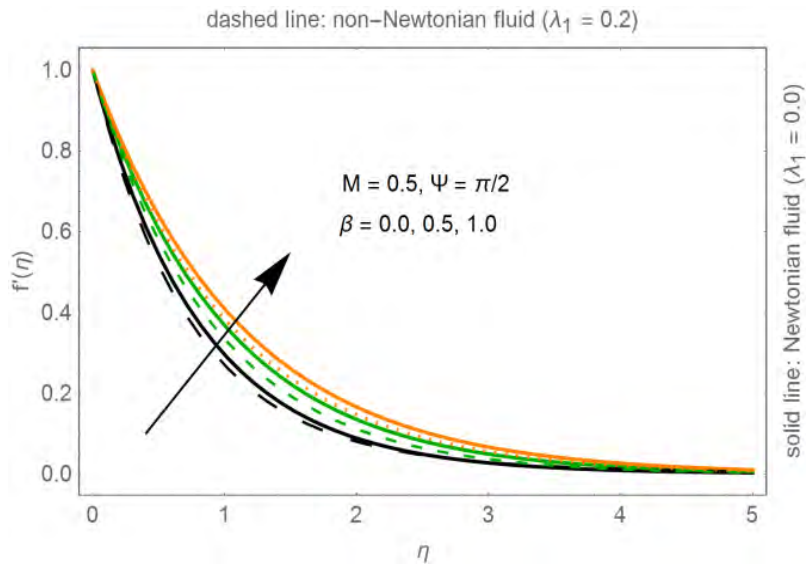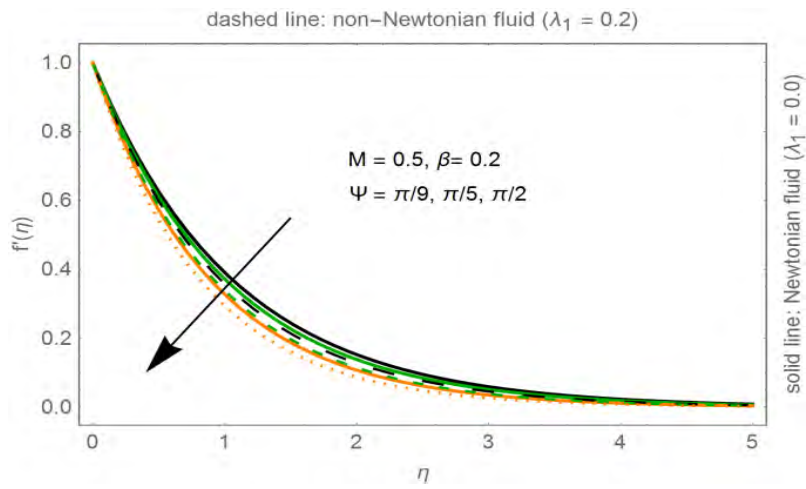
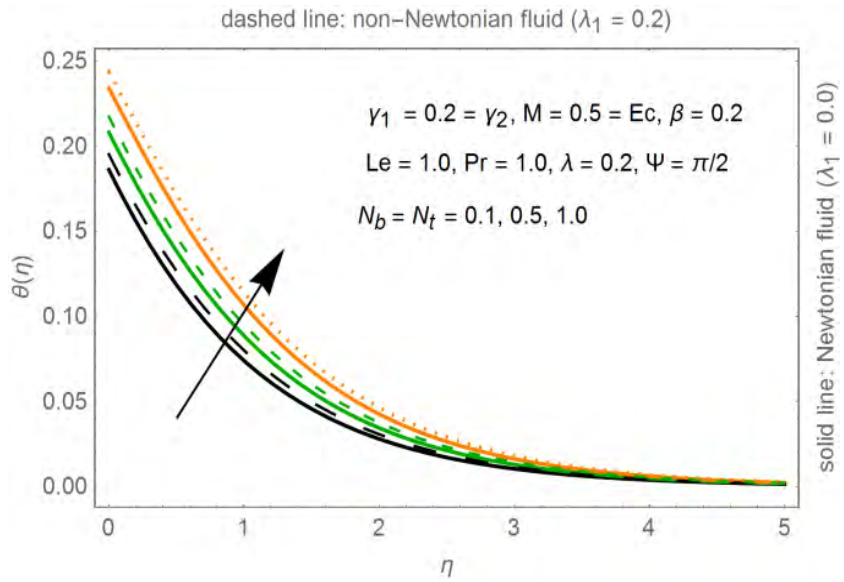Fig. 7.4: Velocity change vs β.

Fig. 7.5: Velocity change vs Ψ.

Fig. 7.6: Temperature change vs $\left(N_b, N_t\right)$.

Fig. 7.7: Variation of γ_1 on $\theta(\eta)$.

γ_1 = 0.2 = γ_2, M = 0.5 = Ec, β = 0.2

Le = 1.0, Pr = 1.0, λ = 0.2, Ψ = $\pi/2$

N_b = N_t = 0.1, 0.5, 1.0

solid line: Newtonian fluid (λ_1 = 0.0)
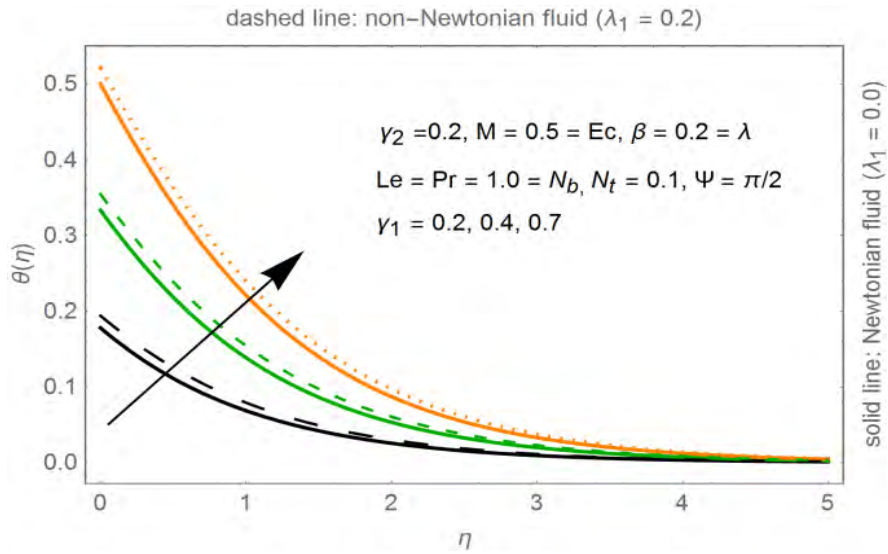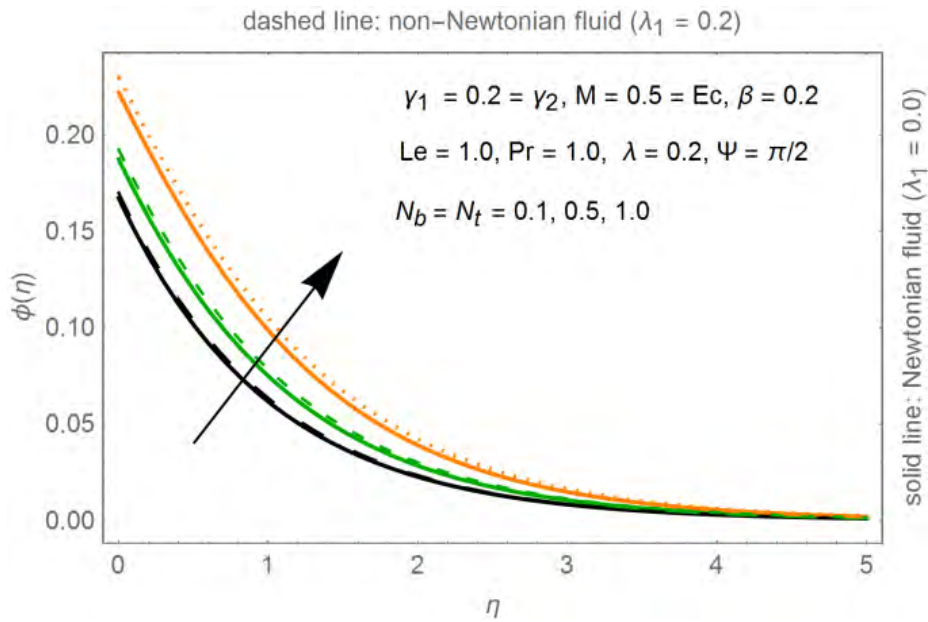
Fig. 7.8: Variation of N_b, N_t on $\phi(\eta)$.

γ_1 = 0.2, M = 0.5 = Ec, β = 0.2 = λ

Le = Pr = 1.0 = N_b, N_t = 0.1, Ψ = $\pi/2$

γ_2 = 0.2, 0.4, 0.7

solid line: Newtonian fluid (λ_1 = 0.0)
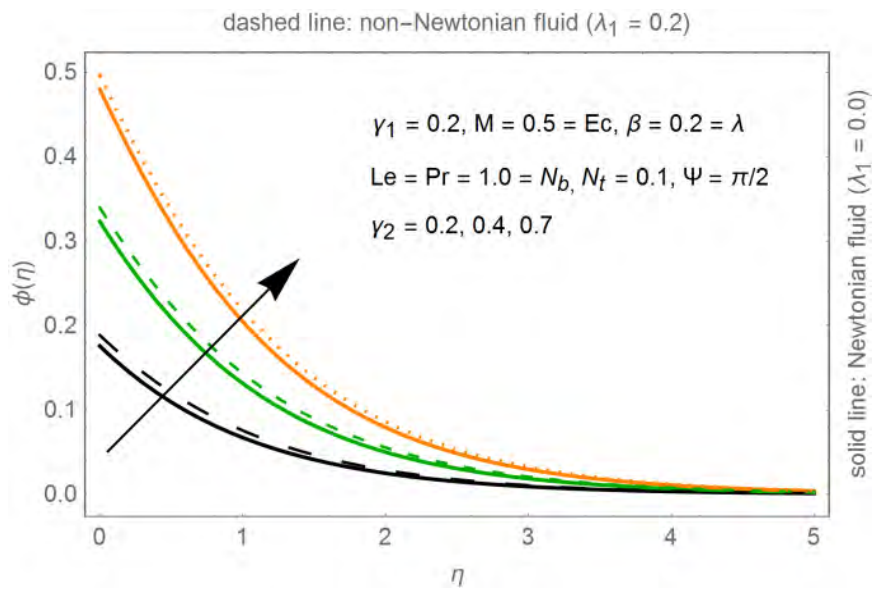
Fig. 7.9: Variation of γ_2 on $\phi(\eta)$.

Table 7.1. Comparison of results

Parameter	HAM (present)	Numerical solution [80]	Exact solution [81]
β	$-f''(0)$	$-f''(0)$	$-f''(0)$
0.0	1.09641491	1.09641580	1.09544512
0.4	0.92723121	0.92724220	0.92582010
0.8	0.81807191	0.81808091	0.81649658
1.2	0.74010411	0.74010502	0.73854895
1.6	0.68073213	0.68074654	0.67936622
2.0	0.63351345	0.63352833	0.63245553
2.4	0.59474926	0.59473195	0.59408853
2.8	0.56201236	0.56205463	0.56195149
3.2	0.53390910	0.53398720	0.53452248
3.6	0.50944571	0.50949569	0.51075392
4.0	0.48782645	0.48784584	0.48989795

Table 7.2. Evaluation of $f''(0)$.

Parameter	HAM (present)	Numerical solution [80]	Exact solution [81]
λ_1	$-f''(0)$	$-f''(0)$	$-f''(0)$
0.0	0.91467231	0.91468190	0.91287093
0.4	1.08101045	1.08100090	1.08012345
0.8	1.22523245	1.22521512	1.22474487
1.2	1.35422340	1.35427540	1.35400640
1.6	1.47211231	1.47212137	1.47196014
2.0	1.58122891	1.58123895	1.58113883
2.4	1.68332391	1.68331479	1.68325082
2.8	1.77956545	1.77955488	1.77951304
3.2	1.87083401	1.87085660	1.87082869
3.6	1.95791792	1.95790896	1.95789002
4.0	2.04126541	2.04125449	2.04124145

Figs. 7.10-7.12 are organized to explore the influence of Brinkman Br, Hartman Ha and Reynolds number Re on entropy number Ns. Fig. 7.13 explains the behavior of temperature difference ς on entropy number Ns. Fig. 7.10 explains entropy against Brinkman number Br. Entropy increases by growing Br. At $(\eta = 0)$ the entropy is larger against Br. It is noted that

entropy is more projecting near the surface. Moreover these effects decline rapidly far from sheet. The effect of Hartman number *Ha* on the entropy number is shown in Fig. 7.11. Entropy increases by growing the value of Hartman number. The entropy is related to the square of Hartman number which is proportionate with the magnetic field. Thus the magnetic field generates additional entropy. Fig. 7.12 portrays the entropy field for several values of the Reynolds number *Re*. It is witnessed that for growing values of Re_l the entropy also increases. We know that by increasing the value of Reynolds number, the inertial forces are improved whereas the viscous forces decay. So, the velocity of fluid particles is increased and the resistance on the fluid motion due to the friction is reduced. Thus, the magnitude of entropy has been enhanced. The effect of finite temperature difference ζ on the entropy is shown in Fig. 7.13. It is seen that by growing ζ the entropy of the system will be reduced. From literature we already know that ζ is inversely related with the velocity distribution which reduce the entropy generation for greater values of ζ .
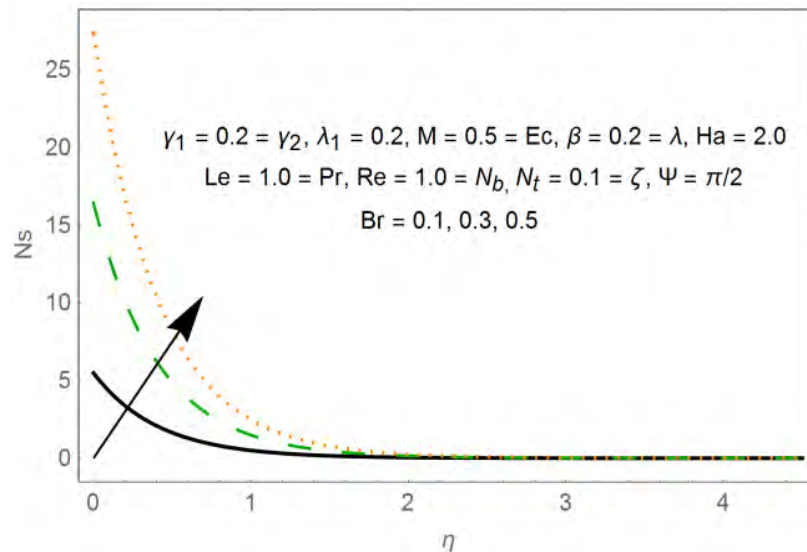
Fig. 7.10. *Br* variations on *Ns* .
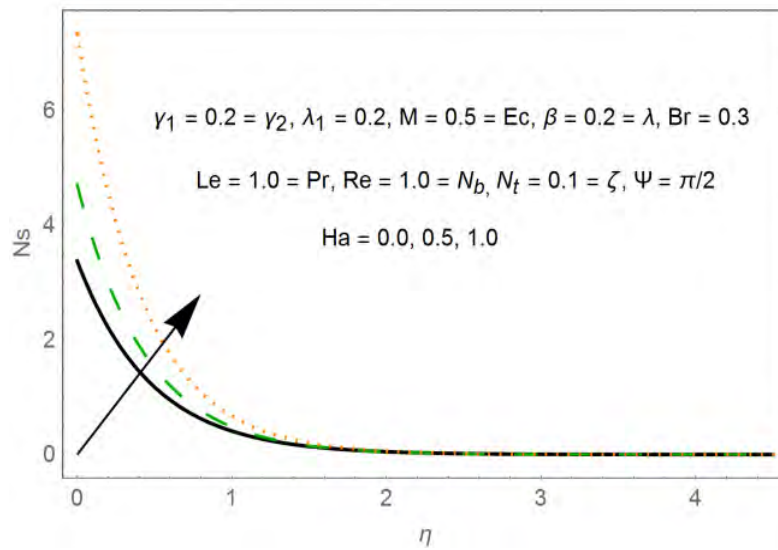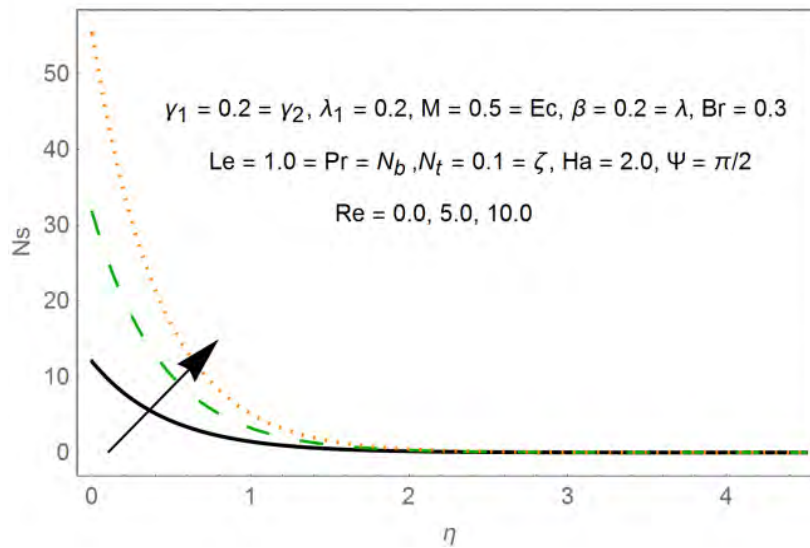
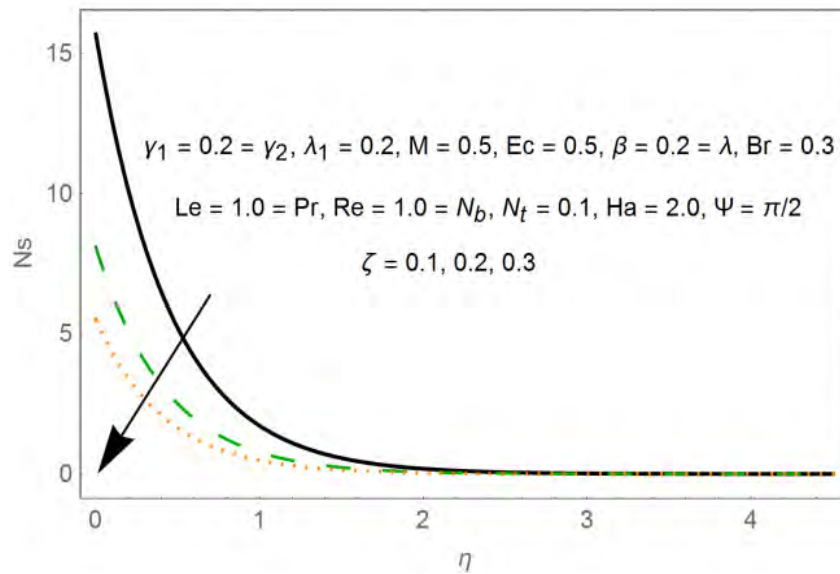Fig. 7.11. *Ha* variations on *Ns*.

Fig. 7.12. Re variations on *Ns*.

Fig. 7.13. ξ variations on Ns.

7.3 Conclusive remarks

- Newtonian flow can be attained by considering $\lambda_1 \to 0$.

- By increasing the value of inclination angle Ψ, the fluid motion slow down.

- The velocity field for Newtonian fluid is lesser than the non-Newtonian fluid model.

- Rise in $\left(N_b, N_t, \gamma_1, \gamma_2\right)$ efficiently improves the temperature and concentration fields.

- Reduction in the magnitude of Brinkman, Hartman and Reynolds number minimize the entropy.

Chapter 8

3D study of Oldroyd-B nanofluid with radiations

In this chapter, 3D dynamics of Oldroyd-B fluid have been discussed while incorporating the effects due to the existence of nanoparticles. The present physical problem is studied under influence of nonlinear radiations. During mathematical formulation, the diffusion equations are shown under thermophoretic and Brownian effect. Bidirectional stretching is taken to study the three-dimensional fluid deformation of non-Newtonian (polymeric) liquid. We achieve set of ODEs by employing similarity analysis on the governing partial differential equations. Further, solution in the series form is calculated by using the Homotopy approach. Graphs and tables are prepared for several quantities.

8.1 Formulating the physical problem

Consider the dynamics of Oldroyd-B model with nanoparticles. The deformation in the fluid particles is due to the bidirectional stretching. Motion of the particles is along *x*- and *y*- direction and deformation is along *z*- direction as revealed in the Fig. 8.1.
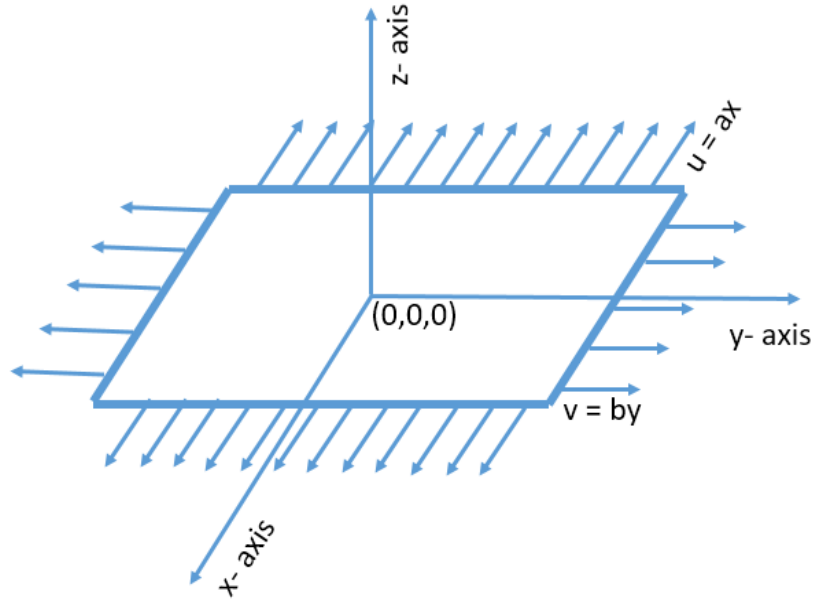
Fig. 8.1: Physical model.

The constitutive equations are

$$\nabla.\mathbf{V} = 0, \tag{8.1}$$

$$\rho \frac{d\mathbf{V}}{dt} = div\mathbf{T}. \tag{8.2}$$

Note that the flow is governed under the assumption that the fluid is incompressible and no body forces are present in the system. In the above equation 8.2, Cauchy stress tensor is denoted by **T** and extra stress tensor is symbolized by **S** and for Oldroyd-B fluid they are

$$\mathbf{T} = -p\mathbf{I} + \mathbf{S}, \tag{8.3}$$

$$\left(1 + \lambda_1 \frac{D}{Dt}\right)\mathbf{S} = \mu\left(1 + \lambda_2 \frac{D}{Dt}\right)\mathbf{A}_1. \tag{8.4}$$

In the above equations, D/Dt represents covariant derivative and Rivlin Ericksen tensor $\mathbf{A}_1$ is

$$\mathbf{A}_1 = \nabla\mathbf{V} + \left(\nabla\mathbf{V}\right)^{tran.}, \tag{8.5}$$

where velocity field is $\mathbf{V} = [u(x,y,z), v(x,y,z), w(x,y,z)]$ and the definition for D/Dt is obtained from literature

99

$$\frac{Da_i}{Dt} = \frac{\partial a_i}{\partial t} + u_r a_{i,r} - u_{i,r} a_r.$$ (8.6)

System of equations for the flow field is

$$\frac{\partial u}{\partial x} + \frac{\partial v}{\partial y} + \frac{\partial w}{\partial z} = 0,$$ (8.7)

$$u\frac{\partial u}{\partial x} + v\frac{\partial u}{\partial y} + w\frac{\partial u}{\partial z} + \lambda_1\left(u^2\frac{\partial^2 u}{\partial x^2} + v^2\frac{\partial^2 u}{\partial y^2} + w^2\frac{\partial^2 u}{\partial z^2} + 2uv\frac{\partial^2 u}{\partial x\partial y} + 2uw\frac{\partial^2 u}{\partial x\partial z} + 2vw\frac{\partial^2 u}{\partial y\partial z}\right)$$
$$= \upsilon\left[\frac{\partial^2 u}{\partial z^2} + \lambda_2\left(u\frac{\partial^3 u}{\partial x\partial z^2} + v\frac{\partial^3 u}{\partial y\partial z^2} + w\frac{\partial^3 u}{\partial z^3} - \frac{\partial u}{\partial y}\frac{\partial^2 v}{\partial z^2} - \frac{\partial u}{\partial x}\frac{\partial^2 u}{\partial z^2} - \frac{\partial u}{\partial z}\frac{\partial^2 w}{\partial z^2}\right)\right],$$ (8.8)

$$u\frac{\partial v}{\partial x} + v\frac{\partial v}{\partial y} + w\frac{\partial v}{\partial z} + \lambda_1\left(u^2\frac{\partial^2 v}{\partial x^2} + v^2\frac{\partial^2 v}{\partial y^2} + w^2\frac{\partial^2 v}{\partial z^2} + 2uv\frac{\partial^2 v}{\partial x\partial y} + 2vw\frac{\partial^2 v}{\partial y\partial z} + 2uw\frac{\partial^2 v}{\partial x\partial z}\right)$$
$$= \upsilon\left[\frac{\partial^2 v}{\partial z^2} + \lambda_2\left(u\frac{\partial^3 v}{\partial x\partial z^2} + v\frac{\partial^3 v}{\partial y\partial z^2} + w\frac{\partial^3 v}{\partial z^3} - \frac{\partial v}{\partial x}\frac{\partial^2 u}{\partial z^2} - \frac{\partial v}{\partial y}\frac{\partial^2 v}{\partial z^2} - \frac{\partial v}{\partial z}\frac{\partial^2 w}{\partial z^2}\right)\right],$$ (8.9)

$$u\frac{\partial T}{\partial x} + v\frac{\partial T}{\partial y} + w\frac{\partial T}{\partial z} = \frac{(\rho C)_P}{(\rho C)_f}\left(D_B\left(\frac{\partial T}{\partial z}\frac{\partial C}{\partial z}\right) + \frac{D_T}{T_\infty}\left(\frac{\partial T}{\partial y}\right)^2\right) + \alpha\frac{\partial^2 T}{\partial z^2} - \frac{1}{(\rho C)_f}\frac{\partial q_r}{\partial z},$$ (8.10)

$$u\frac{\partial C}{\partial x} + v\frac{\partial C}{\partial y} + w\frac{\partial C}{\partial z} = D_B\left(\frac{\partial^2 C}{\partial y^2}\right) + \frac{D_T}{T_\infty}\left(\frac{\partial^2 T}{\partial y^2}\right).$$ (8.11)

Wall conditions are

$$u = U_w(x) = ax, \ v = V_w(y) = by, \ w = 0, \ T = T_w, \ D_B\frac{\partial C}{\partial z} + \frac{D_T}{T_\infty}\frac{\partial T}{\partial z} = 0, \text{ at } z = 0.,$$

$$u \to 0, \ v \to 0, \ T \to T_\infty, \ C \to C_\infty, \quad \text{as} \quad z \to \infty.$$ (8.12)

The radiative flux q_r is expressed as

$$q_r = -\frac{4\delta^*}{3k^*}\frac{\partial T^4}{\partial z} = -\frac{16\delta^*}{3k^*}T^3\frac{\partial T}{\partial z}. \tag{8.13}$$

In the above mentioned equations, k^* is absorption coefficient and δ^* denotes Stefan-Boltzmann constant.

Equation for the temperature field turns to be

$$u\frac{\partial T}{\partial x} + v\frac{\partial T}{\partial y} + w\frac{\partial T}{\partial z} = \frac{\partial}{\partial z}\left(\left(\alpha + \frac{16\delta^* T^3}{3k^*(\rho C)_f}\right)\right) + \frac{(\rho C)_P}{(\rho C)_f}\left(D_B\left(\frac{\partial T}{\partial z}\frac{\partial C}{\partial z}\right) + \frac{D_T}{T_\infty}\left(\frac{\partial T}{\partial y}\right)^2\right). \tag{8.14}$$

Now applying

$$u = axf'(\eta),\ v = ayg'(\eta),\ w = -(a\upsilon)^{1/2}(f'(\eta)+g'(\eta)),$$

$$\theta(\eta) = \frac{T-T_\infty}{T_W-T_\infty},\ \varphi(\eta) = \frac{C-C_\infty}{C_W-C_\infty},\ \eta = \left(\frac{a}{\upsilon}\right)^{1/2}z. \tag{8.15}$$

Using $T = (1-\theta(1-\theta_W))T_\infty$ where $\theta_w = T_w/T_\infty$.

Eq. (8.7) is satisfied individually and Eq. (8.8)-(8.11) are transfigured to

$$f''' + f''(f+g) - (f')^2 + \beta_1\left[2ff''(f+g) - f'''(f+g)^2\right]$$
$$+\beta_2\left[f''(f''+g'') - f''''(f+g)\right] = 0, \tag{8.16}$$

$$g''' + g''(f+g) - (g')^2 + \beta_1\left[2g'g''(f+g) - g'''(f+g)^2\right]$$
$$+\beta_2\left[g''(f''+g'') - g''''(f+g)\right] = 0, \tag{8.17}$$

$$\left(\left(1+R_d\left(1+(\theta_w-1)\theta\right)^3\right)\theta'\right)' + \Pr\left((f+g)\theta' - f'\theta + N_b\theta'\varphi' + N_t\theta'^2\right) = 0, \tag{8.18}$$

$$\varphi'' + Le\Pr(f+g)\varphi' + (N_t/N_b)\theta'' = 0, \tag{8.19}$$

The boundary conditions after employing transformations are

$$f = 0,\ g = 0, f' = 1, g' = A, \theta = 1, N_b\varphi' + N_t\theta' = 0, \quad \text{at} \quad \eta = 0, \tag{8.20}$$

$$f' \to 0, g' \to 0, \theta \to 0, \varphi \to 0, \text{as } \eta \to \infty. \tag{8.21}$$

In the above terms β_1 and β_2 are Deborah numbers, N_b and N_t represent Brownian effect and thermophoresis, Le and Pr are Lewis and Prandtl number and R_d is the radiation parameter and A is the stretching ratio which are further stated as:

$$\beta_1 = a\lambda_1, \beta_2 = a\lambda_2, A = \frac{b}{a}, R_d = \frac{16\delta^* T_\infty^3}{3kk^*}, N_b = \frac{(\rho c)_p D_B (C_w - C_\infty)}{(\rho c)_f \upsilon},$$

$$Pr = \frac{\upsilon}{\alpha}, Le = \frac{\alpha}{D_B}, N_t = \frac{(\rho c)_p D_T (T_w - T_\infty)}{(\rho c)_f \upsilon T_\infty}.$$

(8.22)

Nusselt and Sherwood numbers are

$$Re_x^{-1/2} Nu_x = -(1 + R_d \theta_w^3)\theta'(0) ,$$

$$Re_x^{-1/2} Sh_x = -\varphi'(0).$$

(8.23)

Where $Re_x = U_w x / v$.

The initial guesses and operator which are utilized for computation of solution are

$$f_\circ(\eta) = 1 - e^{-\eta}, g_\circ(\eta) = A(1 - e^{-\eta}), \theta_\circ(\eta) = e^{-\eta}, \varphi_\circ(\eta) = -(N_t / N_b)e^{-\eta},$$

(8.24)

$$L_f = f''' - f', L_g = g''' - g', L_\theta = \theta'' - \theta, L_\varphi = \varphi'' - \varphi.$$

(8.25)

The above mentioned operators have the following features

$$L_f[c_1 + c_2 e^\eta + c_3 e^{-\eta}] = 0, L_g[c_4 + c_5 e^\eta + c_6 e^{-\eta}] = 0,$$
$$L_\theta[c_7 e^\eta + c_8 e^{-\eta}] = 0, L_\varphi[c_9 e^\eta + c_{10} e^{-\eta}] = 0.$$

(8.26)

8.2 Convergence of the solution

The curves as prepared as shown in Figs. 8.2 and 8.3. These geometries present that domain of the convergence is $-1.05 \leq h_f \leq -0.01$, $-1.15 \leq h_g \leq -0.05$, $-1.1 \leq h_\theta \leq -0.1$ and $-1.13 \leq h_\phi \leq -0.1$. The results are convergent in domain of η when we have $h_f = h_g = h_\theta = h_\phi = -0.6$. The geometries describe h curves for the error of $f(\eta)$ and $g(\eta)$, which are utilized to get suitable values of h. Appropriate value for h is taken to obtain convergence upto six decimal place. Figs. 8.4 and 8.5 are drawn to analyze h-curves. Table 8.1 present the convergence.
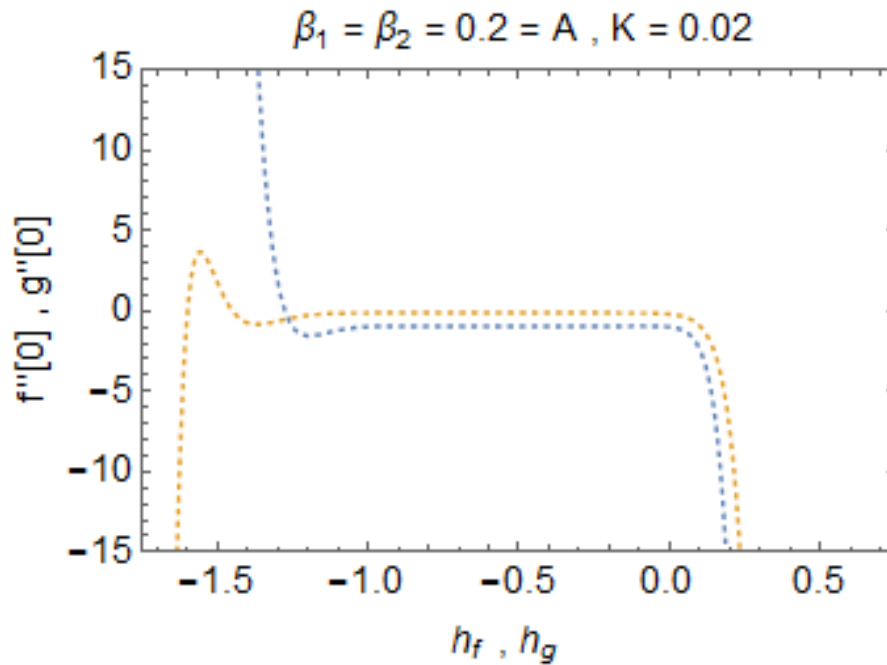
Fig. 8.2: h-curves.
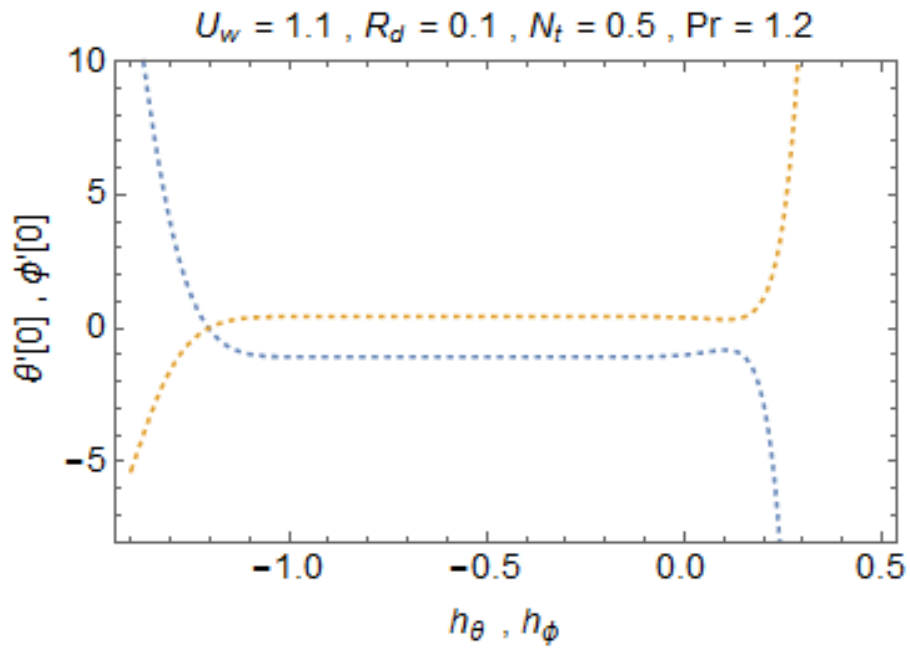
Fig. 8.3: h-curves.
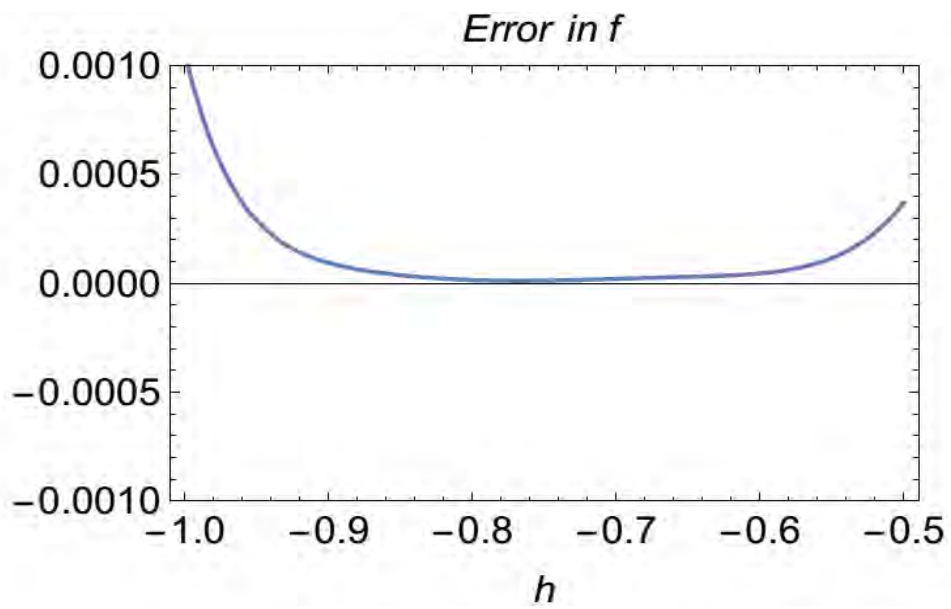
Fig. 8.4: Error graph.
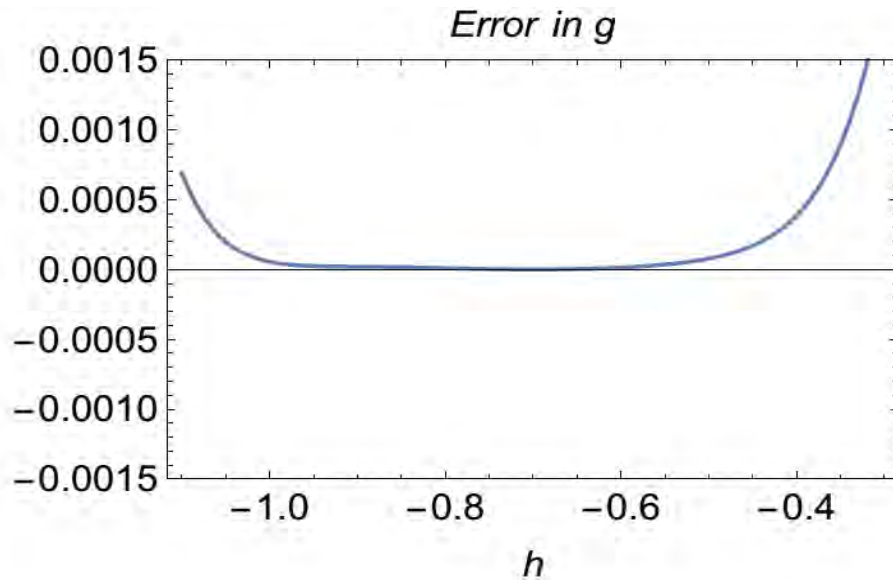
Fig. 8.5: Error graph.

Table 8. 1: Convergence table

Order	$-f''(0)$	$-g''(0)$	$-\theta'(0)$	$-\varphi'(0)$	CPU time
1	0.9360000	0.1456000	1.042402	−0.4169608	2 sec.
5	0.9475450	0.1317675	1.080406	−0.4321625	10 sec.
10	0.9470198	0.1321204	1.074371	−0.4297483	35 sec.
15	0.9470315	0.1321265	1.072644	−0.4290577	80 sec.
20	0.9470355	0.1321210	1.072654	−0.4290617	150 sec.
30	0.9469867	0.1321123	1.072709	−0.4290837	250 sec.

105

8.3 Results and analysis

Influences of Deborah number β_1 on the heat and mass transfer are presented in Figs. 8.6 and 8.7. It is observed that by raising the value of β_1, there is reduction in temperature as well as in concentration flux due to increasing relaxation time. Figs. 8.8 and 8.9 exhibits that Deborah number β_2 depending on retardation time rises temperature as well as concentration flux. Thus it is showing the increasing behavior. Effect of Brownian motion N_b on the concentration flux is displayed in Fig. 8.10. It is witnessed that concentration decreases as N_b grows. It is revealed in Fig. 8.11 that thermophoresis Parameter N_t and temperature flux are in inverse relation. Temperature decays for growth in the value of N_t. However it is observed in Fig. 8.12 that N_t is related directly with mass concentration. Fig. 8.13 defines that an increase in *Le* decreases mass diffusion that indicate reduction in concentration. It is demonstrated in Fig. 8.14 that by raising the value of radiation parameter R_d, temperature flux reduces. Influences of Deborah numbers β_1 and β_2 on $f'(\eta)$ are analyzed in Figs. 8.15 and 8.16. It is noted that β_1 and β_2 have inverse relation on $f'(\eta)$. $f'(\eta)$ lessens with the growth in β_1 but development in fluid velocity $f'(\eta)$ is investigated as β_2 rises. Figs. 8.17 and 8.18 describe the impact of β_1 and β_2 on velocity component $g'(\eta)$. Fig.8. 17 explains that $g'(\eta)$ decays by rising β_1 and grows with the improvement in β_2. It is clear from Fig 8.19 that isolines show growth in behavior by rising the values of R_d. Fig. 8.20 explains the effects of N_b and N_t on $\theta(\eta)$. By rising N_b and N_b, the temperature field is improved. Impact of N_b and N_t on $\phi(\eta)$ are given in Fig. 8.21. It is witnessed that concentration profile decays because of the random motion of nanoparticles. Table 8.2 is displayed to show the effects of different variables over local Nusselt and Sherwood numbers by considering remaining parameters constant. It is investigated that Nusselt number $N_u/\text{Re}^{1/2}$ intensify for increase in *A*, *Pr*, β_2 and decay by rising N_t, *Le* and β_1. However, numerical value of Sherwood number rises by increasing *A*, N_t, *Pr*, β_2 and falls for the greater N_b, Le and β_1.

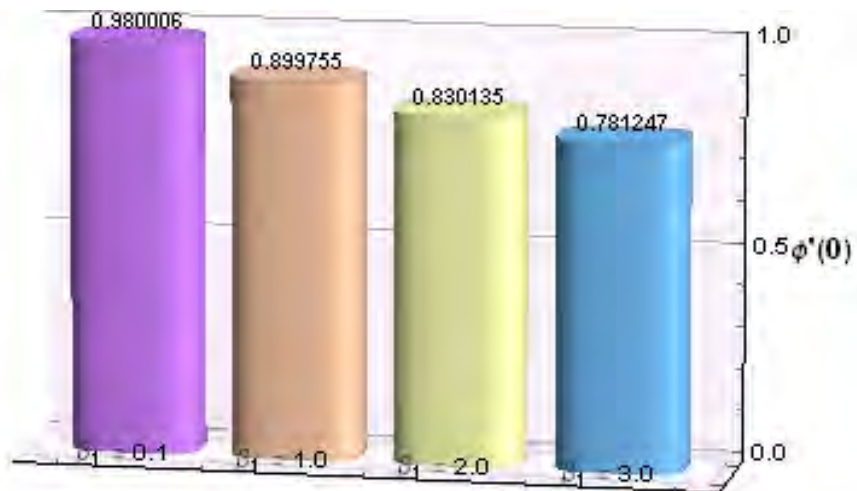Fig. 8.6: Influence of β_1 on temperature derivative.

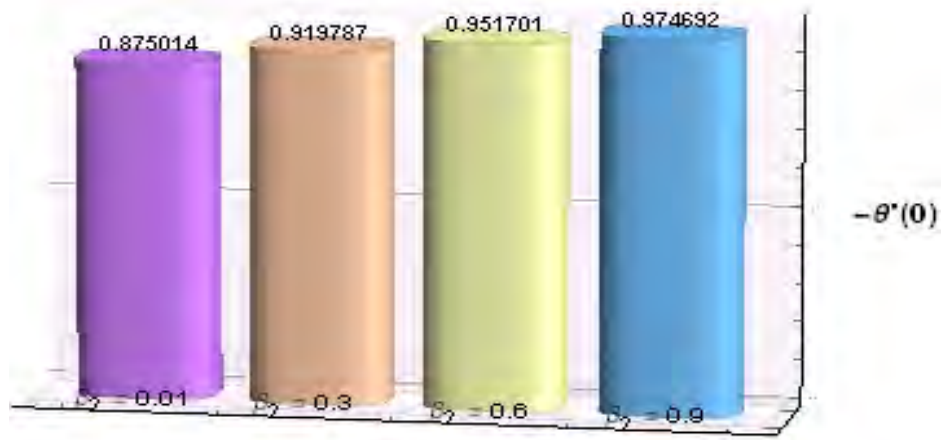Fig. 8.7 Influence of β_1 on concentration derivative.

107

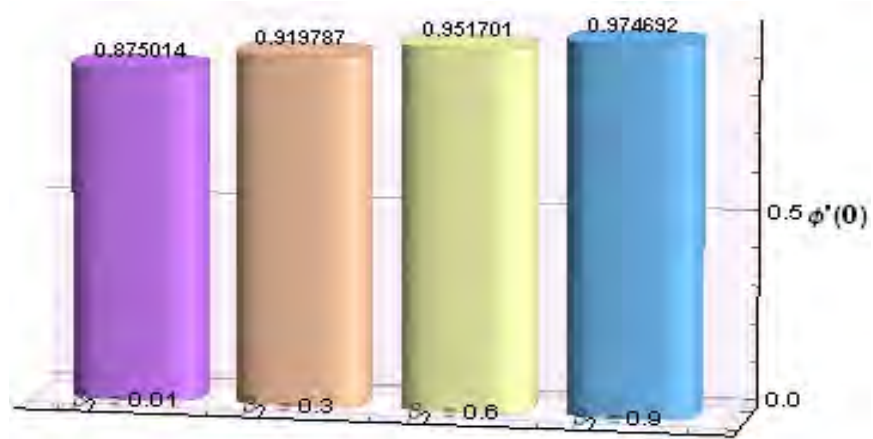Fig. 8.8: Influence of β_2 on temperature derivative.

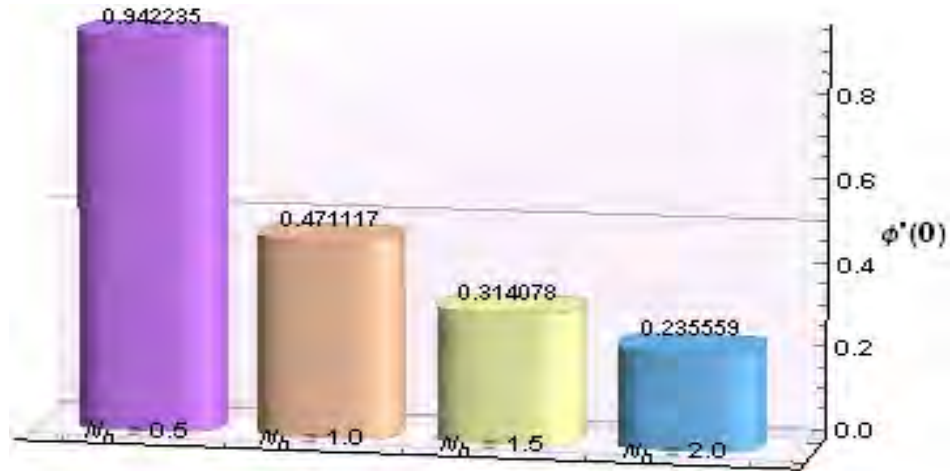Fig. 8.9: Influence of β_2 on concentration derivative.

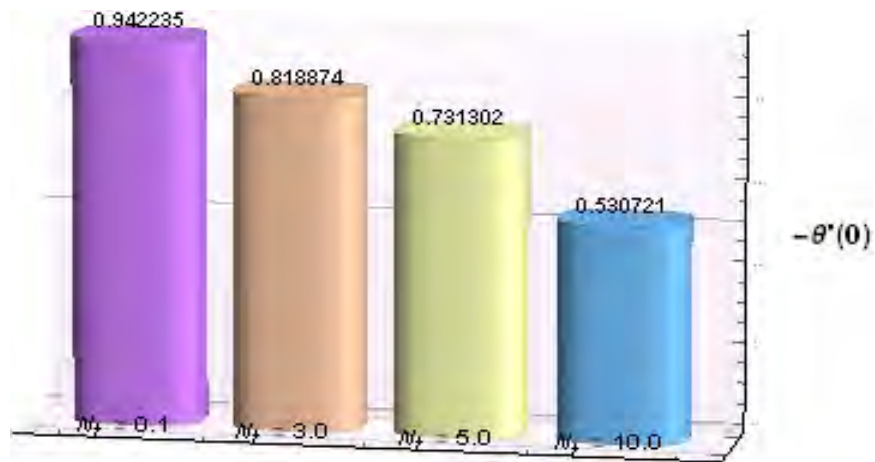Fig. 8.10: Influence of N_b on concentration derivative.
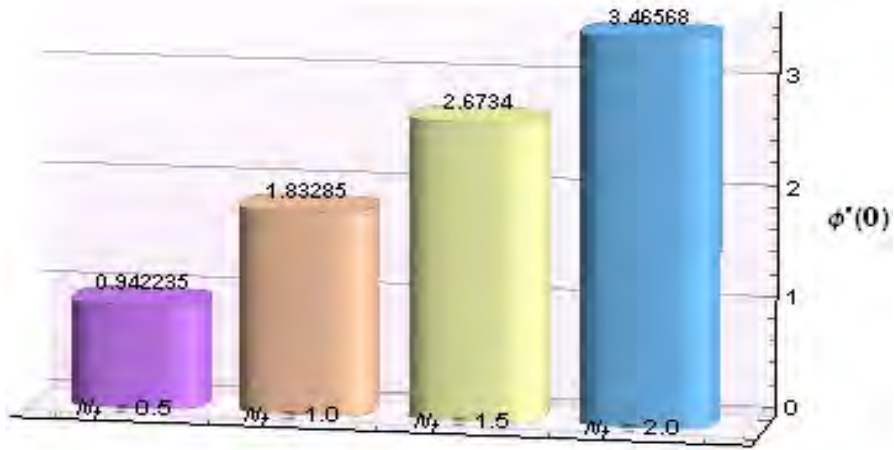

Fig. 8.11: Effects of N_t on temperature derivative.

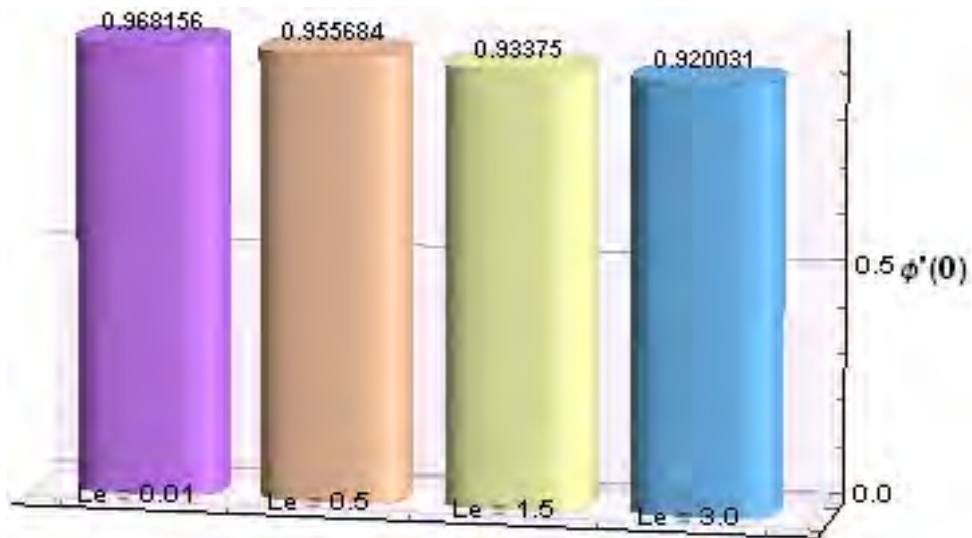Fig. 8.12: Influence of N_t on concentration derivative.

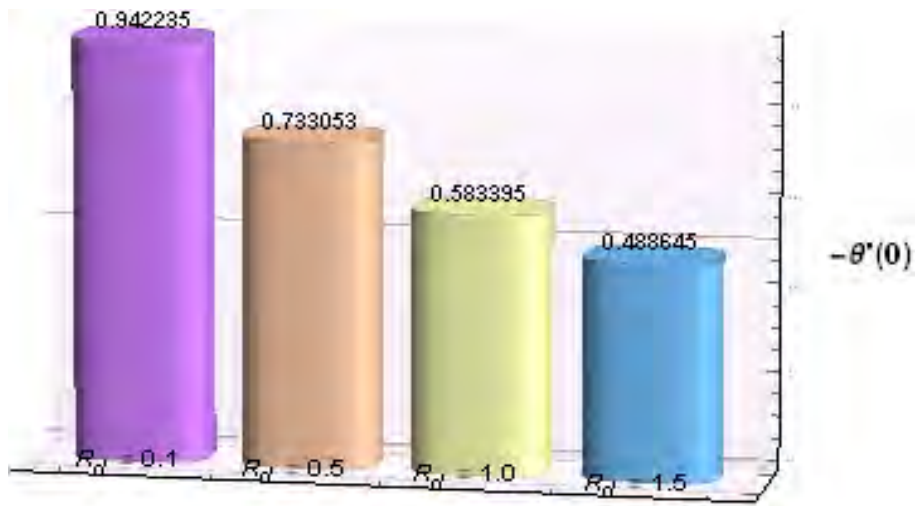Fig. 8.13: Influence of Le on concentration derivative.

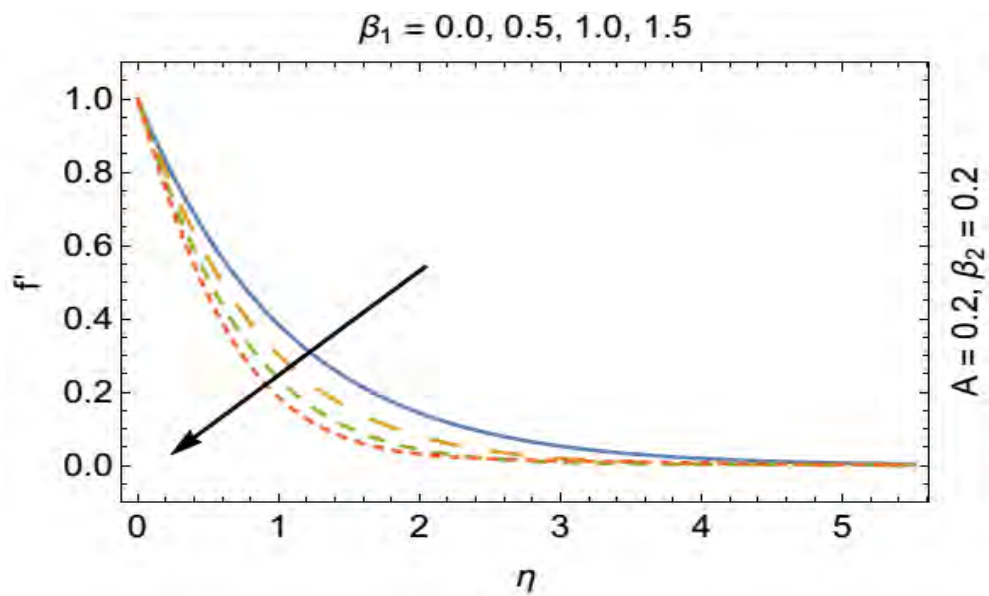Fig. 8.14: Influence of R_d over temperature derivative.
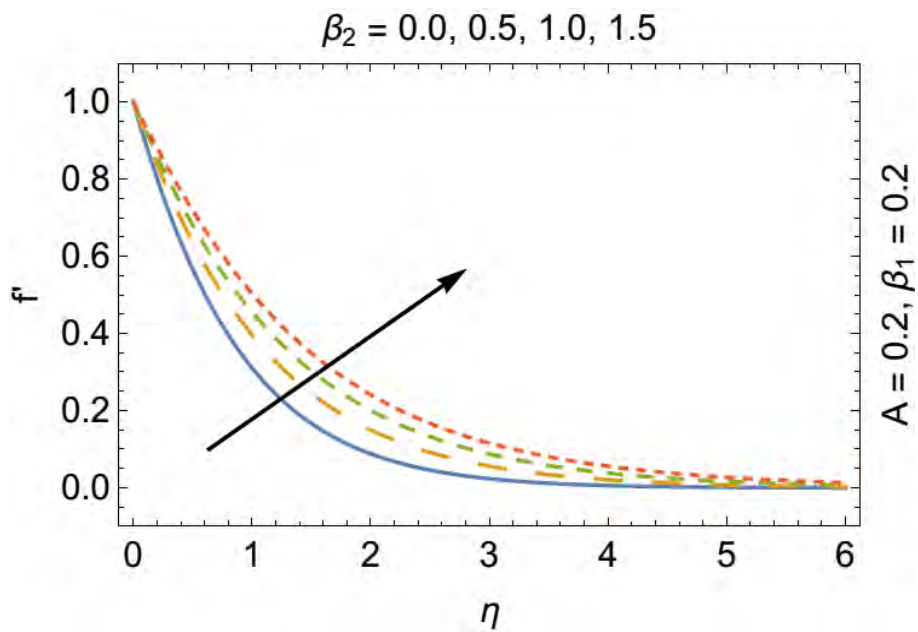

Fig. 8.15: Impact of β_1 on $f'(\eta)$.

$\beta_2 = 0.0, 0.5, 1.0, 1.5$

Fig. 8.16: Impact of β_2 on $f'(\eta)$.

$\beta_1 = 0.0, 0.5, 1.0, 1.5$

Fig. 8.17: Impact of β_1 on $g'(\eta)$.

$\beta_2 = 0.0, 0.5, 1.0, 2.0$

$A = 0.2, \beta_1 = 0.2$

Fig. 8.18: Impact of β_2 on $g'(\eta)$.

$R_d = 0.0, 0.5, 1.0, 1.5$

$\beta_1 = 0.2 = \beta_2, \text{Pr} = 1.2, U_w = 1.2$
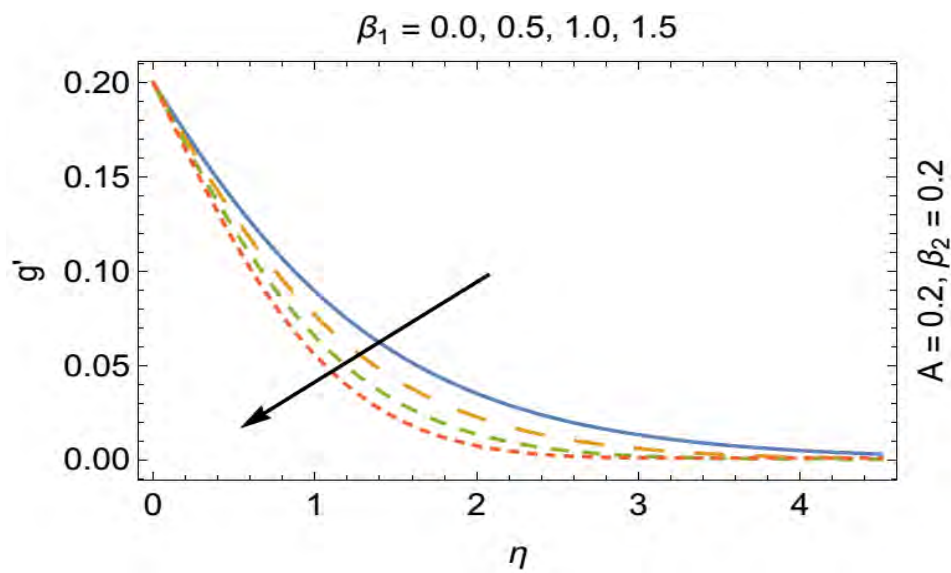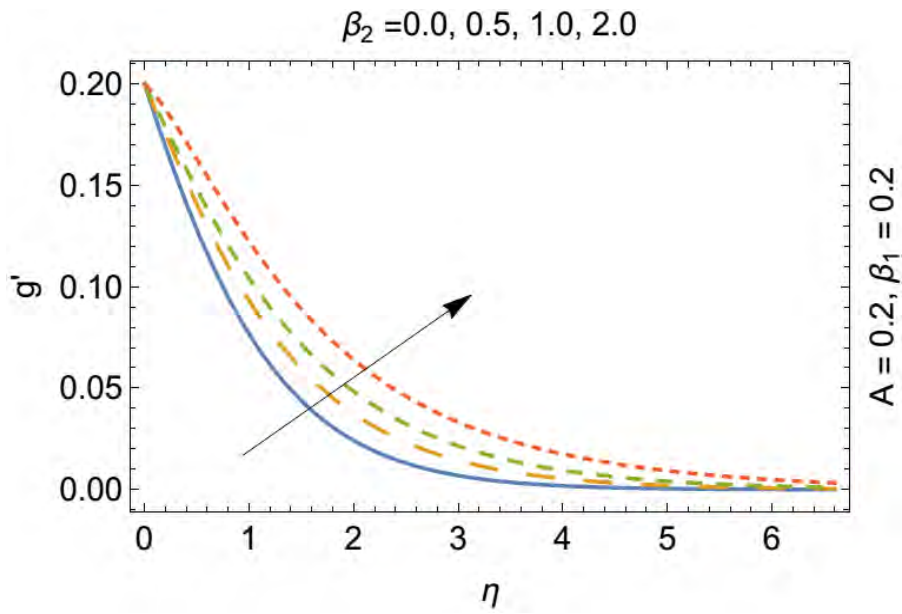
Fig. 8.19: Effects of R_d on $\theta(\eta)$.

113

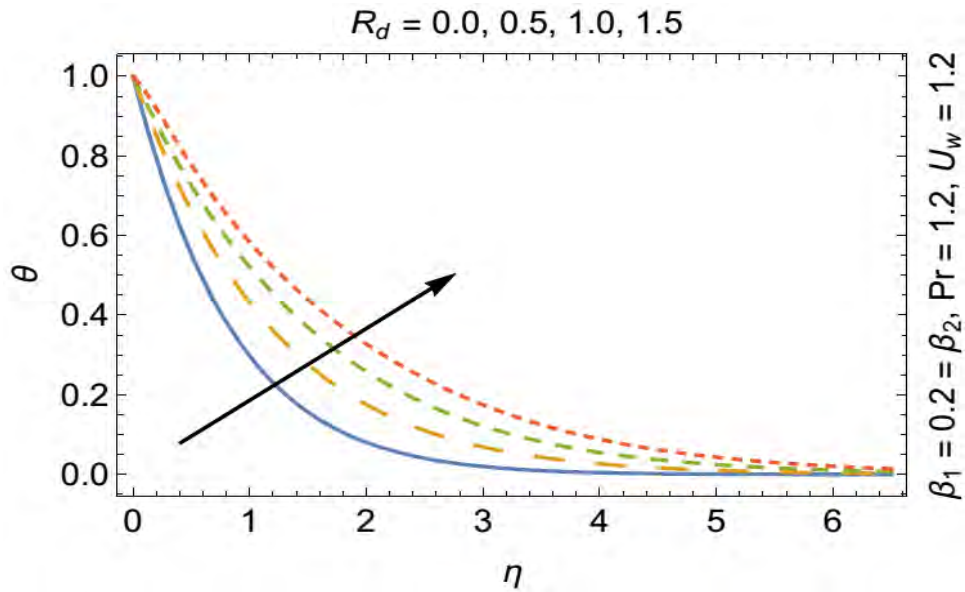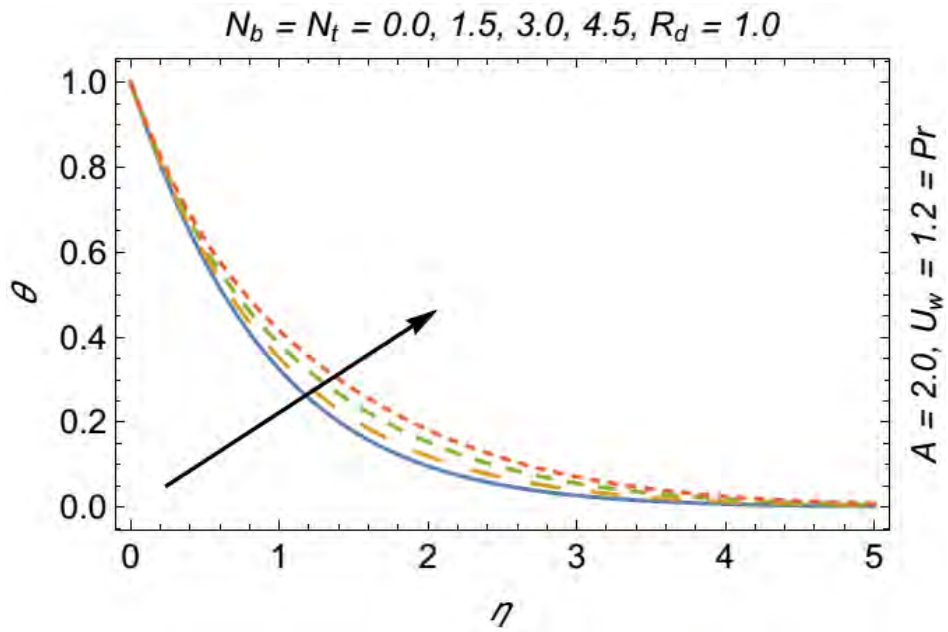Fig. 8.20: Effects of N_b and N_t on $\theta(\eta)$.
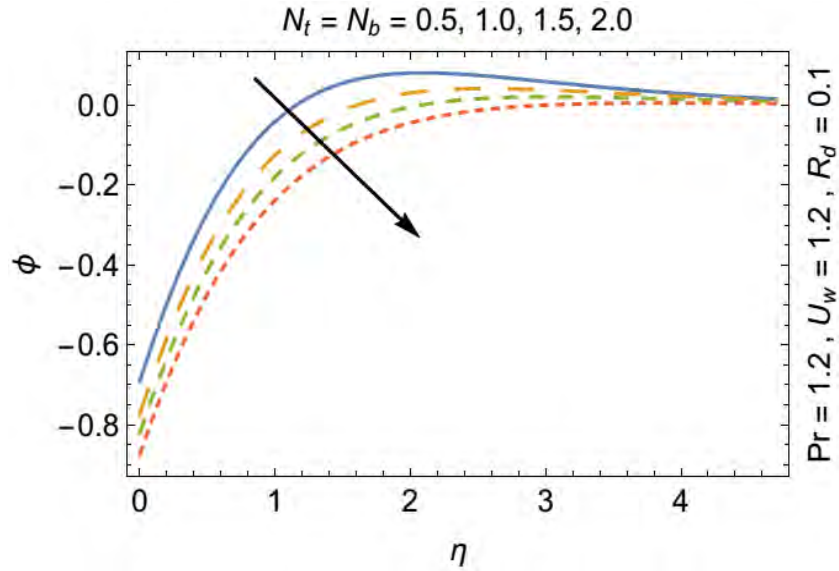
Fig. 8.21: effects of N_b and N_t on $\phi(\eta)$.

Table 8.2: Numerical values of $N_u/\mathrm{Re}^{1/2}$ and $Sh/\mathrm{Re}^{1/2}$.

A	N_t	N_b	Le	Pr	β_1	β_2	$N_u/\mathrm{Re}^{1/2}$	$Sh/\mathrm{Re}^{1/2}$
0.0	0.1	1.0	1.0	1.0	0.2	0.2	1.0349	0.9408
0.5	0.1	1.0	1.0	1.0	0.2	0.2	1.1305	1.0277
1.0	0.1	1.0	1.0	1.0	0.2	0.2	1.2138	1.1034
1.0	0.1	1.0	1.0	1.0	0.2	0.2	1.1305	1.0277
1.0	0.2	1.0	1.0	1.0	0.2	0.2	1.1232	2.0423
1.0	0.3	1.0	1.0	1.0	0.2	0.2	1.1161	3.0432
1.0	0.1	0.1	1.0	1.0	0.2	0.2	1.1305	1.0277
1.0	0.1	0.2	1.0	1.0	0.2	0.2	1.1305	0.5138
1.0	0.1	0.3	1.0	1.0	0.2	0.2	1.1305	0.3426
1.0	0.1	0.3	0.0	1.0	0.2	0.2	1.1820	1.0745
1.0	0.1	0.3	1.0	1.0	0.2	0.2	1.1747	1.0679
1.0	0.1	0.3	1.5	1.0	0.2	0.2	1.1728	1.0662
1.0	0.1	0.3	1.5	0.5	0.2	0.2	0.7523	0.6839
1.0	0.1	0.3	1.5	1.0	0.2	0.2	1.1747	1.0679
1.0	0.1	0.3	1.5	2.0	0.2	0.2	1.7680	1.6072
1.0	0.1	0.3	1.5	1.0	0.0	0.2	1.1636	1.0578
1.0	0.1	0.3	1.5	1.0	0.2	0.2	1.1305	1.0277
1.0	0.1	0.3	1.5	1.0	0.4	0.2	1.0989	0.9991
1.0	0.1	0.3	1.5	1.0	0.2	0.0	1.0855	0.9866
1.0	0.1	0.3	1.5	1.0	0.2	0.5	1.1747	1.0679
1.0	0.1	0.3	1.5	1.0	0.2	1.0	1.2187	1.0755

8.4 Conclusive remarks

The three dimensional Oldroyd-B model together with thermal radiation is analyzed. Fluid deformation is along the stretching surface. The governing equations have been converted into ODEs. Moreover, the results are computed by using HAM. Results are drawn in graphical form to visualize the effect of involved physical parameters. Conclusive remarks drawn from present study are,

- Deborah numbers β_1 and β_2 has opposing effect on $f'(\eta)$.
- Ratio parameter has incompatible influences on $f'(\eta)$ and also on $g'(\eta)$.
- Isotherms and isolines decay by increasing the value of Pr.
- Species concentration $\varphi(\eta)$ descends by growing N_t and N_b.
- Improvement in Pr, β_2 and A enlarge the $Nu_x \operatorname{Re}_x^{-1/2}$ and $Sh/\operatorname{Re}^{1/2}$.
- Positive N_t decreases the $Nu_x \operatorname{Re}_x^{-1/2}$ and enhances $Sh/\operatorname{Re}^{1/2}$.
- For the greater values of Le and β_1, we have reduction in $Nu_x \operatorname{Re}_x^{-1/2}$ and $Sh/\operatorname{Re}^{1/2}$.

Turnitin Originality Report

Rheology of rate type fluid models with heat transfer: Analytical and numerical treatment   by Aqsa Afzal .

From Asssg (ss)

- Processed on 11-Jun-2019 09:46 PKT
- ID: 1142423023
- Word Count: 16104

11/06/2019.
...erson (Turnitin)
...Azam University
Islamabad

Similarity Index
18%
Similarity by Source

Internet Sources:
     5%
Publications:
     0%
Student Papers:
     15%

sources:

1   5% match (student papers from 18-Feb-2016)
Submitted to Higher Education Commission Pakistan on 2016-02-18

2   5% match (student papers from 14-May-2016)
Submitted to Birla Institute of Technology and Science Pilani on 2016-05-14

3   4% match (student papers from 13-Apr-2015)
Submitted to Higher Education Commission Pakistan on 2015-04-13

4   3% match (Internet from 04-Apr-2019)
https://www.grin.com/document/279136

5   2% match (Internet from 19-May-2019)
https://epdf.tips/structural-sensitivity-analysis-and-optimization-2-nonlinear-systems-and-applicaefbd09abf3eec7481e3c1a78b5d27de869657.html

paper text:

Table of Contents

41 Introduction 1.1 Literature survey 1.2 Description of conservation laws 1.

2.1

(signature)